Development and characterization of coated electrode introducing nano particles compatible to austempered ductile iron (ADI)

Thesis submitted by

Tapan Sarkar

Doctor of Philosophy (Engineering)

Metallurgical and Material Engineering Department
Faculty Council of Engineering & Technology
Jadavpur University
Kolkata-700032, India

2018

Jadavpur University

Kolkata-700032

India

Index No.:- 158/15/E

Title of the Thesis:

"Development and characterization of coated electrode introducing nano particles compatible to austempered ductile iron (ADI)"

Name, Designation and Institution of Supervisor/s:

1. Dr. Tapan Kumar Pal
   Professor (Retd.)
   Metallurgical and Material Engineering Department
   Jadavpur University
   Kolkata – 700032
   India

2. Dr. Akshay Kumar Pramanick
   Professor
   Metallurgical and Material Engineering Department
   Jadavpur University
   Kolkata – 700032
   India

List of Publications

Papers Published in International and National Journal

1. **Tapan Sarkar** and Tapan Kumar Pal, "**Austempered Ductile Iron (ADI) Weld Metal Microstructure Study for Optimum Ce Content**", ISIJ International (Accepted)
2. **T. Sarkar**, A. K. Pramanick, S. K. Sahoo, T. K. Pal and A. K. Pramanick, "**Influence of Austempering Temperature and Time on the Microstructure and Mechanical Properties of Ductile Iron Weldment Using Developed Coated Electrode**", Journal of Material Engineering and Performance, 2019, 28(4), 2071-2085., DOI: 10.1007/s11665-019-03989-1.
3. Tapan Kumar Pal and **Tapan Sarkar**, "**Comparative austempering response between weld metals of ADI weldments with and without cerium addition**" Supplemental UE: TMS 2019 148th Anuual Meeting & Exhibition Supplemental Proceedings, The Minerals, Materials & Materials Series, 2019, 217-237., DOI: 10.1007/978-3-030-05861-6_20.
4. **Tapan Sarkar** and Tapan Kumar Pal, "**Response of Austempering Heat Treatment on Microstructure and Mechanical Property in Different Zones of As-Welded Ductile Iron (DI)"**, SAE Int. J. Mater. Manuf., 2018, 11(2), 151-159., DOI: 10.4271/05-11-02-0016.
5. **Tapan Sarkar**, Ajit Kumar Pramanick and Tapan Kumar Pal, "**Some aspects on the welding characteristics and formation of microstructures in a newly developed coated electrode for austempered ductile iron (ADI)**", Indian Welding Journal, 2015, 48(4), 44-60s., DOI:10.22486/iwj/2015/v48/i4 /12605.

Papers Communicated to International Journal

1. **Tapan Sarkar** and Tapan Kumar Pal "**Influence of Cerium on Joint Perrformance of Austempered Ductile Iron (ADI) Welds**", International Journal of Advanced Manufacturing Technology (Communicated)

Papers Presented in International Conference

1. **Tapan Sarkar**, Tapan Kumar Pal and Akshay Kumar Pramanick, "**Effect of Cerium content in Austempered Ductile Iron (ADI) Weld metal**", 1st International Conference on Mechanical Engineering, Jadavpur University (INCOM 2018), on 4-6th January 2018, Kolkata, Published in Proceeding.
2. **Tapan Sarkar**, Tapan Kumar Pal and Akshay Kumar Pramanick, "**Response of Austempering heat treatment in weld metal, HAZ and base metal of ADI weldments",** International Welding Congress 2017, on 7-9th December 2017, Chennai, Published in Proceeding.
3. **Tapan Sarkar**, Ajit Kumar Pramanick and Tapan Kumar Pal, "**Development of SMAW electrode for austempered ductile iron and its respond to austempering**", Published on International welding symposium , 2K14, 28-30th October 2014, Mumbai.

Papers Presented in National Conference

1. Tapan Kumar Pal and **Tapan Sarkar**, "**Development of welding technology for joining/repairing austempered ductile iron (ADI)**", TAME-2019, 15-16th February, 2019, Kalyani.
2. **Tapan Sarkar** and Tapan Kumar Pal, "**Effect of Ce on microstructures of as welded and austempered ductile iron weld metals**", published in NWS 2018 Kochi on 13-15th December 2018, Kochi.
3. **Tapan Sarkar** and Tapan Kumar Pal, "**High cycle fatigue behavior of austempered ductile iron (ADI) welded joints**", published in NWS 2018 Kochi on 13-15th December 2018, Kochi.
4. **T. Sarkar**, S. Banerjee, S. K. Sahoo, T. K. Pal and A. K. Pramanick, "**Development of Coated Electrode and Welding Procedure for Austempered Ductile Iron (ADI)**" Published NWS Kolkata on 15-17th December 2016, Kolkata.
5. **Tapan Sarkar**, Ajit Kumar Pramanick, Hrishikesh Das and Tapan Kumar Pal, "**The influence of austempering temperature and time on the formation of ausferrite in the developed weld deposits on Austempered ductile Iron**" Published NWS Mumbai, 10-12th December 2015, Mumbai.

CERTIFICATE

This is to certify that the thesis entitled **"Development and characterization of coated electrode introducing nano particles compatible to austempered ductile iron (ADI)"** *submitted by* ***Shri*** **Tapan Sarkar**, *who got his name registered on* ***29th October, 2015*** *for the award of Ph.D (Engineering) degree of Jadavpur University is absolutely based upon his own work under the supervision of* ***Prof. Tapan Kumar Pal*** *and* ***Prof. Akshay Kumar Pramanick****. The neither his thesis nor any part of the thesis has been submitted for any degree/diploma or any other academic award anywhere before.*

Dr. Tapan Kumar Pal
Professor (Retd.)
Met. and Mat. Engg. Department
Jadavpur University
Kolkata – 700032
India

Dr. Akshay Kumar Pramanick
Professor
Met. and Mat. Engg. Department
Jadavpur University
Kolkata – 700032
India

JADAVPUR UNIVERSITY
KOLKATA-700032

Index No.:- 158/15/E

BIBLIOGRAPHY OF DOCTORAL DISSERTATION

Faculty	**:** Faculty of Engineering & Technology
Department	**:** Metallurgical and Material Engg.
Name of the Degree	**:** Doctor of Philosophy in Engineering
Name of the Candidate	**:** Shri Tapan Sarkar
Fellow	**:** Junior Research Fellow (DST Purse)
Title of the Thesis	**:** Development and characterization of coated electrode introducing nano particles compatible to austempered ductile iron (ADI)
Date of Registration	**:** 29th October, 2015
Date of submission of thesis	**:** 28th September, 2018
Name of Supervisor/s	**:** Prof. T. K. Pal and Prof. A. K. Pramanick
Nationality	**:** Indian
Signature of the candidate	**:**

Dedicated to My Beloved Parents

and

My Wife

Acknowledgement

I have great privilege and gratification to express my heartiest thanks and deep sense of gratitude to my respected supervisor Dr. T. K. Pal, Professor, Metallurgical and Material Engineering Department, Jadavpur University, Kolkata 700032, India, for his valuable guidance and indefatigable efforts throughout the tenure of this work. He has been an inspiring and driving force where targets appeared to be difficult during the research work. His timely help, constructive criticism, positive attitude, painstaking efforts, humanistic and warm personal approaches made the author capable to compile the thesis in its present form. I must say that my thesis is accomplished because of his great guidance.

I like to extend my sincere thanks to my supervisor Dr. A. K. Pramanick, Professor, Metallurgical and Material Engineering Department, Jadavpur University, Kolkata 700032 for giving me the opportunity to explore my work with freedom and for his timely support, and encouragement that allowed me to complete my research.

Special thanks to Dr. S. K. Sahoo, Associate Professor, Metallurgical and Materials Engineering, NIT Rourkela, Odisha, 769008 for his help and providing me to carried out XRD analysis

I like to extend my sicears thanks to my senior Dr. Ajit Kumar Pramanick presently Asst. Professor, NIFFT, Ranchi 834003 for his special guidance for design the flux formulation and development of coated electrode also shearing his technical knowledge.

I convey my special thanks to Mr. Sumit Banerjee, Head (Quality) Cresmac Foundry, Kolkata and Mr. Anant Jhawar, Kalimata Industries, Durgapur, for their unconditional help regarding materials.

I like to extend my sincere thanks to Mr. Maink Sen, Research Scholar, Metallurgical and Material Engineering Department IIT Kharagpur for carried out TEM analysis for the present work

My heartfelt thanks go to my Seniors Hrishikesh Da, Mani Da, Pritish Da Sushovan Da, Rajorshi Da and Nitesh for their nice company and helping attitudes that made the environment comfortable and tension free.

I owe my deepest gratitude to my parents, my brother, my wife, Krishna Madam and my school friends, whose honest mentally support, carrying and obstinate love give me energy to complete this work successfully.

Tapan Sarkar

Abbreviations

DI	Ductile iron
ADI	Austempered ductile iron
UTS	Ultimate tensile strength (MPa)
YS	Yield strength (MPa)
El	Elongation (%)
OES	Optical emission spectrometer
SMAW	Shielded metal arc welding
PWHT	Post weld heat treatment
BM	Base metal
WM	Weld metal
PMZ	Partial melted zone
HAZ	Heat affected zone
OM	Optical microscopy
SEM	Scanning electron microscopy
EDS	Energy dispersive spectroscopy
XRD	X-ray diffraction
TEM	Transmission electron microscopy
N	Graphite nodularity
r	Nodule size
FCC	Face centered cubic
BCC	Body centered cubic
X_γ	Volume percentage of retained austenite (vol %)
X_α	Volume percentage of bainitic ferrite (vol %)
X_g	Volume percentage of graphite (vol %)
C_γ	Carbon content in austenite (wt. %)
LC	Ledeburitic carbide
AP	Alloyed pearlite
G	Graphite
BF	Bainitic ferrite
RA	Retained austenite
ε	Carbide
M	Martensite
r	Nodule size (μm)
HCF	High cycle fatigue
R	Stress ratio
M_S	Martensite start
Bs	Bainite start
RE	Rare earth
δ	Lattice misfit

Abstract

Austempered ductile iron (ADI) is a new and very promising engineering material with duplex matrix microstructure of bainitic ferrite and retained austenite. Presently the material has gained increasing interest in academic research and industrial application due to its attractive mechanical properties such as high ultimate tensile strength (850-1400 MPa), high fatigue strength, reasonable ductility (elongation 4-10%), excellent wear resistance, fracture toughness and higher fatigue strength along with lower production cost. The excellent combination of these several attractive properties has made ADI for wide applications as structural components in various industries, such as automotive, agricultural, defence, rails and mining industries etc. ADI has also economically replaced as forged steel and cast steel for many of its applications.

Till today ADI is almost always used as cast product and in order to provide more design flexibility and more use of low-cost potential material (ADI) as well as for repairing the casting defects in producing ADI, or in joining several small casings to make a large component that could not, perhaps, have been cast as a single piece, the importance of welding DI which could be later converted to ADI, cannot be overridden. Although different coated electrodes such as ENi-CI, pure nickel (90-97%), stainless steel (Fe-Cr-Ni), ENiFe-CI etc. are available commercially for welding DI, but these electrodes show negligible response to isothermal heat treatment as the alloying elements present in the electrode belong to poor austemperability. As a result weld metals produced by these electrodes can't be converted into ADI structure. In the present work, the suitable coated electrode (Trial 4) for welding DI was first developed based on target chemical composition of weld deposit. Also, three different level of nano size CeO_2 was added in coating of the developed electrode in order to study and understand the effect of Ce on microstructures and mechanical properties of weld metals. Weld procedure was established as per AWS(D11) standard using first single pass bead-on-plate and latter for grove welding of 20 mm thick DI base plate using coated developed electrodes (with and without Ce content) in shielded metal arc welding (SMAW) process with modified U-groove design in order to /extract metallography, transverse tensile, charpy impact and fatigue test specimens.

All the zones of as-welded DI joints and ADI joints, after isothermal heat treatment of as-welded DI joints, i.e weld metal, partially melted zones (PMZ), heat affected zones (HAZ) and base metal were characterized using optical microscopy (OM), scanning electron microscopy (SEM), transmission electron microscopy (TEM), X-ray diffraction (XRD) and energy dispersive spectroscopy (EDS). The mechanical properties such as microhardness, transverse tensile test, room temperature charpy impact test and high cycle fatigue behaviour of the ADI welded joints

have been evaluated in order to find out suitability of developed coated electrode and influence of Ce on weld metal performance.

The results show that there is a significant microstructural variation in particular the proportion of ledeburitic carbide and alloyed pearlite in the matrix structure and morphologhy of graphite such as nodule size, nodularity and nodule count among different zones of as-welded DI joints as well as between Ce and without Ce containing weld metals.

Interestingly, these as-welded microstructures including matrix and graphite largely governed the response of isothermal heat treatment cycle which consists of austenitization at 900°C for 2 h and austempering at 300°C and 350°C for 1.5, 2 and 2.5 h holding time, leading to microstructural variation in particular vol % of retained austenite among the different zones of ADI joints. At 300°C austempering temperature microstructure shows needle-shaped bainitic ferrite with a small amount of film shaped retained austenite and graphite nodules. Whereas, at 350°C austempering temperature microstructure shows feathery shaped bainitic ferrite with a higher amount of blocky shaped retained austenite and graphite nodularity. Increasing holding time from 1.5 to 2 h the size of bainitic ferrite as well as the amount of retained austenite content increased. Further increasing holding time from 2 to 2.5 h the size of the bainitic ferrite increased further, but the amount of retained austenite decreased.

In as-welded condition, maximum hardness exhibited in weld metal followed by PMZ, HAZ and base metal. After isothermal heat treatment of DI weldment microhardness shows opposite trend i.e. weld metal shows lowest hardness followed by HAZ (PMZ could not be distinguished with HAZ) and base metal in both without and with Ce treated ADI weldment. However, in both as-welded and austempered conditions, Ce containing weld metal always shows lower hardness than without Ce content.

The results of transverse tensile tests of the ADI joints (without and with Ce content) showed that all the test samples failed from base metal indicating weld metal and even HAZ are stronger than base metals well as achievement of 100% joint efficiency. Ce containing weld metals show higher charpy impact toughness than without Ce content and maximum toughness is obtained in weld metal containing 0.1% Ce at 350°C for 2 h holding time. Also highest fatigue strength is achieved in ADI weld metal having maximum toughness due to presence of higher amount of high carbon retained austenite.

With respect to the microstructural constituents (maximum amount of retained austenite) and results of mechanical properties of ADI joints, 0.1% Ce is the optimum Ce content in weld metal and 350°C for 2 h holding time is optimum isothermal heat treated condition in the present study.

Contents

List of Figures

List of Tables

Chapter 1

Introduction
&
Scope of work

Chapter 1

Introduction and Scope of Work

1.1 Introduction

Austempered ductile iron (ADI) is a new and very promising engineering material with duplex matrix microstructure of bainitic ferrite and retained austenite **[1-2]**. The material is now of great interest for its low production cost, good recycling capacity, excellent castability and a wide range of mechanical properties such as high yield and tensile strength, good ductility, good fatigue strength, excellent wear resistance and high fracture toughness **[1-4]**. Due to the attractive mechanical properties and low production cost, ADI is now widely used in different commercial applications such as automotive, agricultural, earth moving machinery, railways, defence and structural applications **[5-6]**.

ADI competes favourably with steel forgings, especially for heavy-duty parts where reliability is important. It is used to upgrade from standard ductile irons (DI), and as a substitute for manganese steel and nickel-hard materials **[7]**. When strength is required ADI is particularly cost-effective: tensile and yield strength is twice as high as standard DI; fatigue strength is 50% higher and it can be enhanced by shot penning or rolling. Due to its high strength-to-weight ratio and low production cost, ADI can be replaced aluminium when reduced section sizes are acceptable **[7]**.

This high potential material was first developed by Tecumseh Products in the early 1972 as a form of compressor crankshaft **[8]**. The material was further improved and more companies started in using this material commercially. In 1980 the application of ADI was increased rapidly in North America and first standard of ADI 897/897M was released in the year 1990**[9]**. As per ASTM 897/897M standards **[9]** five different grades of ADI are commercially available according to the ultimate tensile strength (UTS) and percentage of elongation **[10]**.

For ADI initial material is selected as-cast DI. The chemical composition of ADI is similar to conventional DI. However, some alloying elements such as Ni, Cu and Mo are usually added to increasing the austemperbility, to delay the austenite decomposition to pearlite and ferrite upon cooling **[11]**. DI is converted to ADI by two steps isothermal heat treatment process: austenitization and austempering. Austenitization is done at 850-910°C for 30 min -2 h holding time and austempering is performed at 250-450°C for 5 min- 4 h holing time followed by air cooling to room temperature to avoid the formation of martensite **[12]**. The

total heat treatment process of ADI depends on the chemical composition and thickness of the as- cast DI.

Though the microstructure of ADI consists of bainitic ferrite and retained austenite base matrix with graphite nodules, the proportion and morphology of matrix phases can be changed by austempering temperature. At lower austempering temperature the microstructure forms as needle-like (acicular) bainitic ferrite with high carbon untransformed austenite, i.e. called retained austenite **[13]**. By increasing austempering temperature the shape of the bainitic ferrite (acicular) is changed and transforms to plate-like (feathery) shape along with retained austenite. Austempering temperature and holding time show significant effects on the microstructure and mechanical properties of ADI **[13]**. During austempering process a two stage reactions occur, at initial stage (stage I) austenite (residual austenite) decomposes into bainitic ferrite and high carbon austenite (retained austenite). Increasing holding time the stage II reaction starts and high carbon austenite further decomposes to bainitic ferrite and carbide (ε carbide). The time period between the two stages reaction is called the process window which attributes the best combination of microstructural and mechanical properties. Presence of alloying elements such as Ni, Cu and Mn delay the austempering reaction and increase the process window **[11]**. Thus it is important to find out optimum heat treatment conditions for a given composition of DI to avail maximum benefit of ADI.

The mechanical properties of ADI depends on the fine microstructural constituents consisting of retained austenite, carbon content of retained austenite, morphology of ferrite, precipitated carbide if any, the number, size, distribution and nodularity of graphite **[14]**. The graphite nodule count and size distribution play a very important role in determining the final microstructural and mechanical properties of ADI. Borrajo et al **[15]** reported that nodularity in DI is increased with decreasing solidification time and section thickness of the materials. However, higher graphite nodularity with smaller in size shows better mechanical properties than larger size graphite nodules **[16]**.

Several investigators **[17-19]** have shown that rare earth metal such as cerium (Ce) has a beneficial effect on the microstructure and properties of DI. However, the optimum rare earth content varies significantly according to different investigators. For example, X. Diao et al **[20]** showed with increasing Ce content from 0.005 to 0.014% the nodularity increased along with refining the size of the nodules in DI; but further increasing Ce content up to 0.018 or 0.020%, the nodularity decreased and formed some non-spherical graphite with coarsening the nodule size. J.O. Choi et al **[17]** observed that DI castings with 0.3% rare earth content attributed improved graphite nodules, lower tensile strength and hardness, higher elongation than that of

DI castings without rare earth. The addition of 0.5% Ce in high Cr white cast iron (WCI) refined the primary M_7C_3 carbides and impact toughness increased by 50% compared with WCI without cerium modification **[21]**. Addition of Ce is therefore very critical to attain maximumbenefit on the microstructure and properties of DI optimum Ce content needs to be found out.

Till today ADI is mostly used as cast product and in order to provide more design flexibility and more use of low-cost potential material (ADI) as well as for repairing the casting defects in producing ADI, or in joining several small casings to make a large component that could not, perhaps, have been cast as a single piece **[22]**; the importance of welding DI which could be later converted to ADI, cannot be overridden. It is well known that cast iron is difficult to weld, the most common problem being cracking. But a through understanding of the metallurgy involved have enabled in developing a suitable weld procedure. Infact, no.s of coated electrodes for welding DI such as ENi-CI, pure nickel (90-97%) **[23]**, stainless steel (Fe-Cr-Ni) and ENiFe-CI **[24]** etc. are available commercially and these electrodes are being used for joining DI by shielded metal arc welding process (SMAW). The problem of DI welded joints using these electrodes is that joints cannot be converted to ADI by isothermal heat treatment due to poor austemperability of the weld deposits.Thus development of coated electrode with improved austemperability for welding DI, should be the first step for maximum exploitiation of low cost high potential engineering material such as ADI in different commertial applications.

Although research was carried out on the effect of Ce on DI weld metal. But addition of Ce in weld metal other than DI was studied and beneficial effect of optimum Ce content had been reported by previous investigators **[25-29]**. While systematically varying cerium oxide content in the flux formulation of basic coated austenitic stainless steel electrode, G. Srinivasan et al **[25]** expressed that an optimum amount of 0.4% Ce improved mechanical properties of the weld deposits mainly through decrease in oxygen & sulphur content, inclusion size and no.s of inclusions. In another investigation, S. K. Samanta et al **[26]** introduced cerium (Ce) in the form of mischmetal (50% Ce) and Nb in the form of FeNb (50% Nb) into the weld pool as powder form (200 mesh size) through the tubes of 316L stainless steel foil as the filler wire. Refinement of weld microstructure, improvement of oxidation resistance as well as oxide scale adherence of 316L weld was reported. Recently, nanomaterials are being used in commercial welding electrodes as nano-materials have unique mechanical, electrical, magnetic and optical properties differing from traditional materials **[27-29]**. B Chen et al **[30]** replaced conventional microscale marble by marble of nanoscale size in the flux coating of a hardfacing electrode

(D600R). Significantly improved arc stability, greater metal deposition efficiency and increased hardness and wear resistance of the deposit were obtained. In another investigation, improved recovery of Mn, Ni, Mo, Ti etc. and improved strength and toughness of weld deposits were reported with an addition of nano-sized TiO_2 substituting micro size TiO_2 to the coating of SMAW electrode (E11018 M) **[31]**. The review of this literature indicates that Ce has a significant beneficial effect on microstructure and properties of DI and other types of cast iron. Also, microstructure modification and improved properties of weld metals particularly for austenitic stainless steel have been reported with the addition of Ce. Recently beneficial effect of nano-material substituting micro size materials in SMAW electrode has been observed. Thus it is of interest to study and understand the effect of Ce on DI weld metal leading to optimum Ce content as well as its respond to isothermal heat treatment.

In the present research work, development of coated electrode for welding DI based on two fundamental approaches was attempted and then DI groove welded joints were converted to ADI using isothermal heat treatment cycle.

The first approach dealt with the development of suitable coated electrode introducing judicial selection of alloying elements and keeping low Ni content in different flux compositions (ingredient).

Secondly, nano size CeO_2 was added to the flux ingredient by adjusting the micro size elements to study the effect of Ce on the microstructural and mechanical properties of weldments.

The DI plates were then welded by establishing weld procedure as per AWS(D11) standard using the developed electrodes (with and without Ce) and welded DI plates were converted to ADI by applying isothermal heat treatment cycle.

Finally, the weld metals were characterized for microstructural and mechanical properties to find out optimum isothermal heat treatment condition as well as optimum Ce content.

1.2 Scope of work

The aim of the present research work is as follows:

- To develop suitable coated electrodes using solid core wire and flux coating containing spherodizing, graphitizing, fluxing and alloying elements of micro sized particles and replacing partially by nano size CeO_2 particles.
- To develop weld procedure (for sound weld) as per AWS(D11) standard using bead-on-plate and latter using groove weld for welding 20 mm thick DI plate using developed

coated electrodes (with and without Ce) in shielded metal arc welding (SMAW) process.

- To study the influence of isothermal heat treatment cycle on microstructures and mechanical properties of different zones i.e. weld metal, PMZ, HAZ and base metal of ADI weldments.
- Microstructural characterization of weld metal, PMZ and HAZ of as-welded DI and ADI by optical microscopy (OM), scanning electron microscopy (SEM) and phase analysis by X-ray diffraction analysis (XRD), Energy dispersive spectroscopy (EDS) analysis and transmission electron microscopy (TEM) studies.
- To study the mechanical properties such as microhardness, transverse tensile test, room temperature charpy impact test and high cycle fatigue behaviour of the ADI welded joints after different isothermal heat treatment cycle.
- To study the fracture surfaces of broken charpy impact and fatigue tested samples under SEM in order to find out possible micro-mechanism of failure.
- To find out optimum isothermal heat treatment conditions and optimum Ce content of ADI weld metal based on the results of microstructural and mechanical properties studied.

References

1. S. Panneerselvam, C. J. Martis, S. K. Putatunda, J. M. Boileau, "An investigation on the stability of austenite in Austempered Ductile Cast Iron (ADI)", Materials Science & Engineering A, 625(2015) 237-246
2. S. Panneerselvam, S. K. Putatunda, R. Gundlach, J. Boileau, "Influence of intercritical austempering on the microstructure and mechanical properties of austempered ductile cast iron (ADI)", Materials Science and Engineering A, 694 (2017) 72-80
3. S. K. Putatunda, "Development of austempered ductile cast iron (ADI) with simultaneous high yield strength and fracture toughness by a novel two-step austempering process", Materials Science and Engineering A, 315 (2001) 70-80
4. Y. J. Kim, H. Shin, H. Park, J. D. Lim, "Investigation into mechanical properties of austempered ductile cast iron (ADI) in accordance with austempering temperature", Materials Letters, 62 (2008) 357-360
5. P. W. Shelton, A. A. Bonner, "The effect of copper additions to the mechanical properties of austempered ductile iron (ADI)", JMPT, 173 (2006) 269-274
6. J. Yang, S. K. Putatunda, "Influence of a novel two-step austempering process on the strain-hardening behaviour of austempered ductile cast iron (ADI)", Materials Science and Engineering A, 382 (2004) 265-279
7. B. V. Kovacs Sr, "Austempered ductile iron: fact and fiction", Mod. Cast. 80(3) (1990) 38-41
8. Ductile iron Data for Design Engineers - section IV. "Austempered ductile iron", Ductile iron society. http://www.ductile.org
9. K. L. Hayrynen, J. R. Keough, "Austempered Ductile Iron"-The State of the Industry in 2003, in Keith D. Millis Symposium, Louisville, 2003
10. J. Zhang, N. Zhang, M. Zhang, L. Lu, D. Zeng, Q. Song, "Microstructure and mechanical properties of austempered ductile iron with different strength grades", Materials Letters, 119 (2014) 47-50
11. R. B. Gundlach, J. F. Janowak, "Austempered ductile irons combine strength with toughness", Met. Prog., 12 (1985) 231-236
12. A. H. Elsayed, M. M. Megahed, A. A. Sadek, K. M. Abouelela, "Fracture toughness characterization of austempered ductile iron produced using both conventional and two-step austempering processes", Materials and Design, 30 (2009) 1866-1877

13. S. K. Putatunda, A. V. Singara, R. Tackett, L. Gavin, "Development of a high strength high toughness ausferritic steel", Materials Science and Engineering A, 513–514 (2009) 329-339
14. A. Refaey, N. Fatahalla, "Effect of microstructure on properties of ADI and low alloyed ductile iron", Journal of Materials Science, 38 (2003) 351-362
15. J. M. Borrajo, R. A. Martínez, R. E. Boeri, J. A. Sikora, "Shape and count of free graphite particles in thin wall ductile iron castings", ISIJ international, 42(3) (2002) 257-263
16. G. L. Greno, J. L. Otegui, R. E. Boeri, "Mechanisms of fatigue crack growth in Austempered Ductile Iron", International Journal of Fatigue, 21(1) (1999) 35-43
17. J. O. Choi, J. Y. Kim, C. O. Choi, J. K. Kim, P. K. Rohatgi, "Effect of rare earth element on microstructure formation and mechanical properties of thin wall ductile iron castings", Materials Science and Engineering A, 383 (2004) 323-333
18. M. I. Onsøien, Ø. Grong, T. Skaland, K. Jørgensen, "Mechanisms of graphite formation in ductile cast iron containing rare earth metals", Materials science and technology, 15(3) (1999) 253-259
19. C. S. Kanetkar, H. H. Cornell, D. M. Stefanescu, "The Influence of Some Rare Earth (Ce--La--Pr--Nd) and Yttrium in the Magnesium Ferrosilicon Alloy on the Structure of Spheroidal Graphite Cast Iron", AFS Transactions, 92 (1984) 417-428
20. X. Diao, Z. Ning, F. Cao, J. Sun, "Effect of Ce on graphite nodule count and size distribution in ductile iron", International Journal of Modern Physics B, 23 (2009) 1853-1860
21. X. Zhi, J. Liu, J. Xing, S. Ma, "Effect of cerium modification on microstructure and properties of hypereutectic high chromium cast iron", Materials Science and Engineering A, 603(2014) 98-103
22. R. Winiczenko, R. Salat, M. Awtoniuk, "Estimation of tensile strength of ductile iron friction welded joints using hybrid intelligent methods", Trans. Nonferrous Met. Soc. China, 23 (2013) 385–391
23. E. M. El-Banna, M. M. Nageda, Abo El-Saadat, "Study of restoration by welding of pearlitic ductile cast iron", Materials Letters, 42(5) (2010) 311-320
24. M. Pascual, C. Ferrer, E. Rayon, "Weldability of spheroidal graphite ductile cast iron using Ni/Ni-Fe electrodes", Revista de Metalurgia, 45 (5) (2009) 334-338
25. G. Srinivasan, A. K. Bhaduri, S. K. Albert, "Addition of cerium oxide in the flux formulations of a basic-coated stainless steel electrode", Welding in the World, 57 (2013) 55-63

26. S. K. Samanta, S. K. Mitra, T. K. Pal, "Effect of rare earth elements on microstructure and oxidation behaviour in TIG weldments of AISI 316L stainless steel", Materials Science and Engineering A, 430 (2006) 242-247

27. T. Aizawa, "Nanogranulation process into magneto-resistant Co-Cu alloy on the route of bulk mechanical alloying", Materials Science and Engineering A, 285 (2000) 1-7

28. T. Aizawa, K. Kondoh, "Nanostructured materials via bulk mechanical alloying", Scripta Mate., 44 (2001) 1751-1755

29. B. H. Kear, P. R. Strutt, "Chemical processing and application of nano structured materials", Nano structured Materials, 6 (1995) 227-236

30. B. B. Chen, F. Han, Y. Huang, K. Lu, Y. Liu, L. Li, "Influence of Nanoscale Marble (Calcium Carbonate ($CaCO_3$) on Properties of D600R Surfacing Electrode", Welding Journal, (2009) 99-103

31. T. K. Pal, U. K. Maity, "Effect of Nano Size TiO_2 Particles on Mechanical Properties of AWS E11018M Type Electrode", Materials Sciences and Applications, 2 (2011) 1285-1292

Chapter 2

Literature Review

Chapter 2

Literature Review

2.0 Introduction

ADI has become a potential engineering material to the design engineer from economic as well as superior combination of properties point of view. Full exploitation of ADI therefore requires technology of joining and consequently the development of welding filler wire (electrode) material. In this chapter, an overview of the cast iron family, metallurgy of DI and its weldability, the historical upgradation, metallurgical characteristics, applications of ADI have been summarized. Isothermal heat treatment and the important parameters of the heat treatment cycles affecting ADI have been discussed. The problems of DI welding and present status of the welding of DI based on the published work by the previous investigators have been presented. Finally, the development of SMAW electrode and modification of DI microstructure as well as modification of weld metals microstructures with addition of rare earth metal have been brought out.

2.1 Cast Iron

2.1.1 Historical background

Cast iron (CI) was invented in China in the 5^{th} century BC **[1]**. They used to make pots and weapons because it was cheaper. In the west it became available in the 15^{th} century and the first usage to make cannon and shot. Henry VIII initiated the casting of cannons in England by using blast furnaces. These were heavier and cheaper which enabled England to arm her navy better. In 1712 steam engine was developed with CI by Thomas New comen. In the late 1770s CI usage began for structural purposes. Since then it has been used for numerous applications which continues even today.

2.1.2 Cast iron family

CI is a generic term used to designate a family of metals with a wide variety of properties **[2]**. The physical properties of CI will greatly influenced by the shape distribution of the free carbon **[3]**. CI is a Fe-C-Si alloy that often contains other alloying elements and is used in the as-cast condition or after heat treatment. The demands for iron casting are based on the nature of CI is an engineering materials and their economic cost advantages. CI offers

a wide range of mechanical properties such as strength, hardness, machinability, wear resistance, abrasion resistance, corrosion resistance etc. Thus, from a commercial point of view the most important cast alloys are CIs. All CIs contain more than 2% carbon and an appreciable amount of silicon (usually 1-3%) **[4]**. The high carbon and silicon content means that they are easily melted, have good fluidity in the liquid state and have excellent pouring properties. The basic types of CI are best differentiated by their microstructures as opposed to their chemical analysis because the various types overlap. There are four main types of CIs, 1) gray, 2) ductile, 3) white and 4) malleable as given in flow chart **(Fig.2.1)**. The microstructures of different CI are shown in **Fig.2.2**. Typical chemical composition of unalloyed CI and applications is given in **Table 2.1**.

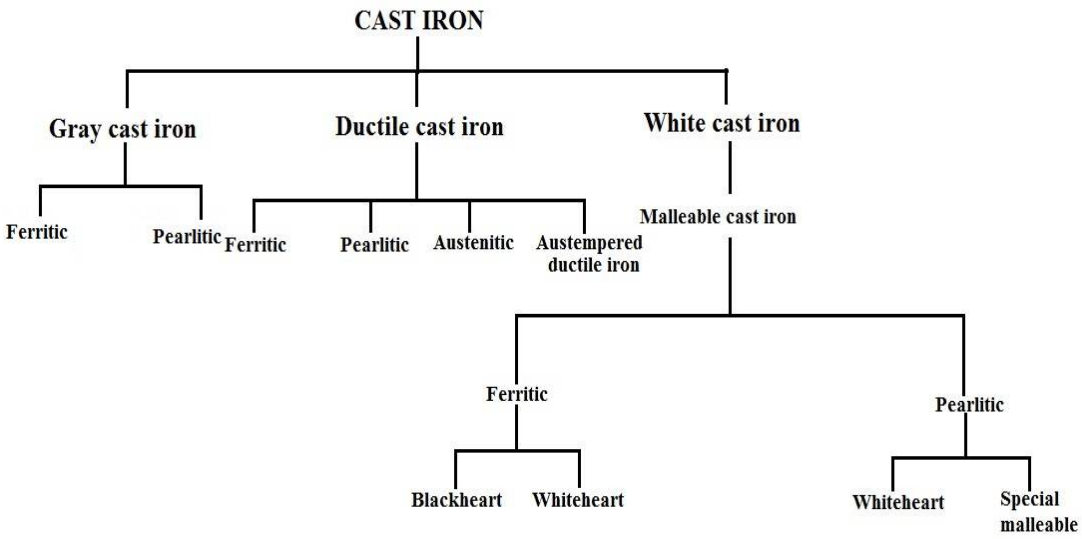

Fig.2.1: Classification of cast iron (CI)

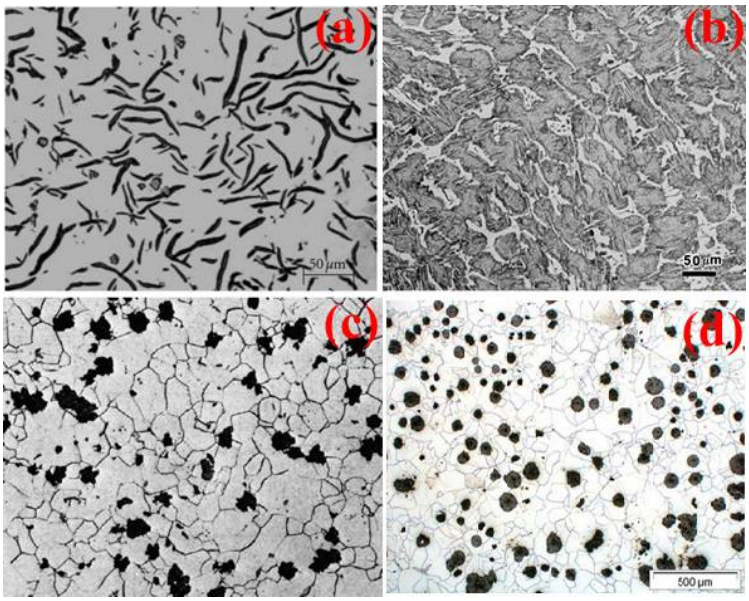

Fig.2.2: Optical microstructure of different cast iron (a) gray cast iron, (b) white cast iron, (c) malleable cast iron, (d) ductile cast iron **[5]**

Table 2.1 Typical chemical composition of unalloyed cast iron (CI) and application **[6]**

Iron	C	Si	Mn	S	P	Application
Gray	2.5-4.0	1.0-3.0	0.4-1.0	0.05-0.025	0.05-1.0	Motor blocks, Piston rings, heavy machine tool
Ductile	3.6-4.2	2.25-2.75	0.35	0.03 max	0.08	Pressure casting, valve and pump bodies, shock resisting parts
White	1.8-3.6	0.5-1.9	0.25-0.80	0.06-0.20	0.06-0.18	General purpose
Malleable	2.7-3.2	0.60-0.80	0.45-0.60	0.15 max	0.15 max	Malleable iron pipe fitting

2.1.3 Metallurgy of CI

The metallurgy of CI is more complex than its economics and in fact, is one of the more complex metallurgical systems. Iron-carbon alloys with less than 2% carbon are metastable; the true stable system being iron-graphite (Fe-C). If an iron alloy exceeds about 2% carbon, the carbon does not have to nucleate from decomposition of austenite, but instead, it can form directly from the melt by a eutectic reaction. Cementite (Fe_3C) can still nucleate at the eutectic more readily than graphite, but on sufficiently slow cooling, graphite itself is able to form and grow **[7]**. The graphite is the thermodynamically stable phase, whereas the Fe_3C is actually a metastable phase. For kinetic reasons it is more difficult for the graphite to form than the Fe_3C **[8]**. To understand the role of Si in cast irons it is useful to examine the binary Fe-C phase diagram shown in **Fig.2.3**. Liquid eutectic iron (4.3%) may

solidify as either austenite + graphite or as austenite + carbide (Fe_3C). The carbides form at 1148°C which is 6°C below the formation of graphite. This temperature difference ($\Delta T_{G\text{-}C}$) increases by addition of Si as shown in **Fig.2.4**.

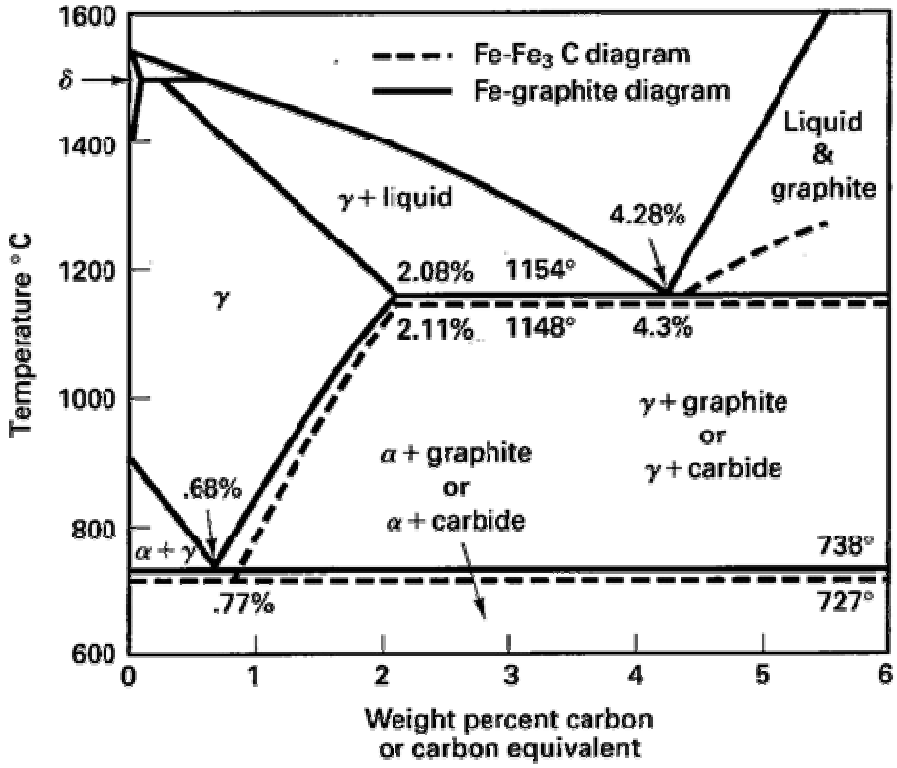

Fig.2.3: Fe-C phase diagram for cast iron **[9]**

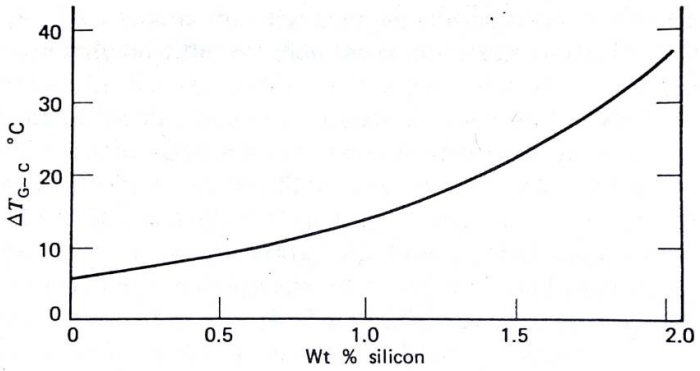

Fig.2.4: Difference of eutectic temperature, $\Delta T_{G\text{-}C}$ as a function of Si content **[8]**

As $\Delta T_{G\text{-}C}$ increases the thermodynamic driving force forming graphite prior to forming Fe_3C increases. Thus probability of forming graphite eutectic rather than a carbide eutectic is increased. The kinetics of CI solidification may be understood from **Fig.2.5**. The crossover

point on **Fig.2.5** gives the rate above which the cementite eutectic forms. It is seen from the dashed curve that by increasing $\Delta T_{G\text{-}C}$ the rate required to form cementite is raised. Hence, Si allows to from graphite at higher rates.

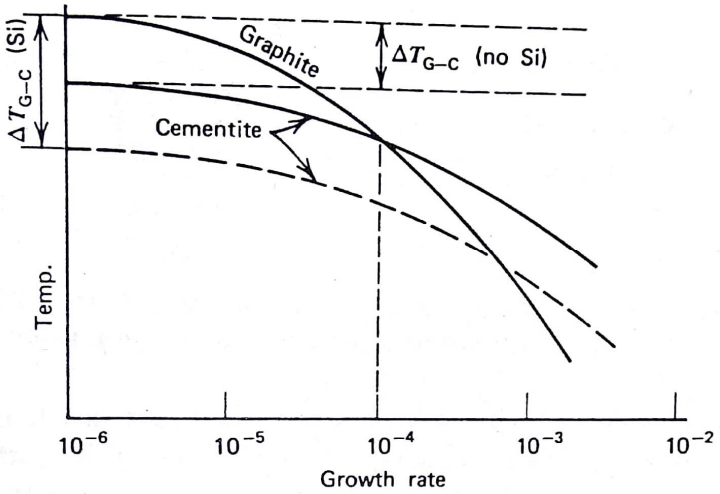

Fig.2.5: Solid, liquid interface temperature as a function growth rate for growth of cementite eutectic and graphite eutectic **[8]**

2.1.4 Theories about graphite nucleation

The nucleation of graphite in CI has been debated over many decades and many theories have been proposed.

2.1.4.1 The graphite theory

According to Boyles **[10]**, graphite grows from already present small sizes crystalline graphite in the melt. Eash **[11]** presented the idea of Si rich regions around the dissolving graphite particles, when the melt is treated with Si based inoculants. The solubility of Carbon (C) is sufficiently low in those regions which can promote the precipitation of graphite, but Feest et al.**[12]** showed that the dissolution time of ferrosilicon in liquid iron was a few second and graphite formed at the interface between dissolving particle and liquid iron. They modified the theory and proposed that these seed crystal will be preserved in the melt provided that Ba or Sr is present in sufficient amounts to prevent the graphite from dissolving back into the melt.

2.1.4.2 The gas bubble theory

Karasy **[13]** presented this theory in 1976. According to him, graphite can only crystallize if it is protected by some boundary such as the gas bubble of CO and the graphite will grow in this bubble. However, it is not possible to grow full graphite into the bubble as carbon cannot diffuse into the solid of grown graphite.

2.1.4.3 The salt-like carbide theory

Lux **[14]** considered both homogeneous and heterogeneous nucleation of graphite. According to him certain elements like Ca, Sr and Ba forms salt like carbides in the liquid which offers a close match of lattice parameters to graphite and reduces the interfacial energy between the nucleus and the substrate to allow for extensive graphite nucleation during solidification.

2.1.4.4 The silicon carbide theory

Following the dissolution of ferrosilicon in liquid CI, Wang and Fredriksson **[15-16]** observed that SiC crystals and graphite particles were formed in the melt close to the dissolving ferrosilicon particles. A theory was developed and calculations were performed to explain the nucleation of graphite and the fading mechanism of these particles. The theory was based on the assumption of the existence of local supersaturation of C and Si in the melt subsequent to the SiC dissolution which provides the necessary driving force for homogeneous nucleation of graphite. The fading effect was explained by the homogenization of C and Si in the melt through convection and diffusion.

2.1.4.5 The oxide/sulfides theory

Non-metallic and metallic inclusions play an important role in precipitating oxides, sulfides and nitride particles. Kusakawa et al **[17]** reported that non-metallic inclusions show the highest inoculation effect. It is believed that oxides, especially silica acts as a nucleus for graphite. The technique of X-ray microanalysis and electron diffraction pattern were used in **[18]** identifying the nucleating particles. Several other researchers have suggested the growth of graphite on sulfides, oxides and nitrides **[19]**.

2.2 Ductile Iron (DI)

Ductile cast iron (DI) was first announced to the foundry industry as a new engineering material at 1948 annual meeting of American foundry society. This revolutionary material, discovered independently by British cast iron research association (BCIRA) and the international nickel company (INCO), is also referred to as nodular spheroidal graphite CI. The BCIRA process consists of an addition of Ce to molten hypereutectic CI of essentially the same analysis of gray iron. Ce removes the sulphur (S) and with about 0.02% residual Ce, produce graphite spheroids instead of flakes **[20]**. The INCO process, on the other hand, similarly employs magnesium additions to either hypo or hypereutectic cast iron.

Essentially DI consists of graphite spheroids dispersed in matrix similar to that of steel. The only significant difference between gray cast iron and DI is the shape of the graphite shape; however the matrix structure is similar **[21-22]**.

DI is an important cast material to the designer which combines the advantages of CI, such as cheapness, ease of machining, low melting temperature, good fluidity, good wear resistance properties, high damping capacity, excellent heat resistance properties and those of steel, such as high strength, ductility, toughness, hot workability and hardenability. The matrix of DI can be controlled by base composition, by foundry practice and or by heat treatment to produce 415 MPa minimum tensile strength, with over 25 percent of elongation, up to 1050 MPa minimum tensile strength yet having 1 to 4 percent elongation **[23-24]**. A summary of the principle types of DI is presented in **Table. 2.2**.

Table 2.2 Principle types of ductile iron and their application **[6]**

Ductile iron grades	Hardness (Brinell)	Characteristics	Application
80-60-03	200-270	Essentially pearlitic matrix, high strength as cast, responds readily to flame or induction hardening	Heavy duty machinery, gears, dies, rolls for wear resistance, and strength
60-45-10	140-200	Essentially ferritic matrix, excellent machinability and good ductility	Pressure castings, valve and pump bodies, shock resisting parts
60-40-15	140-190	Fully ferritic matrix, maximum ductility and low tension temperature (has analysis limitations)	Navy shipboard and other uses requiring shock resistance
100-70-03	240-300	Uniformly fine pearlitic matrix normalized and tempered or alloyed. Excellent combination of strength, wear resistance and ductility	Pinions, gear, crankshaft, cams, guides, track roller
120-90-02	270-350	Matrix of tempered martensite, may be allowed to provide hardenability, maximum strength and wear resistance	Pinions, gear, crankshaft, cams, guides, track roller

2.2.1 Development of graphite solidification

The solidification of spheroidal graphite eutectic in DI starts at temperature above those of the flake graphite eutectic for similar carbon equivalent. In this case the graphite spheroid is enveloped by a shell of austenite so that only one phases, austenite, is in contact with the eutectic liquid. Solidification of this type has been neo-eutectic. Each unit of graphite spheroid and austenite shell may be considered a cell where carbon must diffuse

through the shell of austenite in order to grow spheroid. Thus this process is slower than that of gray iron eutectic solidification and the neoeutectic freezing range is extended to about 49°C. Liquid metal is then present over a wider temperature range and a lower temperature for DI than gray iron.

No nucleation of spheroidal graphite occurs once the growth of the neo-eutetic starts. The number of graphite spheroids is therefore determined at an early stage of solidification. Subsequent cooling of the solidification DI is accompanied by graphite precipitation on the existing spheroids at temperatures down to eutectoid range. As with gray cast iron, the cooling rate through the eutectoid range and/or alloying treatment determines the matrix structure.

The importance of an adequate number of spheroids in obtaining fully spheroidal graphite structures must be stressed. When the number of spheroids is low, there is an inadequate number of site to which the carbon may diffuse. Depending on the composition and processing variables, either graphite or carbide will form from the liquid during further cooling. Both alternative results in properties inferior to fully spheroidal graphite structure.
The number of nodules per unit area i.e. the nodule count, can be between 100/mm^2 and, in extreme cases, 1000/mm^2 and it depends on the section size, cooling rate (moulding materials), inoculation, spheroidizing agents present in casting **[23-24]**.

2.2.2 Role of alloying elements in DI solidification

2.2.2.1 Magnesium (Mg)

A number of elements can be used at least practical spheroidization of graphite in CI, Mg is by far the most effective and economical method. The mechanism by which Mg causes graphite spheroids to occur is unknown; however, the function of Mg addition is well known. First Mg serves as a deoxidizer and desulfurizer of the molten metal. If the oxygen/or sulphur content of the melt is too high, a subsequent amount of Mg will be consumed in the formation of MgO and MgS. However, Mg prevents the nucleation of flake graphite during the solidification process and thereby promotes the growth of graphite spheroids; generally 0.05% residual Mg content is necessary to achieve spheroid formation in most DI.

2.2.2.2 Carbon

The carbon content in commercially DI varies from 3.0-4.0%. Nodule count is directly affected by the carbon content; greater number of spheroids formed at the higher carbon contents. Increasing the carbon content also increases the castability by improving

fluidity and feeding. The carbon content level should be correlated with the carbon equivalent formula **[25]**:

$$CE = \%C + 1/3\%Si \quad \text{..... (2.1)}$$

Carbon equivalent as excess of 4.3% promote the development and growth of graphite spheroid.

2.2.2.3 Silicon

The normal range of Si in DI is 1.80 to 2.8%. Since Si affects the carbon equivalent value, it also affects the number of spheroids and occurrence of flotation. Si increases the amount of ferrite formed during eutectoid transformation and also strengthens the iron by strengthening the ferrite. Addition of Si is more influential graphite control when the addition is made late.

The major effect of Si is to increase the value of temperature difference ΔT_{G-C} as shown in **Fig.2.4**. As ΔT_{G-C} increases the thermodynamic driving force for forming graphite prior to cementite is increased, and hence probability of forming of graphite eutectic rather than a carbide eutectic is increased. Hence, Si is responsible for the formation of graphite for a DI microstructure.

2.2.2.4 Sulfur

The most striking effect of sulpfur in DI is to increase the amount of Mg required to achieve spheroidal graphite. The level of sulfur in the iron prior to Mg treatment is a function of the melting practice used. Sulfur content after treatment is usually 0.015%.

2.2.2.5 Phosphrous

Phosphorus forms very brittle structure known as stedite in DI. Since phosphrous adversely affects toughness and ductility, a maximum of 0.05% is usually specified.

2.2.2.6 Other elements

In addition to the elements C, Si, S, and P discussed above, a number of alloying elements may be present in DI such as Mn, Ni, Mo, and Cu. Alloy of these elements increase the toughness or increase the high temperature corrosion resistance.

2.2.3 Types of ductile iron

The importance of matrix in controlling mechanical properties is emphasized by the use of matrix names to designate the following types of DI **[26-27]**.

2.2.3.1 Ferritic ductile iron

Graphite spheroids in a matrix of ferrite provide an iron with good ductility and impact resistance and with a tensile and yield strength equivalent of low carbon steel. Ferrite

ductile iron can be produced as-cast, but may be given an annealing heat treatment to assure maximum ductility and low temperature toughness **[26-27]**.

2.2.3.2 Pearlitic ductile iron

Graphite spheroids in a matrix of pearlite result in an iron with high strength, good wear resistance, and moderate ductility and impact resistance. Machinability is also superior to steels of comparable physical properties. The preceding three types of DI are the most common and are usually used in the as-cast condition, but DI can also be alloyed/or heat treated to provide the following grades for a wide variety of additional applications **[26-27]**.

2.2.3.3Austenitic ductile iron

DI alloyed to produce an austenitic matrix offers good corrosion and oxidation resistance, and good strength and dimensional stability at elevated temperatures **[26-27]**.

2.3 Austempered ductile iron (ADI)

2.3.1 Introduction

ADI also known as ausferritic ductile iron is the most recent addition in the DI family. It is produced by giving conventional DI by a special heat treatment process called "austempering" **[28]** and converts to ADI, bringing about an excellent combination of strength, toughness, and fatigue characteristics. For the design engineer ADI is a most versatile material, enabling innovative solutions to new and current problems. By selecting precise heat treatment parameters a specific set of properties can be achieved.

2.3.2 Historical background of ADI

ADI was developed with a mixed microstructure of bainitic ferrite with carbon enriched austenite and graphite nodules after austempering heat treatment. The austempering process was first developed by two researchers working of United States Steel Laboratories, Davenport and Bain, in the early 1930's for heat treating steels **[29]**. Much later, the unique ausferrite banite microstructure of CI was discovered in 1937 **[30]**. However, commercialization of austempered cast irons has lagged. Soon after DI was developed, International Harvester and General Motors started to use the austempering process on DI in research studies in the year1960 **[31]**. However, ADI was not produced commercially until the early 1970's. In 1972, the Tecumseh Products announced the first commercial ADI product a compressor crankshaft **[32]**. Since then, more and more companies have started to use ADI. The Finnish company Kymi Kymmene Metal used ADI to replace forged steel for a set of gears in the early 1970's. In late 1970's, General Motors replaced a wide range of steel gears, pinions, and velocity joints in light vehicles with ADI **[32]**. Since 1980's ADI

applications have been continuously increasing in North America. The Cummins Engine started to make ADI timing gears produced to AGMA class 8 standards, in their B and C series diesel engines in 1984 **[32]**, for the market expansion due to cost reduction. The price per unit of mass for DI was typically half that of steel. When the extra cost of austempering process was added, the ADI products are still much more economical than steel **[31]**. Because of the increasing application of ADI in 1980's, specifications for ADI material started to develop.

2.3.3 Standards of ADI

The acceptable standards of ADI was first published in 1990 by ASTM 897M-90 **[33]** which was later revised in 2002. In 2003, SAE J2477 standards of ADI has been approved and published in the same year. The comparison of the ISO, SAE and ASTM standards for ADI are shown in **Table 2.3**. It is to be noted that ISO designations are applicable for sections thickness less than 30mm. The convention used in (**Table 2.3)** is based on tensile strength (MPa), yield strength (MPa) and elongation (%) **[34]**.

Table 2.3 Austempered ductile iron standards (ISO, ASTM and SAE)

ISO/CD 17804	ASTM J2477	ASTM A897/A 897 M
800-500-10	900-650-09	850-550-10
900-600-08	1050-750-07	1050-700-07
1050-700-06	1200-850-04	1200-850-04
1200-850-03	1400-1100-02	1400-1100-01
1400-1100-01	1600-1300-01	1600-1300-00

2.3.4 Application of ADI

In the past twenty years ADI has changed from experimental interest to a competitive engineering material. In the early seventies limited production of ADI was initiated in the United States and Europe and in the late seventies many practical applications were opened in the industrially advanced nations. The production of ADI in Japan is estimated to be about 8000t in 1990 which are seven times that of five years ago. It is estimated that ADI in the world may be produced in excess of 50000t in 1991**[35]**. Now is the period of trial applications to industrial components and ADI will be used in large quantities in the near future.

ADI now have wide application as parts in automotive, construction, mining, military and railroad components worldwide as given in **Table 2.4 [36-37]**.

Table 2. 4 Application of austempered ductile iron (ADI) **[36-37]**

Classification	Parts
Automotive Industry	Crankshafts, camshafts, Timing Gears, Tie rods, Suspension arms, Differential Gears, CV Joints, Break components, ball joint sprockets, Pump components, Engine mounting brackets, gear cases, spindle supports, connecting rods, torque arms, planer carrier, Drive yokes.
Construction and Industry	Truck-rear spring pads, Truck connecting seats, digger teeth, slides, yokes, collars, structural members, sprockets, connectors, truck-plates, track-shoes, End connector, Gears, Crankshafts, Camshafts, Snow shoes, Bulldozer-cases, Chain sprockets, Housings, Concrete mixer car-shaft, Power take of components.
Agriculture	Plow points, Chisels, Tillage, Points, Sickle, Guards, Tie rods, Slip Clutches, Hitches, Pins, Fertilizer, Lift arms, Lift crank, Power take off components
Rail road	Wheel, Suspension parts, Covers, Shoes, Tie bars, Hardware
Military	Ordnance, Armours, Truck components, Other vehicle components.

2.3.5 Effect of alloying elements on ADI

The purpose of addition of alloying elements is to increase the hardenability of DI and also to avoid the formation of pearlite and martensite during the cooling of austempering process. The composition must be compatible with production of the quality of iron and free of iron carbide. The hardenability elements are limited primarily to Mn, Cu, Ni and Mo used alone or in combinations. Other hardenability alloying elements can result in undesirable poor nodularity of graphite nodule or as cast carbides in the iron upon solidification. The alloy additions delay not only the initiation of the austempering reaction but also the embrittling effect of the second reaction, thereby creating a wide process window to get higher mechanical properties. Some works **[38]** reported that, addition of Ni-Mo and Cu-Mo to delay the stage I reaction slightly, but delay the embrittling effect of the stage II reaction much more, thereby creating a wide process window for austempering leading to high toughness. The effect of Ni and Mo to improve the hardenability is shown by TTT diagram (**Fig.2.6)**.

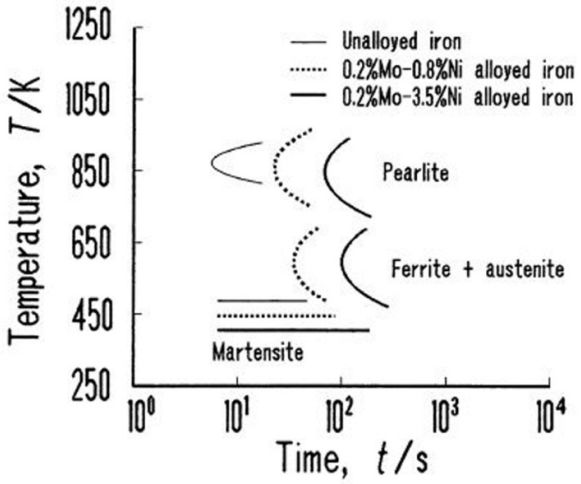

Fig. 2.6: TTT diagram for unalloyed and Mo-Ni alloyed DI irons austenitized at 900°C (1173K) **[39]**

The effect of the alloying elements on ADI in details is discussed given below:

2.3.5.1 Carbon (C)

Carbon acts as a graphitizing element in DI casting. The appropriate amount of carbon will be beneficial to obtain the spheroidal graphite with a number of nodules, a small nodule diameter with good roundness also reduce the carbides and casting defects. Graphite floatation occurs relatively easily when the CE is too high. Too low CE may give rise to porosity and carbides. The general range of carbon content should be between 3.4 and 3.8 wt. % in ADI **[40]**.

2.3.5.2 Silicon (Si)

Silicon is the most important alloying element of ADI and it's effect is mostly observed in diffusion of carbon during the austempering process. In DI, Si acts as a ferrite stabilizing element and its solution in ferrite leads to enhancement of its strength and hardness, but reduce ductility **[41]**. Si is a stronger graphite stabilizing alloying element than Cu and Ni. Increasing the Si content leads to better nodularity and nodule count in DI. Si also retards the formation of carbide and presence of minimum 2% Si content in composition is required to avoid the carbide formation. It is reported **[42]** that Si acts as a great role to avoid the formation of carbide during austempering from 300-370°C. During the austempering process Si segregates at the eutectic cell boundaries and also encourages the Mn segregation in eutectic cell boundaries to delay the austempering reactions **[43]**.

2.3.5.3 Molybdenum (Mo)

Mo is the most powerful alloying elements to increase the austemperability and hardenability in DI. The maximum amount of Mo present in DI is 0.3%. Presence of higher

Mo content during solidification leads to unsuitable structure such as carbide. Mo also acts as graphitizing element and in heavy section DI, Mo increases the amount of graphite nodules and thus improves the mechanical properties. Presence of Mo to narrow the austenite region in Fe-C phase diagram and increases the eutectoid transformation temperature. There are no such considerable effects in austempering temperature but has little effect in process windows with presence of Mo. Elliot et al **[44]** reported that Mo content increase the austemperability without any significant change in austempering kinetics. However, it increases the amount of intercellular carbides formed during solidification and this leads to decrease in elongation and reduction in area. This also leads to decrease in UTS and 0.2% proof stress for each austempering temperature.

2.3.5.4 Manganese (Mn)

Manganese is the second most powerful alloying element after Mo to increase the austemperability and hardenability of DI. Mn is a carbide forming alloying element and segregates into the eutectic cell boundaries during solidification like Mo. Mn is a austenite stabilizer and reduces the eutectoid transformation temperature and increases the amount of high carbon retained austenite during the transformation of bainitic ferrite (up to 0.8% Mn) **[45]**. It also increases the carbon content of parent austenite ($C\gamma$) and decreases the carbon content in high carbon austenite ($C\gamma_H$). However, the driving force for stage I austempering reaction is considerably reduced and it progresses slightly with delays **[46]**.

2.3.5.5 Nickel (Ni)

Ni is the third powerful alloying element of ADI after Mo and Mn. Ni is an austenite stabilizing element and reduces the austenitizing temperature. It segregates at the eutectic cell near the graphite nodules during solidification. It also decreases the probability of carbide formation, makes them thinner and unstable. In case of DI, it increases the amount of pearlite in the structure and makes it thinner **[47]**. Ni also decreases the carbon content in the residual austenite and high carbon retained austenite. It has no considerable effects in process window. It increases the rate of transformation of bainitic ferrite formation and refused higher amount of carbon content through the austenite to increase the amount of retained austenite with presence of maximum amount of Ni content (2%). The effect of Ni on the mechanical properties of ADI shows that increasing Ni content leads to increase of impact energy without any major change in their tensile strength due to increased of high carbon retained austenite in ADI structure **[48]**.

2.3.5.6 Copper (Cu)

Cu is the least expensive alloying element used for increasing the austemperability and hardenability of ADI. It increases the pearlite content in DI structure and shows comparatively stronger effect than others. Presence of pearlite content in base DI to reduce the austenitization speed and shows dangerous effect on low austenitizing temperature. Cu also widens the austenite zone in the Fe-C phase diagram and reduces the austenitization temperature. It segregates on the eutectic cells near the graphite nodules during the solidification (reverse segregation) and offsets the positive segregation of Mn and Mo to some extent like Ni. It also decreases the probability of carbide formation **[49]**. Cu increases the carbon content of the residual austenite ($C\gamma$) and decreases the carbon content of high carbon retained austenite ($C\gamma_{HC}$).

2.3.5.7 Rare Earth Elements

The addition of rare earth elements has significant effects on the properties of DI **[50]**.

(i) Cerium (Ce)

Ce shows significant effects in DI microstructure. The microstructural and mechanical properties of DI depend on the amount of Ce level and the section thickness of the materials **[51]**. In DI, presence of 0.02 % Ce shows higher graphite nodularity with smaller in size than without Ce content. However, increasing Ce from 0.02-0.03% the graphite shape was increased and further increasing from 0.03-0.4% the shape of the graphite nodules was decreased. It has been reported that 0.03% Ce shows more than 10% higher ductility than normal DI and lower strength and hardness in small section castings **[52]**.

(ii) Lanthanum (La)

La also acts as a nodularizing element in DI and shows mixed results. Horie et al **[53]** claimed that nodule count increases and carbides are reduced when the La: S ratio is between 2.5 and 6.0. However, Stefanescu et al. **[54]** found that nodule count steadily decreases as the lanthanum content in Mg-Fe-Si increases.

The typical chemical composition of the ADI is given in **Table 2.5 [33]**.

Table 2.5 Typical chemical composition of the ADI

Element	C	Si	Mn	Cu	Ni	Mo	Al	S	P	Ce
wt.%	3-4	2.4-2.8	0.3	0.8	2	0.2	0.6	0.015	0.035	0.03

2.3.6 Heat treatment for ADI

ADI is produced with the help of isothermal heat treatment process knows an austempering. The complete heat treatment process consists of two main stages, such as austenitization and austempering. The schematic diagram of the typical isothermal treatment cycle is given in **Fig.2.7**.

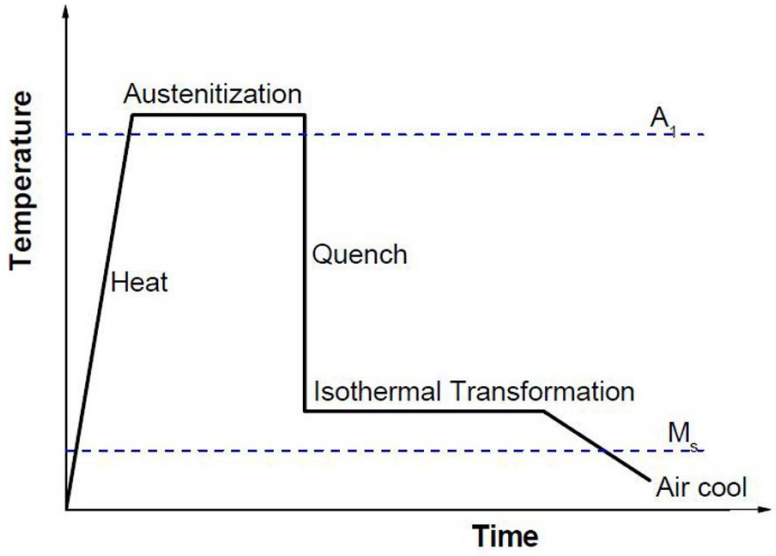

Fig.2.7: Typical isothermal heat treatment cycle **[55]**

2.3.6.1 Austenitization process

Austenitization is the first step of isothermal heat treatment process. During this process as-cast DI is usually heated between 850-900°C for about 30 minutes to 2.5 h holding time **[55]**. The austenitization temperatures and holding time is an important factor to control the microstructure and mechanical properties of ADI. The optimum temperature and holding time of austenitization depends on the chemical composition, graphite nodularity, nodule size and the section thickness of the cast DI **[56]**. During austenitization, the austenitization temperature controls the total carbon content of the austenite, which affects the structure and properties of the ADI. The temperature should be selected to ensure that sufficient amount of carbon was transferred from the graphite nodules to the matrix structures. Furthermore, all the ferrite and pearlite needs to be dissolved as well as the alloying elements to segregate even out the matrix **[57]**. However, at higher austenitization temperature, the diffusion rate of carbon is very fast, as a result the concentration of impurity elements at the austenite grain boundaries is lower leading to a reduction of segregations, but the austenite grain becomes larger in size leading to a coarser bainitic ferrite structure. The solution of carbon is both time

and temperature dependent, thus at higher austenitization temperatures it is necessary to shorten the time to attain uniform carbon content in the matrix structure **[58]**. However, increasing the austenitization temperature, the amount of retained austenite and its carbon content will increase which is favourable for the higher toughness and fatigue strength. On the other hand, at a lower austenitizaton temperature an incomplete transformation is being taken place and as a result the mechanical properties have been affected by the presence of cell boundary cemnetite/carbide **[57]**. Therefore, it is necessary to select a high enough austenitization temperature to obtain a homogeneous bainitic ferrite and retained austenite based structure, to minimize the presence of impurities in the grain boundary in order to improve the mechanical properties.

2.3.6.2 Quenching

Quenching is to be done interface between the austenitization and austempering process. During quenching, the cooling rate is controlled to avoid the formation of pearlite around the graphite nodules, which reduce the mechanical properties. Generally the time of quenched must be controlled within few seconds and the temperature must be above the martensite start temperature (Ms) **[59]**. Addition of Mn and Mo are often made to reduce the rate of pearlite formation during the cooling process and allow in largecasting sections of DI to be produced without pearlite formation. The degree to which, the formation of pearlite can be avoid during quenching is known as austemperability of cast iron. The shift of the pearlite nose due to the addition of Mo, and the effect of slow cooling rate is shown in schematic TTT diagram (**Fig.2.8)**.

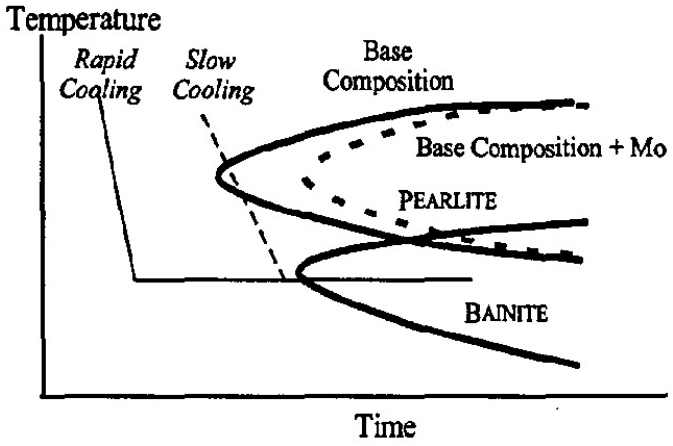

Fig.2.8: TTT diagram of the ADI from austenitization to austempering

2.3.6.3 Austempering process

During austempering process, the bainitic ferrite and retained austenite transformation occur isothermally which determine the final microstructure of the ADI. The austempering temperature and time must be controlled to obtain the desired microstructure to achieve the optimum mechanical properties. Generally the austempering temperature varies from 250 to 450℃ for 5 min to 4 h holding time **[60]**. During austempering process, a two-stage transformation reactions occurr **[60]**. In the first stage austenite (γ) decomposes into ferrite (α) and high carbon content or untransformed austenite (γ_{HC})

$$\text{Stage I:} \quad \gamma \rightarrow \alpha + \gamma_{HC}$$

However, in the second stage the high carbon austenite (γ_{HC}) decomposes into ferrite (α) and carbide (ε carbide) **[61]**.

$$\text{Stage II:} \quad \gamma_{HC} \rightarrow \alpha + \varepsilon \text{ (carbide)}$$

In order to obtain the optimum mechanical properties of ADI the process must be carried out upto the stage I reaction but before the stage II reaction. The time periods between the complication of stage I and onset between the stage II reaction is called the "process window" **(Fig.2.9)**. The process window could be enlarged by the addition of alloying elements, and casting thickness **[62]**. Presence of alloying elements such as Ni, Mn, Mo and Cu enlarge the process windows. At larger process windows high amount of C is diffused from the ferrite into surrounding austenite and attributes more carbon enriched retained austenite. The graphite nodularity can play a decisive part in the austempering heat treatment process **[63]**. Austempered with lower graphite nodules content forms less stable retained austenite than higher graphite nodules. The graphite nodularity has a significant effect on the stage I for both higher and lower austempering temperatures. Decreasing the graphite nodularity delays the end of stage I reaction and accelerates the start of the stage II reaction, thus narrowing the process window **[52]**.

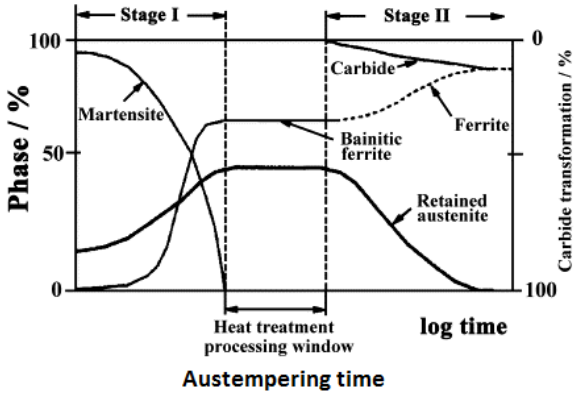

Fig.2. 9: Typical heat treatment processing window **[64]**

The effect of austempering temperature can be optimized within the confines of this window; to short an austempering time leads to an inadequate enrichment of the austenite and hence consists of lower carbon-enriched stabilized austenite content. However, austempering process beyond the commencement of stage II reaction causes carbide precipitation again to reduce the carbon-enriched stabilized austenite content **[65-66]**.

Appropiate austempering process produces a unique bainitic ferrite structure consisting of high carbon enriched retained austenite (γ_{HC}) and graphite nodules dispressed on it. This unique microstructure provides the excellent combination of mechanical and physical properties **[67-70]**.

2.3.7 Mechanism of bainitic ferrite transformation

Bainitic ferrite is diffusionless process and the transformation occurs at temperature below T_0, when the free energy of bainitic ferrite becomes less than austenite at the same composition. A locus of T_0 temperature of the function of the carbon content is called the T_0 curve **[71]** which is plotted on the Fe-C phase diagram shown in **Fig.2.10**. Growth without diffusion can only occur if the carbon concentration of the austenite lies to the left of the T_0 curve.

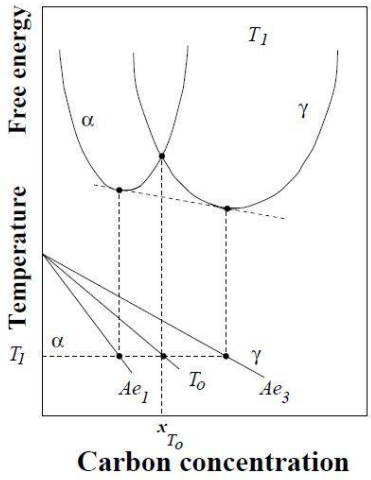

Fig.2.10: Schematic illustration of the origin of the T_0 curve on the phase diagram **[71]**

If the bainitic ferrite plate forms without diffusion, but any excess carbon is soon afterwards rejected into residual austenite. The next plate of bainitic ferrite then has to grow from carbon enriched austenite **(Fig.2.11a)**. This process must cease when the austenite carbon concentration reaches T_0 curve. The reaction is said to be incomplete reaction **[71-72]** since the austenite has not achieved its equilibrium composition (given by Ae_3 curve) at the point

the reaction stops. If on the other hand, the ferrite grows with equilibrium carbon concentration then the transformation should cease when the austenite carbon concentration reaches Ae_3 curve.

In the case of steels, it is found experimentally that the transformation to bainite does indeed stop at the T_0 boundary (**Fig.2.11b**). The balance of the evidence is that the growth of bainitic ferrite below the *Bs* temperature involves the successive nucleation and martensitic growth of sub-unit, followed in upper bainite by diffusion of carbon into the surrounding austenite (**Fig.2.12)**. The effect of austempering can be optimized within the confines of this process window to short the austempering time leads to an inadequate enrichment of the austenite and hence a low retained austenite content. Austempering beyond the component of stage II causes carbide precipitation and hence a reduction in the retained austenite content.

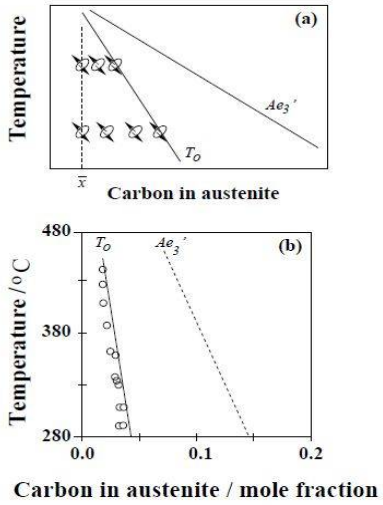

Fig.2.11: (a) Illustrated showing the incomplete phenomenon, (b) experimental data shows the growth of bainitic ferrite complete when austenitic carbon content reaches T_0 curve **[71]**

It is known that the extent of transformation to bainitic ferrite in DIs, as in steel, decresses ultimately to zero when increasing the isothermal transformation temperature towards the bainite start temperature **[73]**. This is because the austenite can only transform to banite if its carbon concentration is less than a value x_{T0} given by the T_0 curve. It follows that the distribution of carbon at the point where the bainite reaction stops is given ideally by

$$\bar{x} = V_{ab}x_{ab} + V\gamma x_{T0} \quad \text{..... (2.2)}$$

Where $\bar{x}$ is the average carbon concentration of the austenite prior transformation, V_{ab} and $V\gamma$ are the volume fraction of bainitic ferrite and residual austenite respectively, at the point where the reaction stops. x_{ab} is the carbon concentration of bainitic ferrite.

Given that in silicon-rich alloy, such as DI consider here, $V\gamma$ = 1- V_{ab}

The maximum fraction of bainitic ferrite is given approximately by

$$V_{ab}^{max} = (xTo - x^{-})/(xTo - xab) \ldots\ldots\ldots\ldots \textbf{(2.3)}$$

Since x_{T0} is the carbon concentration of the residual austenite, its value can be used to calculate the martesite start temperature (M_s) of that austenite. If M_s falls below room temperature, the austenite is retained completely. The maximum volume fraction of retained austenite V_{γ}^{max} will then equal 1- V_{ab}^{max} which is calculated using equation **2.3**.

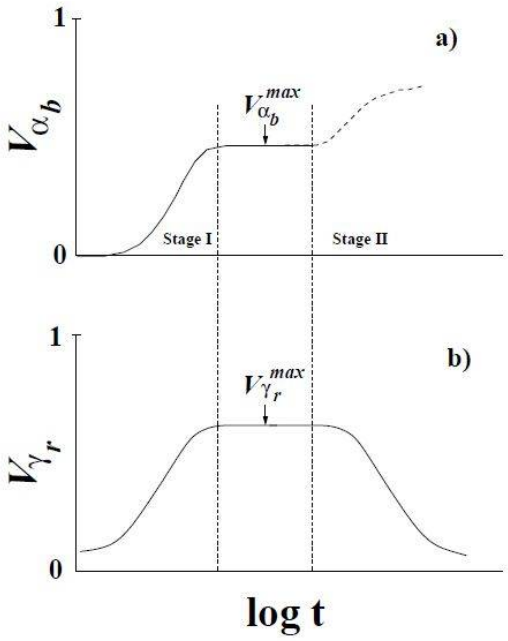

Fig.2.12: Schematic representation of (a) bainitic ferrite and (b) retained austenite, as a function of time. V_{ab} and $V\gamma_r$ represent the volume fractions of bainitic ferrite and retained austenite, respectively

The concentration of carbon in the austenite may not be limited exactly by the T_0 line when the distribution of carbon in the austenite is not uniform as shown in **Fig. 2.13** [**74]**. Studies specific to cast iron using X-ray diffraction, by Niesawaah and Hijhof **[75-76]** have shown that the average carbon concentration in the retained austenite tends to be slightly higher than indicated by the T_0 curve.

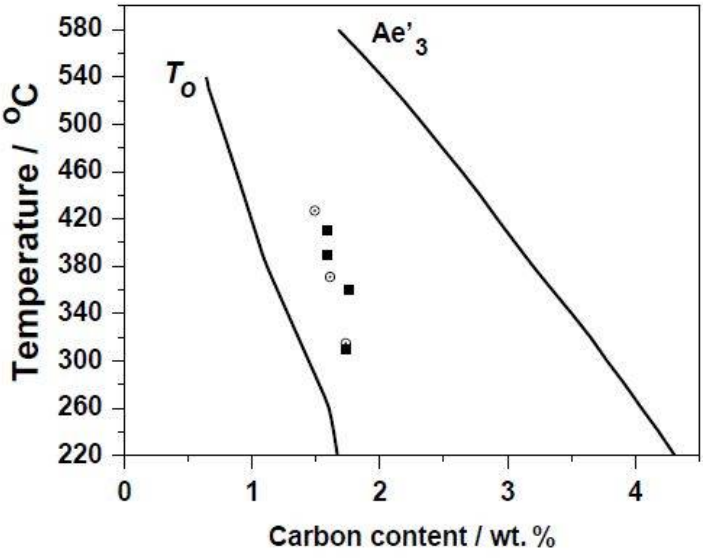

Fig.2.13: The calculated T_0 and para equilibrium Ae'^3 curves for Fe–3.5C–2.5Si–0.55Mn–0.15Mo–0.31Cu (wt. %) **[74]**

2.3.8 ADI Microstructure

The Austempered microstructure that optimises the ductility and toughness consists of bainitic ferrite and high carbon retained austenite with graphite nodules. Other constituents include martensite, carbide and pearlite, all of which tend to reduce ductility. It is difficult to avoid these constituents completely during processing since the composition of the component is rarely uniform to the structure.

2.3.8.1 Upper bainitic ferrite

Upper bainitic ferrite **(Fig. 2.14)** consists of fine ferrite plates, each of which is about 0.2 μm thick and about 10 μm long **[77]**. The plates grow in clusters called sheaves. Within each sheaf the plates are parallel and of identical crystallographic orientation, each with a well-defined crystallographic habit. The individual plates in a sheaf are often called sub-units of bainitic ferrite. They are separated by low misorientation boundaries or cementite particles in the context of conventional steels **[77]**. Cementite is not found in austempered ductile iron, or in high-silicon steels. It is replaced by films of carbon-enriched austenite with or without some metastable carbide such as ε or Hagg depending on the chemical compositions **[77-78]**.

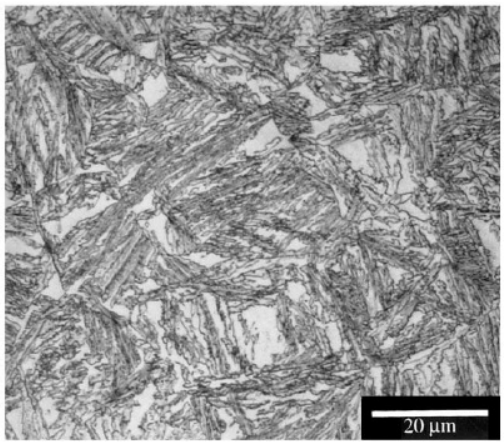

Fig.2.14: Upper bainitic ferrite **[56]**

2.3.8.2 Lower bainitic ferrite

Lower bainitic ferrite **(Fig.2.15)** is the predominant morphology in cast irons transformed below 330°C **[79]**. It has a microstructure and crystallographic feature which are similar to those of upper bainite. The major distinction is that the transformation is at lower temperature so that carbides can also precipitate inside the plates of ferrite. There are, therefore, two kinds of carbide: those which may grow from the carbon-enriched austenite, and others which precipitate inside the supersaturated bainitic ferrite **(Fig. 2.16)**. In conventional steels these carbides are cementite but in high silicon steels and in ADI they could be ε or other transition carbides. The formation of this microstructure is substantially independent austempering time and composition.

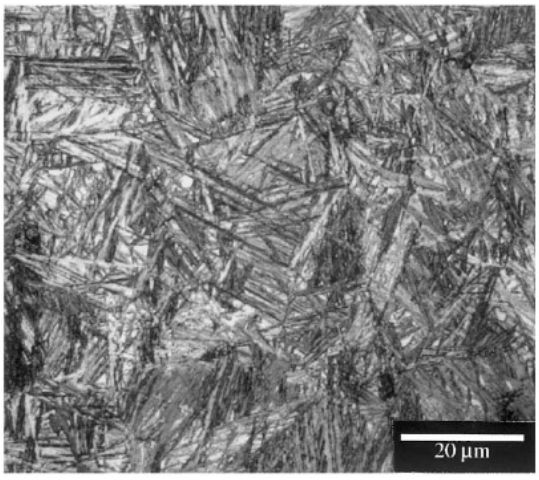

Fig.2.15: Lowe bainitic ferrite **[56]**

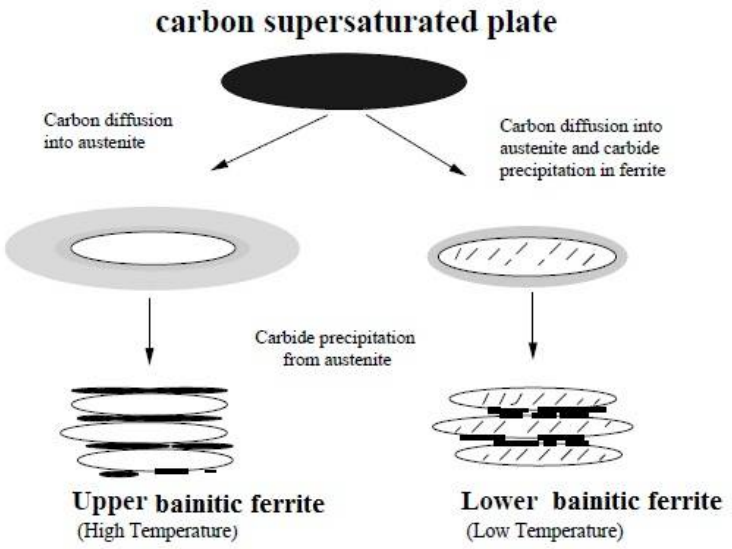

Fig.2.16: Transformation of bainitic ferrite **[79]**

2.3.8.3 Retained Austenite

In ADI austenite forms during the austenitization process above the A_1 temperature. and C content of the austenite changed markedly and determined by the factors such as- (i) The austenitising temperature which determines the equilibrium carbon content in austenite **[80]**, (ii) The substitutional element concentration that also affects the equilibrium carbon content of austenite **[81]**, and (iii) The austenitizing time to determine how close the austenite gets to equilibrium **[82]**.

At the start of austempering process, during quenching the austenite does not transform and hence is metastable and supersaturated with respect to carbon. During transformation of bainitic ferrite carbon is rejected from the austenite and some of the carbon may be transformed to carbide and remainder partitions to the remaining austenite. The remaining austenite is called the untransformed austenite or retained austenite **[83]**.

2.3.9 Mechanical properties of ADI

ADI is a family of DI and its mechanical properties could be varied over a wide range by varying the isothermal heat treatment cycle.

2.3.9.1 Tensile properties

Fig.2.17 illustrates the relationship between austempering temperatures with tensile properties of the ADI **[84]**. With increasing austempering temperature both UTS and YS monotaniously decreases, but ductility is progressively increases. However, at about 350°C

decrease in strength and increase in ductility become more appreciable. In fact, the ADI grades are classified based on the tensile properties. Lower grade of ADI shows lower tensile strength (UTS 850 MPa) and higher elongation (10%), whereas higher grade shows higher tensile (1400 MPa) strength and poor elongation (1%). The tensile strength of ADI varies with varying the alloying elements present and graphite nodularity. The strength of alloyed ADI shows lower value than unalloyed ADI due to the segregation of alloying elements. With decreasing the size of the nodules, both tensile strength and elongation show higher value (**Fig.2.18**) **[85]**. **Fig.2.19** shows typical tensile vs. elongation curve for various alloys highlighting the mechanical properties and product advantage of ADI, replacing forge or wrought steel **[86]**.

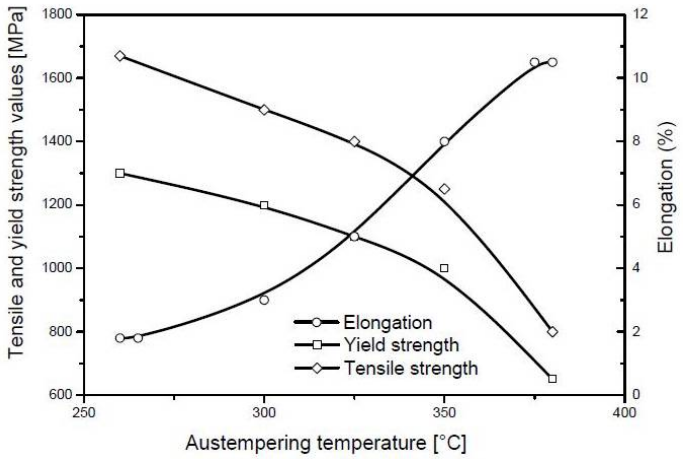

Fig.2.17: Austempering temperature vs. mechanical properties **[84]**

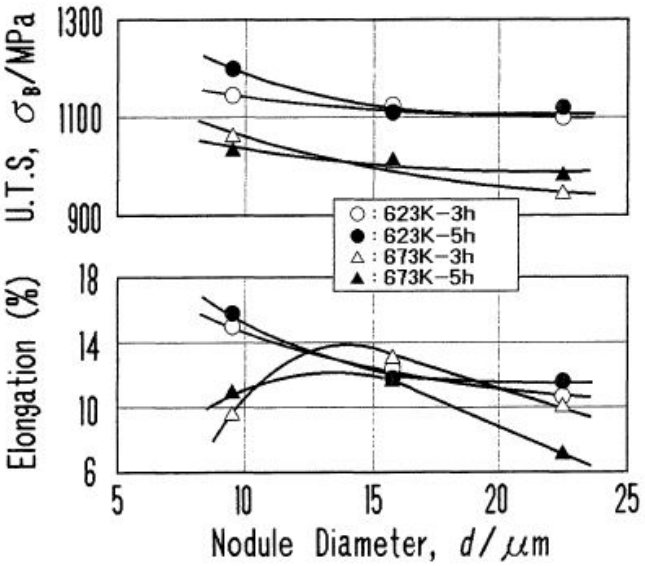

Fig.2.18: Effect of nodule size on tensile properties of ADI **[85]**

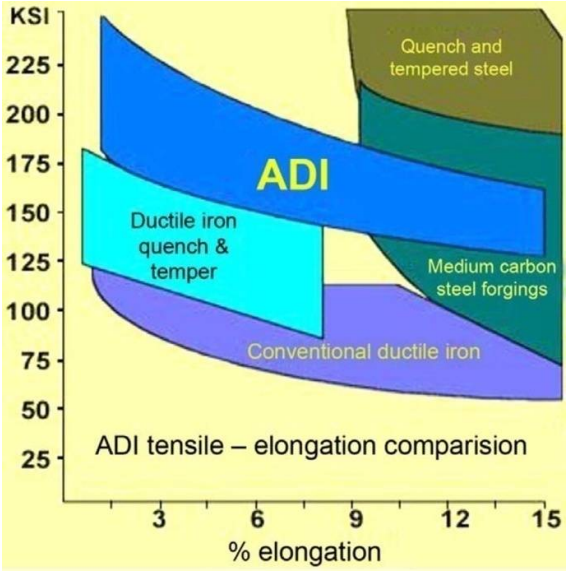

Fig.2.19: Typical tensile vs. elongation curves for various alloys **[86]**

2.3.9.2 Fracture toughness

Fracture toughness, which is an intrinsic resistance of the material to crack propagation, has become an essential part of material properties used by designers to select materials for critical applications. Fracture toughness of ADI is influenced by its microstructure. It has been reported **[87-88]**, that ADI with feathery shape bainitic ferrite along with higher amount of retained austenite shows generally better fracture toughness than that with needle shaped bainitic ferrite based microstructure. The fracture toughness also varies with the austempering temperature. It is found that the fracture toughness initially increases with increasing temperature, reaches a maximum at an intermediate temperature of around 350°C, and then decreases with further increasing austempering temperature. The fracture toughness depends on the bainitic ferrite grain size and the amount of retained austenite **[88]**. Ferrite has the maximum fracture toughnessat the lower austempering temperature because it has the finest grain size. However, with increasing austempering temperature the contribution to fracture toughness from retained austenite increases.

2.3.9.3 Fatigue properties

ADI shows higher fatigue properties as like as forge steel. Its fatigue strength is typically 50% higher than that of standard DI **[89]** and it will be further increased by surface treatment. When subjected to surface treatments such as rolling, peening or machining after heat treatment, the fatigue strength of ADI is increased significantly **[90]** and it will be further increased by surface treatment. The fatigue strength depends on the austempering temperature and varies with changing the temperatures. The amount of retained austenite, the

carbon content of the retained austenite and the coarseness of the bainitic ferrite structure influence the fatigue limit of ADI **[91]**.

The nodularity, nodule size, bainitic ferrite shape and size, volume fraction of retained austenite and its carbon content strongly affect the fatigue limit of ADI **[92]**. These microstructures act to arrest or decrease the short crack propagation rate. Larger shape of the bainitic ferrite or packet boundary and prior grain boundaries arrest short fatigue crack nuclei in ADI. Decreasing the prior austenite grain size via lower austenitization temperature to decrease the subcritical nucleus size, while increasing the carbon-enriched stabilized austenite volume fraction and carbon content increase the barrier strength of dislocation. It is reported that ADI with austempered at higher temperature shows more fatigue crack growth resistance as a result of the toughness from its bainitic ferrite microstructure and large amount of carbon-enriched stabilized austenite, as compared to that austempered at low ausferritic austempering temperature **[93]**. Larger volume fraction of carbon-enriched stabilized retained austenite at higher austempering temperature produces more beneficial effects of its martensitic transformation ahead of the crack tip to retard the crack growth.

2.4 Welding of DI

2.4.1 Introduction

CI is not easy to weld the most common problem being cracking; but a through understanding of the metallurgy involved will assist in prescribing a suitable procedure. The starting point for developing a weld procedure must therefore be an understanding of the type of iron being considered, how it was produced and how it will respond to the thermal effects of welding. The weldability of the DI depends on several factors, namely the chemical composition of parent materials and filler metals used, mechanical properties, type of microstructure, adopted welding process and working conditions **[94]**. Since DI is used primarily for castings, welding of DI is somewhat uncommon due to their well-known poor weldability **[95]**. But there are an occasion when welding is necessary. For example, it is quite common to repair cracks in castings/damaged in service by welding; or in joining several small casings to make a large component that could not, perhaps, have been cast as a single piece **[96]**.

2.4.2 Basic considerations in DI welding

2.4.2.1 Formation of different zones

During welding of DI different zones such as fusion zone (FZ), partial melted zone (PMZ), heat affected zone (HAZ) are formed having different microstructures as shown in **Fig 2.20**. Presence of high carbon content in DI facilitates to form hard brittle phases, namely martensite and carbides in the FZ, the PMZ and the HAZ. Both carbide and martensite, being hard and brittle, are detrimental to the ductility, toughness and machinability of the weld and also may cause cracking in the joint **[97]**.

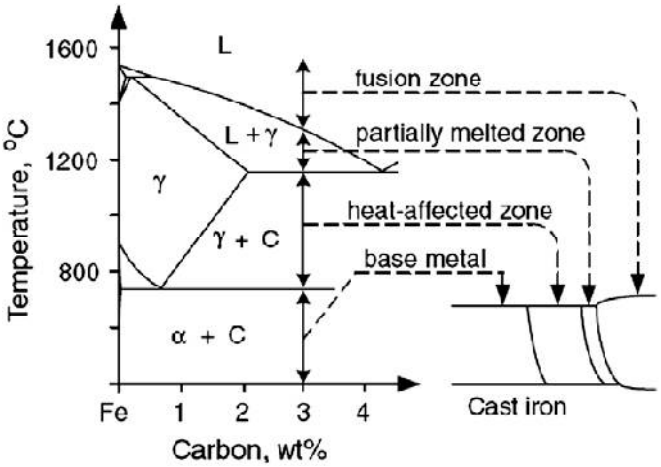

Fig. 2.20: Temperatures experienced by various microstructural zones in a cast iron weld **[98]**

Fusion Zone (FZ): In fusion zone (FZ), the base metal (DI) is melted with the filler metal/electrodes during welding. In FZ the cooling rate is very high compared to all others zone to form very hard, brittle ledeburitic carbides in as-welded condition. This reduces the impact properties of the weldments. Also, inability of FZ to yield and relieve welding stresses can result in cracking in the adjacent HAZ of the DI.

PartiallyMelted Zone (PMZ): This is the zone immediately outside the FZ where liquation can occur during welding. In this zone the base metal near the primary graphite nodules melted during the weld pass, while the remainder of the matrix transformed to austenite.

Heat Affected Zone (HAZ): This is the part of the base metal that reaches a temperature high enough to effect metallurgical changes, but not high enough to cause any melting. In this zone, the graphite is not altered sufficiently to cause carbide problems. The matrix however, is transformed to a hard, martensitic structure upon rapid cooling. Brittleness associated with the martensite can be reduced by slow cooling or PWHT. In DI the widths of the HAZ is

affected by the original microstructure of the base metal as well the welding heat input and preheat temperature.

2.4.2.2 Preheat

Preheat is required in DI before welding due to the following advantage such as:

(a) To prevent the crack.
(b) To reduce the residual stress and distortion.
(c) To minimize the HAZ and reduced the hardness.
(d) To improve the fusion of weld metal to the groove face for obtaining the complete fusion.
(e) To reduce the temperature gradient during welding.

The preheat temperature of DI depends on the hardenability of the iron, chemical composition or carbon equivalent, the size and complexity of the weld and the type of filler materials **[95]**. The preheating must be sustained for a time sufficient to avoid the formation of martensite and to prevent secondary graphite from developing in the matrix upon annealing or multi-pass welding process **[99]**. Higher preheat temperature of about 435°C is required to reduce solidification cooling rate to a level such that iron carbide does not form in PMZ. However, such high preheat temperature can cause undesirable distortion of work pieces. Ebrahimnia et al. **[100]** achieved good results in terms of avoiding crack formation by performing a local pre-heat treatment with a temperature of 300°C before welding large forming dies (found in presses for the production of vehicle body panels), as well as varying PWHT from 300 -500°C with different cooling rates. El-Banna **[95]** performed DI welding using four different preheating temperatures (25°C, 200°C, 300°C and 400°C) and concluded that the best range of preheating temperatures for these types of irons is between 200°C and 300°C.

2.4.2.3 Electrodes for DI welding

For welding conventional DI, commercially available coated electrodes include ENi-CI, pure nickel (90-97%) **[95]**, stainless steel (Fe-Cr-Ni) and ENi Fe-CI **[101]** etc. The details compositions of the available electrodes are given in **Table 2. 4**. Nickel and nickel alloys are widely used for welding cast irons and offer many advantages. Nickel in solid state does not have a high solubility for carbon. When nickel is diluted with cast iron during welding carbon is rejected on solidification and forms graphite. The nickel matrix remains ductile. The process of graphite formation is accompanied by volumetric expansion which counter balances the shrinkage due to cooling. Various performances of these electrodes have been reported by previous investigators. For example, while welding of pearlitic DI, Fe-Cr-Ni

alloy filler metals appeared to be poorly suited because of a strong tendency towards fusion zone cracking **[101]**. Also between nickel and nickel-iron filler materials, authors **[94]** have expressed that the latter one have a smaller coefficient of expansion, good machinability and lower cost in comparison to the earlier one. In another study, the authors **[95]** concluded that nickel-copper deposits also had limited use for welding pearlitic DI because of the hot-cracking sensitivity. It is to be mentioned that steel filler wire such as E7018 and cast iron filler wire are sometimes used. For example, steel electrodes are normally recommended for repairs in non-structural applications where subsequent machining is not required. But due to different contraction coefficients, mild steel shrinks more than cast iron during the solidification process, generating residual stress in the weld interface **[94]**. CI as filler may use in some cases due to lower melting point and no dilution effect. But filler must make up the loss of carbon and silicon. Experiments carried out by Pascual et al. **[102]** reported that the use of cast-iron as a filler metal gave rise to the worse mechanical properties when welding DI using SMAW or OAW technologies, while Ni-Fe and Ni alloys led to the best results in terms of mechanical properties as well as ensuring good toughnes values **[102]**. It is to be mentioned here that cast iron electrodes are included in AWS a5.15-90 **[103]** specification for welding electrodes and rods for cast iron.

However, the inherent drawback of these commercially available coated electrodes used for DI is that they do not respond austempering heat treatment to form ADI from DI weld due to poor austemperability.

Table 2. 6 Chemical composition of the electrodes available for DI welding **[103]**

AWS Classification	C	Mn	Si	S	Fe	Ni	Cu	Al	Others
ENi-Cl	2.0	2.5	4.0	0.03	8.0	85 min	2.5	1.0	1.0
ENi-Cl-A	2.0	2.5	4.0	0.03	8.0	85 min	2.5	1.0-3.0	1.0
ENiFe-Cl	2.0	2.5	4.0	0.03	Rem.	45-60	2.5	1.0	1.0
ENiFe-Cl-A	2.0	2.5	4.0	0.03	Rem.	45-60	2.5	1.0-3.0	1.0
ENiFeMn-Cl	2.0	10-14	1.0	0.03	Rem.	35-45	2.5	1.0	1.0
ENiCu-A	0.35-0.55	2.3	0.75	0.025	3.0-6.0	50-60	35-45		1.0
ENiCu-A	0.35-0.55	2.3	0.75	0.025	3.0-6.0	60-70	25-35		1.0

2.4.2.4 Post weld heat treatment (PHWT)

After welding, post weld heat treatment may be necessary for the following advantages:

(a) To improve the ductility of the HAZ of the weld.

(b) To decompose the formation of carbide during welding.

(c) To relive the residual stress.

(d) To improve the machinability of the weld and HAZ.

The PWHT of the DI depends on the section size of the casting, the chemical composition of the DI base iron and electrodes. Generally the PWHT varies from 300 - 500°C with different cooling rates.

2.4.3 Welding Processes for DI

Several arc welding processes have been successfully used to join DI, such as Shielded Metal Arc Welding (SMAW), Flux Cored Arc Welding (FCAW), Gas Metal Arc Welding (GMAW), Gas Tungsten Arc Welding (GTAW) and Laser Welding (LW) **[94, 104]**, as well as Oxyacetylene Welding (OAW).

SMAW is one of the most utilized methods for welding DI **[105]** and is an ideal candidate for this application, mainly for allowing easier maneuverability and access of welding electrodes (essential factor for performing repairs). It is also one of the most common and economical methods of welding in the industry. Furthermore, highly productive or automated welding processes such as **GMAW** and **FCAW** are not advantageous to perform arbitrary and interrupted tasks such as repairs. Other method such as **GTAW** has higher heat intensity during welding, which is highly detrimental to cast irons for promoting the appearance of brittle microstructures such as martensite and carbide.

2.4.4 Literature review on DI welding

Pascual et al. **[102]** studied welding nodular cast iron with oxyacetylene (OAW) and shielded metal arc welding (SMAW) using 98.2% Ni and Fe-Cr-Ni alloy filler materials respectively. They concluded that welding DI with or without preheat was possible but preheating almost always increased weld quality and ductility. OAW resulted very poor weld metal properties; whereas SMAW yielded reasonable amount of ductility in the weld metal. Actually Ni increased the ductility and hindered the carbide formation.

El-Banna **[95]** studied welding DI in as-cast and fully ferritized states using SMAW process with ENiFe-CI filler material. He worked on different preheating temperatures and concluded that DI can successfully be welded with or without preheating using Ni based electrodes. But in order to achieve certain mechanical properties a preheating temperature of 200-300°C is required. In as-welded specimens ledeburitic carbide structures and local melting around the graphite nodules are observed. With application of preheating various pearlite and martensite ratios instead of carbide were formed.

Kelly et al. **[106]** studied the weldability of DI using four different process of welding, namely GMAW, GTAW, SMAW and SAW using Ni- Fe-Mn as filler metal, and without preheat. The Ni-Fe-Mn filler metal system was reported to be capable of welding DI without preheat or postheat and retaining 100% of the base metal tensile properties in spite of

formation of iron carbide, secondary graphite, and/or martensite in the HAZ. It was concluded that HAZ microstructure alone could not be used to predict weldment performance.

Voigt et al. **[107]** studied general HAZ structures of DI welded by SMAW process with ENi-CI filler material using 300°C of preheating. In as -weld DI, formation of carbides surrounding the graphite nodules and in intercellular regions between nodules in PMZ and martensite in HAZ could not be overcome in spite of preheating temperature for sufficient times after welding. However, after subcritical annealing martensite was decomposed to ferrite and secondary graphite.

2. 5 Coated electrode

2.5.1 Historical background

In 1907, Kjellberg from Sweden proposed the idea of using heavy flux coating to prevent atmospheric contamination. In his first patent, he stated that as the electrode was consumed a crater like cavity was formed at the electrode tip which served to guide the molten metal across the arc from the electrode. The coating decomposition acted as a shielding against air contamination **[108-109]**. Despite significant advances, covering developed during that period aimed more to stabilize the arc than to protect or refine the weld metal. In 1930's several slag system were explored ($FeO - SiO_2$, $CaO - SiO_2$, $FeO - SiO_2 - MnO$) **[110]** in both steel refining and welding. A dramatic incident during World War II revealed the capabilities of arc welding **[108]**. The development of low hydrogen electrodes were characterized in 1940's **[111]**. Calcium carbonate became increasingly used in flux coatings to produce basic slags and to yield shielding gas. Low hydrogen electrodes with iron powder additions to coatings were successfully designed and commercialized in both titania and lime type coatings. Compared with conventional low hydrogen type, the E7018 type electrodes (with approximately 30% iron) exhibited excellent welding characteristics. The post World War II period was marked by the commercial introduction of the basic low hydrogen and iron – powder cover electrode to the American market.

Advances in material as well as new materials demand suitable electrodes/filler materials for various applications of welded joints. Scientific research leading to an understanding of the fundamental behavior of welding consumables is still in progress.

2.5.2 Function of coating

The coating of the electrode has to fulfill the following functions:

- To increase the arc stability with the help of low ionization potential elements like Na, K
- To provide protective shielding gas environment to the arc zone and weld pool with the help of suitable gases generated by thermal decomposition of constituents present in coatings such as hydrocarbon, cellulose, charcoal, cotton, starch, wood flour etc.
- To remove impurities from the weld pool by forming slag as constituents present in coatings such as titania, feldspar, china-clay react with impurities and oxides in present weld pool (slag being lighter than weld metal floats over the surface of weld pool which is removed after solidification of weld)
- For alloying of the weld metal (to achieve specific properties) which can be done by incorporating required alloying elements in electrode coatings and during welding these get transferred from coating to the weld pool.
- To deoxidize weld metal. For this purpose, deoxidizers like Ferro-Mn, Ferro- silicates etc. are frequently added in the coating material.
- To maintain required viscosity of the molten metal so as to reduce tendency of falling down of molten weld metal in horizontal, overhead and vertical welding as well as to facilitate slag-metal reaction.

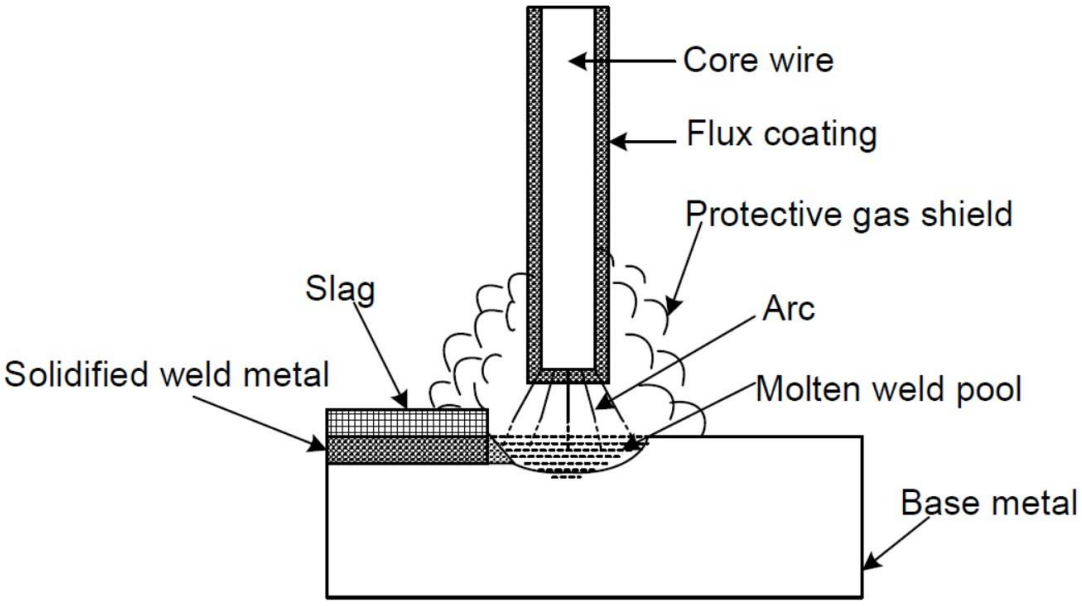

Fig.2.21: Schematic diagram showing constituents of SMAW

2.5.3 Type of coating in coated electrode

Coatings of coated electrodes used in SMAW process are classified as acid, oxide, rutile, cellulosic and basic on metallurgical premises.

2.5.3.1 Acid and oxide coating

They contain the largest amount of iron and manganese ores and large amount of hydrated aluminosilicates. The molten metal at the electrode tip is therefore metallurgical rimming and very active because it contains large quantities of oxygen and hydrogen. The boiling of the liquid metal at the electrode tip cause the surface tension forces to be easily overcome favouring spray droplet transfer. The larger the concentration of sodium and potassium ions and their compounds the more the arc is ionized and the smaller is its total voltage. Such electrodes are very suitable for AC welding.

2.5.3.2 Rutile coating

In rutile coating the iron and manganese ores are replaced by titania (TiO_2) i.e. rutile. As a result, the molten metal from the electrode is not so oxidized and is therefore metallurgically nearly killed. Rutile electrode melting is therefore less of the spray type than acid or oxide electrodes. Rutile is recognised as a mineral which stabilises the arc better than iron and manganese.

2.5.3.3 Cellulosic coating

The cellulosic coating contains large amount of organic matters, mostly cellulose upto about 30%. Other components of the covering do not show any significant difference compared with acid and rutile electrode. Because the ionisation potential of gases (CO, CO_2, H_2O) from electrode coating is high, the electron emission is impeded leading to increased arc voltage.

2.5.3.4 Basic coating

The basic coating contains carbonates (mainly of calcium), fluorite (CaF_2), relatively small amounts of aluminosilicates, metal powders, and deoxidisers which have relatively greater effect than other coatings. When compared with the other coatings, they produce well deoxidised, killed and low hydrogen droplets deposited metal. Unlike other types of electrode, basic electrode coatings contain fluorine compounds, mostly fluorite which is introduced to decrease melting point and viscosity of slag. The electrodes with fluorides in their coatings exhibit stable melting when positive.

Table 2.7 Commoncoating constituents and their functions **[110]**

Name	Chemical formula	Gaseous Protection	Deoxidation	Slag Formers	Viscosity Control	Arc Stabilizers	Binders	Slipping Agents	Alloy Agents	Colour Coating
Cellulose	$(C_6H_{10}O_5)_x$	X	X					X		
Limestone	$CaCO_3$	X	X	X	X	X				
Lime	CaO		X		X	X				
Flourspar	CaF_2	X	X		X					
Rutile	TiO_2		X	X	X	X				X
Zirconium	ZrO_2					X				
Alumina	Al_2O_3				X	X				
Silica	SiO_2		X	X	X	X				
Iron Oxide	FeO, Fe_2O_3, Fe_3O_4		X	X	X	X				X
Ferro Alloys	FeMn, FeSi, FeTi		X	X					X	
Dolomite	$MgOCaO(CO_2)_2$	X	X	X						
Sodium oxide	NaO		X			X				
Sodium silicate	Na_2SiO_2, nH_2O			X	X	X	X			
Potassium silicate	K_2SiO_3, nH_2O			X		X	X			
Feldspar	$K_2OAl_2O_36SiO_2$			X	X	X				
Talcs	$3MgO4SiO_24H_2O$		X	X	X	X		X		
Clays	$Al_2O_32SiO_22H_2O$			X	X	X	X	X		
Iron powder	Fe					X			X	
Pigments	----------									X

2.5.4 Nano -size rare earth elements in coating

The rare earth oxides added into the flux coating play a dual role. During welding, major portions of the REM oxides from the electrode coating end up in the slag. Thus it enhances the removal of sulphur from the weld metal along with Mg, Mn and Ca into the slag, leading to increase the impact strength of the weld metal **[112]**. On the other hand, a minor portion of the REM only will remain in the weld metal as micro alloyed addition in the

weld metal. Minor addition of Ce is found to be highly effective in removing O and S in the steel through the formation of Ce_2O_2S **[113]**. **Fig.2.22** is an associated projection drawing of precipitation diagram of the $lga_{[Ce]}$-$lga_{[O]}$-$lga_{[S]}$ space which shows the conditions for the formation of rare-earth oxides, sulfides or oxy-sulfides depend upon the activity of oxygen and sulphur **[114]**.

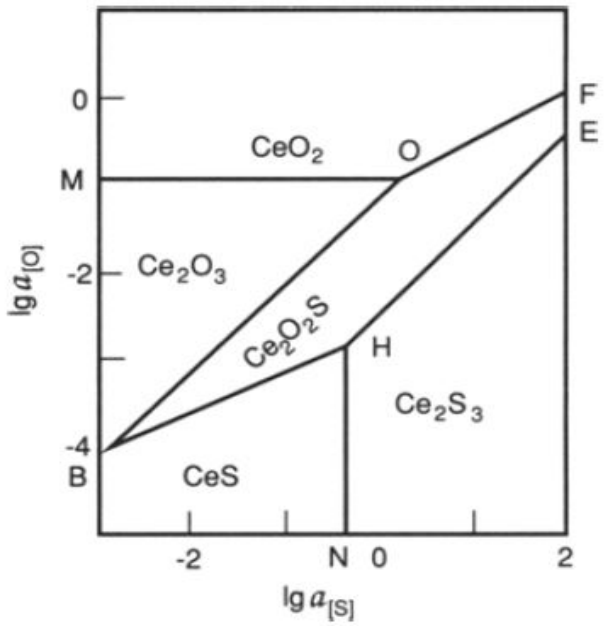

Fig.2.22: Projection drawing of ($lga_{[Ce]}$-$lga_{[O]}$-$lga_{[S]}$)

References

1. D. B. Wagner, "Science and Civilization in China", Volume 5: Chemistry and Chemical Technology, Part 11: Ferrous Metallurgy. Vol. 46. Cambridge: Cambridge University Press, 2008
2. D. H. Herring, "The HERRING GROUP, Inc., Elmhurst, III., Heat Treatment of Cast Irons", Thermal Processing, (2004) 23-26
3. G. Lesoult, M. Castro, J. Lacaze, "Solidification of spheroidal graphite cast iron", Acta Mater., 46 (1998) 983-1010
4. R. Elliott, "Cast Iron Technology", Butterworths,1988
5. Ductile Iron Society, "Ductile Iron Data, Section 2, Introduction and Section 4, Austempered Ductile Iron", Revised by J. R. Keough (August 1998). USA, 2013
6. R. W. Heine, C. R. Loper, P. C. Rosental, "Principle of Metal Casting", Tata Mcgraw-Hill Edition, 493-494
7. H. F. Taylor, M.C. Flemings, J. Wulff, "Foundry Engineering", John Wiley & Sons Inc., 1959
8. The solidification of metals, Iron and steel institute, London, 1968, Pub 110
9. W. F. Smith, J. Hashemi, "Foundations of materials science and engineering", McGraw-Hill, 2011
10. A. Boyles, "The Structure of Cast Iron", Ohio: Metals Park, 1947
11. J. T. Eash, "Effect of ladle inoculation on the solidification of gray cast iron", AFA Transactions, 49 (1941) 887-906
12. G. A. Feest, G. McHugh, D. O. Morton, l. S. Welch and I. A. Cook, in Proc. Sol. Tech. in the Foundry and Casthouse, 1983
13. S. I. Karsay, "Ductile Iron I-Production", Quebec: Quebec Iron and Titanium Corporation, 1976
14. B. Lux, "Giesserei", techn.-wiss. Beih. Mod. Cast 45 (1964) 222-232
15. C. H. Wang, H. Fredriksson, in 48th International Foundry Congress, Varna, Bulgaria, 1981
16. H. Fredriksson, "Inoculation of iron-base alloys", Materials Science and Engineering, 65(1) (1984) 137-144
17. T. Kusakawa, S. Okimoto, K. Kobayashi, K. Ide, H. Okita, "Inoculation Effect of Rare Earth Metals and Rare Earth oxides to Spheroidal Graphite", Cast Iron Rep. Cast. Res. Lab., Waseda Univ., 39 (1988) 25-32

18. K. M.Muzumdar, J. F. Wallace, “Effect of Sulfur in Cast Iron”, AFS Transactions, 81(1973) 412-423
19. M. A. Gadd, G. H. J. Bennett, “Physical Chemistry of Inoculation in Cast Iron”, MRS Online Proceedings Library Archive, 34 (1984)
20. H. Morrogh, “Production of nodular graphite structures in gray cast irons”, Trans. AFS., 56 (1948) 72-90
21. H. Morrogh, W. J. Williams, “The Production of Nodular Graphite Structures in Cast Iron”, J. Iron Steel Inst.,158 (1948) 306-322
22. D. J. Reese, “Symposium on nodular graphite cast iron”, Trans. AFS, 57 (1949) 576-587
23. C. C. Reynolds, C.M. Adams, H. F. Taylor, “Prediction of Mechanical Properties from Chemical Composition for fully annealed ductile cast iron”, Trans. AFS, 61(1953) 510-515
24. C. F. Reynolds, H. F. Taylor, “Mechanical properties of spheruidic graphite cast iron”, Trans. AFS, 60 (1952) 687-713
25. H. Horie, T. Kowata, A. Chida, “Effect of Rare Earth Elements on Chill Formation and Nodule Count in Thin-section Spheroidal-Graphite Cast Iron”, Cast Metals, 1(2) (1988) 90-97
26. S. K. Swain, “Effect of Chemistry and Processing Variables on the Mechanical Properties of Thin-wall ductile iron castings”, M.Tech Thesis, 2008
27. J. E. Shigley, “Shigley's mechanical engineering design”, Tata McGraw-Hill Education, 2011
28. J. F. Janowak, P. A. Norton, “A guide to mechanical properties possible by austempering”, AFS Trans., 88 (1985) 123-135
29. J. Zimba, D. J. Simbi, E. Navara, “Austempered ductile iron: an alternative material for earth moving components”, Cement & Concrete Composites, 25(6) (2003) 643–649
30. J. R. Keough, K. L. Hayrynen, G. L. Pioszak, “Designing with Austempered Ductile Iron (ADI)”, AFS Proceedings, (2010) 1-15
31. K. L. Hayrynen, J. R. Keough, “Austempered Ductile Iron-The State of the Industry in 2003”, Keith D. Millis Symposium, Louisville
32. Ductile iron Data for Design Engineers - section IV. “Austempered ductile iron" Ductile iron society, 2016, http://www.ductile.org

33. ASTM A897 / A897M-16, "Standard Specification for Austempered Ductile Iron Castings", ASTM International, West Conshohocken, PA, 2016, www.astm.org
34. T. Dorn, J. R. Keough, T. Schroeder, T. Thoma, "The Current State of Worldwide Standards for Dcutile Iron", in Keith Mills Symposium On Ductile Cast Iron, 2003
35. T. Yuichi, H. Kage, "Development and application of austempered spheroidal graphite cast iron", Materials Transactions, JIM, 33(6) (1992) 543-557
36. T. Shiokawa, "69th general meeting of Ductile Iron Society Lynchburg", (1980); 1st Int. Conf. On ADI Chicago, (1984) 107
37. J. R. Keough: "World Conf. On ADI", Bloomingdale, (1991) 638
38. J. F. Janowak, R. B. Gundlach, "Development of a Ductile Iron for Commercial Austempering.(Retroactive Coverage)", Transactions of the American Foundrymen's Society, 91 (1983) 377-388
39. Y. Tanaka, K. Hidehiko, "Development and application of austempered spheroidal graphite cast iron", Materials Transactions, JIM, 33(6) (1992) 543-557
40. G. Wenbang, C. Guodong, L. Li, H. Jing, Z. Zhonghe, "Design and control of chemical compositions for high performance austempered ductile iron", China Foundry, (2012) 143-147
41. A. Nazarboland, R. Elliott, "The relationship between austempering parameters, microstructure and mechanical properties in a Mn-Mo-Cu alloyed ductile iron", International Journal of Cast Metals Research, 10 (1997) 87-97
42. T. N. Rouns, K. B. Rundman, "Constitution of Austempered Ductile Iron and Kinetics of Austempering", AFS Transactions, 95 (1987) 851-874
43. J. M. Velez, A. Garboggini, A. P. Tschiptschin, "Effect of silicon on Kinetics of bainitic reaction in austempered ductile cast iron", Materials Science and Technology, 12(4) (1996) 329-337
44. S. Yazdani, R. Elliott, "Influence of Mo on austempering behaviour of ductile iron – part 1". Materials Science and Technology, 15(5) (1999) 531-540
45. D. J. Moore, T. N. Rouns, K. B. Rundman, "Structure and mechanical properties of austempered ductile iron", AFS Transactions, 93 (1985) 705-718
46. B. V. Kovacs, "The effects of alloying elements and their segregation in ADI". In: Proceedings of 3rd World Conference on ADI, ASM, Chicago, USA, March (1991) 241-269

47. S. K. Yu, C. R. Loper, "The Effect of Molybdenum, Copper and Nickel on the Pearlitic and Martensitic Hardenability of Ductile Cast Irons", AFS Transaction, 96 (1988) 811-821
48. S. Yazdani, M. A. Rahimi, "Wear behavior of an austempered ductile iron containing Mo-Ni-Cu", Materials Science Forum, 475-479 (2005) 199-202
49. Y. Mi, "Effect of Cu, Mo, Si on the content of retained austenite of austempered ductile iron", Scripta Metallurgica et Materialia, 32(9) (1995) 1313-1317
50. S. M. Heydarzadeh, M. Nili Ahmadabadi, A. B. Vahdat, "The role of austempering parameters on the structure and mechanical properties of heavy section ADI", Journal of materials processing technology, 153 (2004) 203-208
51. J. O. Choi , J. Y. Kim, C. O. Choi, J. K. Kim, P. K. Rohatgi, "Effect of rare earth element on microstructure formation and mechanical properties of thin wall ductile iron castings", Materials Science and Engineering A, 383 (2004) 323-333
52. M. Ramadana, A. A. Nofal , I. Elmahalawi , R. Abdel-Karim, "Influence of graphite nodularity on microstructure and processing window of 1.5% Ni–0.3% Mo austempered cast iron", Materials Science and Engineering A, 435-436 (2006) 564-572
53. H. Horie, S. Hiratsuka, T. Kowata, Y. Twamochi, Y. Shobuzawa and M. Nakamura, "Effect of Eight Individual Rare-earth Elements on the Graphite Nodule Count of a Thin-section of Spheroidal-graphite Cast Iron", Cast Metals, 3(2) (1990) 73-81
54. D. M. Stefanescu, R. J. Warrick, L. R. Jenkins, G. Chen and F. Martinez, "Influence of the chemical analysis of alloys on the nodule count of ductile iron", Transactions of the American Foundrymen's Society, 93 (1985) 835-848
55. Y. J. Kim, H. Shin, H. Park, J. D. Lim, "Investigation into mechanical properties of austempered ductile cast iron (ADI) in accordance with austempering temperature", Materials Letters, 62(3) (2008) 357-360
56. S. K. Putatunda, "Development of austempered ductile cast iron (ADI) with simultaneous high yield strength and fracture toughness by a novel two-step austempering process", Materials Science and Engineering A, 315(1-2) (2001) 70-80
57. A. F. Sergio, "Evaluation of impact and fatigue properties on austempered ductile iron", MS thesis. 2009
58. M. A. Yescas, "Prediction of the Vickers hardness in austempered ductile irons using neural networks", Int. J. Cast Metals Res., 15 (2003) 513–521

59. C. Glondu, "Improving the Toughness of Austempered Ductile Iron", Master Thesis, Sweden, 2007
60. S. K. Putatunda, S. Kesani, R. Tackett, G. Lawes, "Development of austenite free ADI (austempered ductile cast iron)", Materials Science and Engineering A, 435-436 (2006) 112-122
61. J. F.Janowak, P. A. Norton, "A guide to mechanical properties possible by austempering, 1.5% Ni, 0.3% Mo iron", AFS Trans, 88 (1985) 123-135
62. J. Aranzabal, I. Gutierrez , J. M Rodriguez-Ibabe, J. J. Urcola, "Influence of the amount and morphology of retained austenite on the mechanical properties of an austempered ductile iron", Metallurgical and materials transactions A, 28(5) (1997) 1143-1156
63. I. Riposan, M. Chisamera, "Conf. Proc. Cast Iron IV Proc", Materials Research Society, Pittsburgh, PA, (1990) 195-202
64. M. A. Yescas, H. K. D. H. Bhadeshia, D. J. MacKay, "Estimation of the Amount of Retained Austenite in Austempered Ductile Irons Using Neural Networks", Mater. Sci. Eng., 311(1-2) (2001) 162-173
65. M. Bahmani, R. Elliot, "Isothermal Transformation Diagrams for Alloyed Ductile Cast Iron", Mater. Sci. Technol., 10(12) (1994) 1050-1056
66. H. Bayati, R. Elliot, "Influence of Austenitising Temperature on Mechanical Properties of High Manganese Alloyed Ductile Iron", Mater. Sci. Technol., 11(9) (1995) 908–912
67. D. J. Moore, T. N. Rouns, K. B. Rundman, "The Relationship Between Microstructure and Tensile Properties in ADI", AFS Trans., 95 (1987) 765–774
68. L. Bartosiewicz, B. V. Kovacs, A. R. Krause, S. K. Putatunda, "Fatigue Crack Growth Behaviour of Austempered Ductile Cast Iron", AFS Trans., 92 (1992) 135–142
69. H. R. Erfanian-Naziftoosi, N. Haghdadi, A. R. Kiani-Rashid, "The Effect of Isothermal Heat Treatment Time on the Microstructure and Properties of 2.11 % Al Austempered Ductile Iron", J. Mater. Eng. Perform., 21(8) (2012) 1785–1792
70. P. O. Atanda, O. E.Olorunniwo, B. I. Imasogie, "Effect of Process Parameters on the Mechanical Properties of Iso-Thermal Treated Ductile Iron", Mater. Perform. Character.,3(1) (2014) 255–264
71. H. K. D. H. Bhadeshia, "The lower bainite transformation and the significance of carbide precipitation", Acta metallurgica, 28(8) (1980) 1103-1114

72. H. K. D. H. Bhadeshia, D. V. Edmonds, “The bainite transformation in a silicon steel”, Metallurgical Transactions A, 10(7) (1979) 895-907
73. S. A. Khan, H. K. D. H. Bhadeshia, “Kinetics of martensitic transformation in partially bainitic 300M steel”, Materials Science and Engineering A, 129(2) (1990) 257-272
74. H. K. D. H, Bhadeshia, A. R. Waugh, “Bainite: An atom-probe study of the incomplete reaction phenomenon”, Acta Metallurgica, 30(4) (1982) 775-784
75. H. Niesawaag, J. W. Nijhof, Proceedings of the International Symposium on Physical Metallurgy of Cast Iron, 34 (1985) 411
76. M. N. Ahmadabadi, “Bainitic transformation in austempered ductile iron with reference to untransformed austenite volume phenomenon”, Metallurgical and Materials Transactions A, 28(10) (1997) 2159-2173
77. H. K. D. H. Bhadeshia, “Bainite in steels”, The institute of Materials, 1992
78. W. Dubensky, K. B Rundman, “An Electron Microscope Study of Carbide Formation in Austempered ductile Iron”, AFS Transactions,93 (1985) 389-394
79. D. A. Harris, B. Tech, R. J Maitland, “The Products of the Isothermal Decomposition of Austenite in a Spheroidal Graphite Cast Iron”, Iron and steel, (1970) 53-60
80. L. Sidjanin, R. E.Smallman, J. M.Young, “Electron Microstructure and Mechanical Properties of Silicon and Aluminium Ductile Irons”, Acta Metallurgica et Materialia, 42 (1994) 3149-3156
81. J. M.Velez, A. Garboggini, A. P. Tschiptschin, “Effect of Silicon on the Kinetics of the Bainitic Reaction in Austempered Ductile Cast Iron”, Materials Science and Technology, 12 (1999) 329-337
82. N. Darwish, R. Elliott, “Austempering of Low Manganese Ductile Irons Part 2 Influence of Austempering Temperature”, Materials Science and Technology, 9 (1993) 586-602
83. P. P. Rao, S. K. Putatunda, “Investigations on the Fracture Toughness of Austempered Ductile Irons Austenitised at Different Temperatures”, Mater. Sci. Eng., 349(1–2) (2003) 136–149
84. D. M. James, “A Design Engineer’s Digest of Ductile Iron”, Sorelmetal Technical Services Rio Tinto Iron & Titanium, Inc., USA (2005) 9-12
85. Y. Tanaka, H. Kage, “Development and application of austempered spheroidal graphite cast iron”, Materials Transactions, JIM, 33(6) (1992) 543-557

86. B. V. Kovacs, "Austempered ductile iron, facts and fiction", Mod.Cast., 36(1990) 38–41
87. H. Bayati, R. Elliot, G. W Lorimer, "Influence of Austenitising Temperature on Austempering of High Manganese Alloyed Ductile Iron", Mater. Sci. Technol., 11(8) (1995) 776–786
88. S. K. Putatunda, R. Gupta, P. P. Rao, "Understanding Microstructure: Key to Advances in Materials, presented at the 25th Annual Technical Meeting of the International Metallographic Society", Columbus, OH, July 27, 1996, International Metallographic Society, Materials Park, OH, 103–110
89. J. Yang, S. K. Putatunda, "Effect of Microstructure on Abrasion Wear Behavior of Austempered Ductile Cast Iron (ADI) Processed by a Novel Two-Step Austempering Process", Mater. Sci. Eng., 406(1–2) (2005) 217- 228
90. S. B. Amir, Y. Sasan, A. Behzad, "Effect of Shot Peening Process on Fatigue Behavior of an Alloyed Austempered Ductile Iron", China Foundry, 8(3) (2011) 325–330
91. H. A. Mohamed, "Fatigue Properties of an Alloyed Austempered Ductile Iron of Initially Ferritic Matrix Structure Using Thermography as NDT", presented at the 2nd International Conference on Technical Inspection and NDT (TINDT2008), Tehran, Iran, October 21–22, 2008
92. T. J. Marrow, H. Centinel, "Short Fatigue Cracks in Austempered Ductile Cast Iron (ADI)", Fatigue Fract. Eng. Mater. Struct., 23(5) (2000) 425–434
93. L. Chin-Kuang, C. Chin-Wei, "Influence of Heat Treatment on Fatigue Crack Growth of Austempered Ductile Iron", J. Mater. Sci., 37(4) (2002) 709-716
94. M. Pouranvari, "On the weldability of grey cast iron using Nickel based filler metal", Mater. Des.,31 (2010) 3253-3258
95. E. M. El-Banna, "Effect of preheat on welding of ductile cast iron", Mater. Lett., 41 (1999) 20-26
96. S. M. Mirhedayatian, S. E. Vahdat, M. J. Jelodar, R. F.Saen, "Welding process selection for repairing nodular cast iron engine block by integrated fuzzy data envelopment analysis and TOPSIS approaches" Mater. Des., 43 (2013) 272–282
97. E. E. Huke, H. Udin, "Welding metallurgy of nodular cast iron", Weld Journal, 32(3) (1953) 78-85
98. S. Kou, "Welding metallurgy", 2nd ed. New Jersey: John Wiley and Sons; 2003

99. G. Hallen, "Some aspects on the formation of microstructure in multipass welds in ferritic ductile iron", 3rd Int. Symp. On the Physical Metallurgy of Cast Irons, Stockholm, Sweden, Aug., (1984) 457-465
100. M. Ebrahimnia, F. M. Ghaini, S. Gholizade, M. Salari, "Effect of cooling rate and powder characteristics on the soundness of heat affected zone in powder welding of ductile cast iron", Mater. Des., 33 (2012) 551-556
101. E. M. El-Banna, M. S. Nageda, M. M. Abo El-Saadat, "Study of restoration by welding of pearlitic ductile cast iron", Materials letters, 42(5) (2000)311-320
102. M. Pascual, J. Cembrero, F. Salas, M. Pascual-Martínez, "Analysis of the weldability of ductile iron", Mater. Lett., 62 (2008) 1359-1362
103. Guide for Welding Iron Castings: "ANSI/AWS D11.2-89 (R2006)", An American National Standard Institute, (1988) 52-54
104. R. Winiczenko, R. Salat, M. Awtoniuk, "Estimation of tensile strength of ductile iron friction welded joints using hybrid intelligent methods", Trans. Nonferrous Met. Soc. China, 23 (2013) 385-391
105. M. Askary-Paykani, M. Shayan, M. Shamanian, "Weldability of Ferritic Ductile Cast Iron Using Full Factorial Design of Experiment", J. Iron Steel Res. Int., 21 (2014) 252-263
106. T. J. Kelly, R. A. Bishel, R. K. Wilson, "Welding of Ductile Iron with Ni-Fe-Mn Filler Metal", In: Welding Research Supplement, (1985) 79-85
107. R. C, Voigt C. R. Loper Jr, "A study of heat-affected zone structures in ductile cast iron", Welding Journal, 62(3) (1983) 82-88
108. C. E Jackson, "Fluxes and Slags in welding, WRC Bulletin, 190 (1973) 1- 25
109. G. E. Claussen, The metallurgy of covered electrode weld metal", Welding Journal, 28(1) (1949) 12-24
110. W. Spraragen, C. E. Claussen, Welding Journal, 19(1) (1940) 24-30
111. R. Shutt, Welding Journal, 35(12) (1955) 1207-1213
112. X. Zhao, W. Wang, L. Chen , F. Liu , J. Huang , H. Zhang, "Microstructures of cerium added laser weld of a TiNi alloy", MaterialsLetters, 62 (2008) 1551-1553
113. F. Cosandet, L. D Sczerzenie, J. K. Tien, "The effect of cerium on high temperature tensile and creep behaviour of a super alloy", Met. Trans A, 14(3) (1983) 611-621
114. Y. Jingsheng, Y. Zongsen, W. Chengjian, "Rare earths and the mechanical properties off steel", JOM, 40(5) (1988) 26-31

Chapter 3

Methodology

Chapter 3

3.0 Methodology

In the present investigation total work have been divided into four parts: (i) development of coated electrode with and without Ce content, (ii) welding of cast ductile iron (DI) after establishing weld procedure on bead-on-plate as well as groove weld using developed electrodes (with and without Ce content), (iii) imparting isothermal heat treatment cycle to as-welded DI plates with changing austempering temperature and holding timeand, (iv) characterization of microstructures and mechanical properties of as-welded DI plates and ADI joints.

In the first part, the formulation of the coated electrode was designed based on the available published literature and practically developed by trial and error method. All the developed electrodes are basic coated in which graphite powders, alloying elements in the form of ferro-alloys and pure metal powders were added to obtain the target weld chemistry leading to desired microstructure and mechanical properties of the weld deposits. Among the six developed coated electrodes one having composition close to the target chemical composition was selected. Further, three levels of nano size CeO_2 were added to the coating of selected electrode to study and understand the effect of Ce on microstructure and mechanical properties of as-welded DI weld metals and after isothermal heat treated (ADI) weld metals.

In the second part, weld procedure for welding cast DI plate of 20 mm thick was developed as per AWS(D11) standard using bead-on-plate studies by varying preheat temperature and PWHT immediate after welding in SMAW process. Also weld procedure for groove welding on 20mm thick DI base plate was developed by modifying U groove design and using same welding parameters for bead-on-plate weld procedure.

In the third part, all the DI welded joints were converted to ADI by applying isothermal heat treatment cycle which consists of austenitizing at 900°C for 2 h holding time and austempering at 300°C and 350°C for 1.5 h, 2 h and 2.5 h holding time.

In the fourth part, the as-welded and heat treated weld metals, PMZ, HAZ and base metal were characterized for microstructure and mechanical properties. Microstructural studies were performed under optical microscopy (OM), scanning electron microscopy (SEM) and transmission electron microscopy (TEM) studies. Phase analysis was done by XRD and EDS analysis. The mechanical properties of the welded joints have been evaluated

by Vickers microhardness testing, transverse tensile testing, and high cycle fatigue testing. Room temperature charpy impact testing was done only for weld metals. The fracture surfaces of charpy impact and fatigue test samples were examined under SEM.

The details methodology of total work is presented with the help of tree diagram as given in **Fig.3.1**.

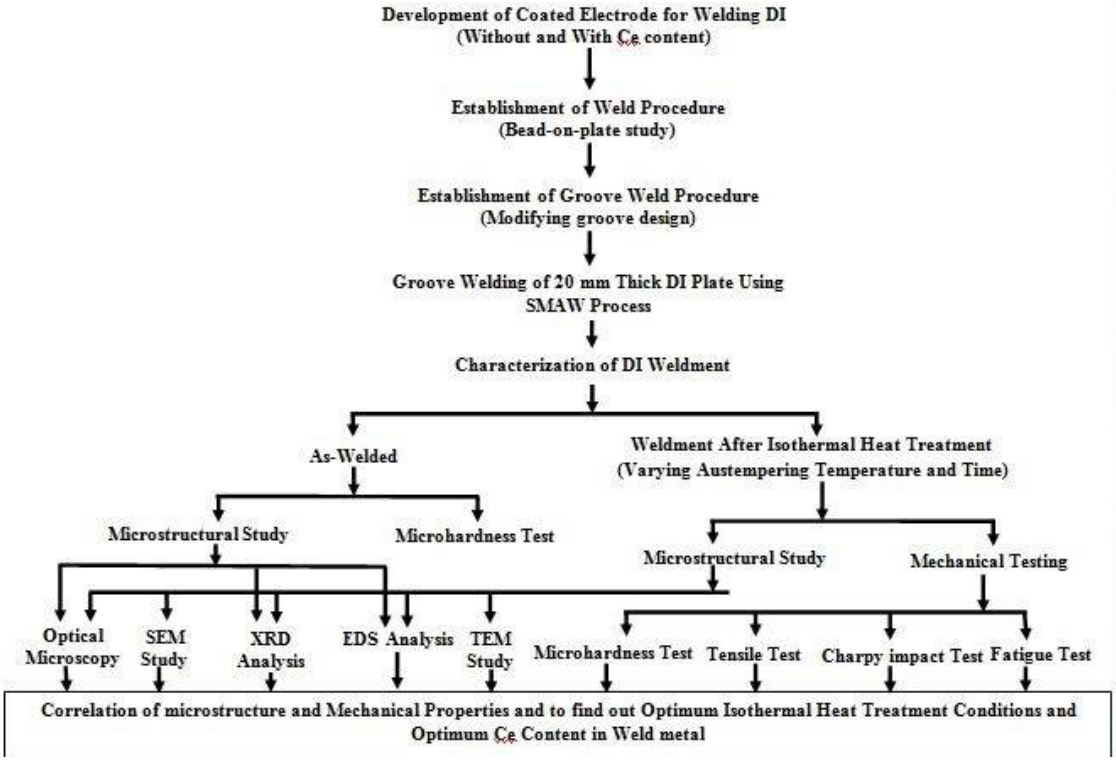

Fig.3.1: Tree diagram of the present work

Chapter 4

Experimental Procedure

Chapter 4

4.0 Introduction

This chapter deals with the experimental work and techniques applied in order to fulfil the objective of the work. The total experimental work have been divided into five parts: i) first manufacturing of developed coated electrodes through extrusion process using core wire, flux ingredients and alloy powder etc. followed by drying, ii) secondly, establishment of weld procedure (sound weld) for ductile iron (DI) with selected developed electrodes as per AWS(D11) standard using bead-on-plate test by varying preheat and post weld heat treatment in SMAW process and also groove welding with modified U-groove design using established weld procedure, iii) thirdly application of same isothermal heat treatment cycle (austenitization and austempering with varying the austempering temperature and holding time) to all the as-welded DI joints including weld metal, HAZ and base metal, iv) fourthly characterization of weld metals, PMZ, HAZ and base metal microstructure by optical microscopy (OM), scanning electron microscopy (SEM), transmission electron microscopy (TEM), X-ray diffraction analysis (XRD), Energy dispersive spectroscopy (EDS) analysis, and (v) finally evaluation of the mechanical properties of the ADI welded joints by microhardness testing, room temperature transverse tensile testing, and high cycle fatigue testing as well as evaluation of room temperature toughness of weld metals by charpy impact testing.

4.1 Development of coated electrode

4.1.1 Core wire

In this present work, 4 mm dia and 450 mm long low carbon steel wires were used as a core wire for manufacturing of coated electrodes. The typical chemical composition of the core wire contains 0.05% C, 0.48% Mn, 0.018% Si, 0.018% S and 0.022% P. The core wires were reasonably free from dirt, oil, rust and other contamination.

4.1.2 Flux formulation

The flux formulation was designed for development of coated electrode in order to weld DI castings and convert DI weldment into ADI after isothermal heat treatment. Accordingly, the flux formulation of coated electrodes were made by systematically varying the flux ingredients in the coating to achieve the target weld metal composition (3.7% C, 3.4% Si, 0.4% Mn, 0.23% Cu, 0.7% Ni, 0.5% Al) **[1-2]**. Further, three levels of nano size CeO_2 was added to the coating of selected developed coated electrode to study and

understand the effect of Ce on weld metal microstructure and properties in as-welded and after isothermal heatreatment. The typical flux composition of the different trial electrodes with and without the addition of nano size CeO_2 is given in **Table 4.1** and **Table 4.2** respectively.

Table 4.1 Typical flux formulation for development of coated electrode

Flux Ingredient	Weight %					
	Trial 1	**Trial 2**	**Trial 3**	**Trial 4**	**Trial 5**	**Trial 6**
$BaCO_3$ Powder	1	0.2	0.2	0.2	0.2	0.77
Acidic Fluorspar	10	8	8	8	8	6.88
Graphite Power	20	27	30	30	30	25.8
Fe-Si powder	18	21	21	25	30	25.8
Fe-Ti Powder	2	1.7	1.7	1.7	1.7	4.13
Ni Powder	0.5	3.5	3.5	3.5	3.5	3.01
$BiCO_3$	0.5	0.2	0.2	0.2	0.2	0.17
Mo Powder	0.4	2.5	2.5	2.5	2.5	2.15
Al Powder	4	6.6	6.6	6.6	6.6	5.68
Cu Powder	5	1.5	1.5	1.5	1.5	1.29
Calcite	32	24.6	24.6	24.6	24.6	21.6
Fe Powder	9	4.2	1.21	1.2	1.2	1.03
$MgCO_3$ Powder	0.2	0.1	0.1	0.1	0.1	0.088
Na-Alg	1.5	1.1	1.11	1.11	1.11	0.95
CMC	0.5	0.5	0.5	1.5	1.5	1.29

Table 4.2 Typical flux formulation for development of coated electrode introducing CeO_2

Flux Ingredient	Weight %		
	Trial 7	Trial 8	Trial 9
$BaCO_3$ Powder	0.2	0.2	0.2
Acidic Fluorspar	8	8	8
Graphite Power	30	27	30
Fe-Si powder	25	21	21
Fe-Ti Powder	1.7	1.7	1.7
Ni Powder	3.5	3.5	3.5
$BiCO_3$	0.2	0.2	0.2
Mo Powder	2.5	2.5	2.5
Al Powder	6.6	6.6	6.6
Cu Powder	1.5	1.5	1.5
Calcite	24.6	24.6	24.6
Fe Powder	1.2	4.2	1.21
$MgCO_3$ Powder	0.1	0.1	0.1
Na-Alg	1.11	1.1	1.11
CMC	1.5	0.5	0.5
Nano CeO_2	3	1.5	5

4.1.3 Manufacturing of coated electrode

Manufacturing of coated electrode for SMA welding is a complex process that requires several steps. During the extrusion process of coated electrodes in the laboratory mainly three different aspects were looked into. Firstly, the core wire was flattened at the ends and re-straightened to ensure good feeding through the wire/rod feeder. Secondly, each flux coating was prepared suitably as per flux formulation listed in **Table 4.1** and **Table 4.2**. Thirdly, the eccentricity of the electrode is required to be adjusted several times using the adjusting bolts on the face of the extrusion die.

The flux ingredients and alloy powders were weighted and blended to form a dry mix. Particle sizes of the flux ingredients are very important for mixing and extrusion. Generally, fines less than 200 mesh are minimized. The mixing of the dry powders was performed in a mixture machine as shown in **Fig. 4.1**. The dry powders were mixed for a minimum of 2 h for thorough mixing. After dry mixing, the required amount of binder (potassium silicate and

sodium silicate) was gradually added to the dry mix. Optimum addition of potassium and sodium silicate will make strong wet mix which will not crumble even by compressed into hand–size balls. This wet mix is now called as paste and ready for extrudable. However, the optimum addition of binder to make it as paste is highly experience dependent.

Fig.4.1: Mixture machine

After preparation of core wires/rods and flux/binders mixture (paste), the actual extrusion of the coated electrodes was started using a laboratory scale extrusion machine **(Fig 4.2)**. The core wires/rods were placed into the wire/rod feeder and the total paste was placed into the paste compartment of the extruder and compressed with a hydraulic ram. The core wire/rods feeding speed and the extrusion ram speed must be adjusted to an acceptable pace for extrusion. This adjustment was done by first feeding one rod through the rod guide of the extruder into the extrusion die. The hydraulic ram was then used to compress the flux paste into the extrusion die. The speed of the ram was then adjusted to an acceptable range relative to the rod feeding speed. Typically, the speed of the ram should be adjusted number of times to establish a good flow of the paste. If the ram speed is too low, the flux paste will not coat the wire/rod continuously. On the other hand, if the ram speed is too high, the coat will appear as rippled and swollen. Simultaneously the eccentricity of the electrode should be adjusted when the core wire/rod and paste both pushed through the extrusion die. Extrusion pressure in the present investigation was typically around 130 N/mm^2 which is dependent on the flow consistency of the paste. The extrusion process in detail is presented in the flow chart as shown in **Fig.4.3**. Electrode eccentricity was measured by the relative position of the

core rod with respect to the layer of flux coating as shown in **Fig.4.4**. It is to be mentioned here that the eccentricity of the electrode is required to be adjusted several times using the adjusting bolts on the face of the extrusion die.

In the present investigation, 6 mm die is used for extrusion process to yield a coating factor which is the ratio of the electrode diameter and the wire/rod diameter of 1.5.

After extrusion, coating of 25-30 mm in length is removed by brush from one end of the electrode to provide space for the electrode holder and little coating is also removed from the opposite end of the electrode to expose the tip of the core wire/rod for electrical contact at the time of arcing.

Fig.4.2: Laboratory extrusion machine

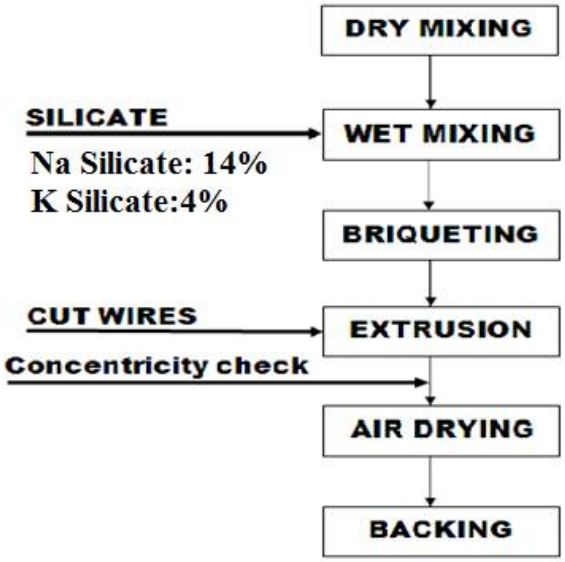

Fig.4.3: Flow diagram of the total extrusion process

Fig.4.4: Measurement of eccentricity applied dial indicator

4.1.4 Electrode baking

Electrode baking is another important part of the electrode manifesting process to remove all the moisture, which could be a source of hydrogen from the coating surface of the electrode. After successful extrusion the electrodes were dried in open air at 24 h followed by baking in PID control baking furnace **(Fig. 4.5)**. When higher graphite powder was present in the coating, baking was done at lower temperatures and controlled holding times. The total baking cycle is given in the flow diagram **(Fig. 4.6)**. After successful baking, the electrodes were removed from the furnace and packed in airtight container for further processing. The developed electrodes are shown in **Fig.4.7**.

Fig.4.5: Baking furnace

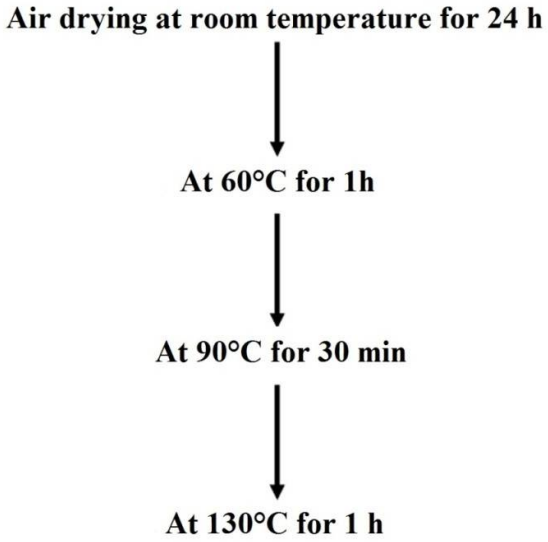

Fig.4.6: Flow diagram of electrode baking cycle

Fig. 4.7: Developed coated electrode

4.2 Base metal

The base metal used in this work was as-cast ductile iron (DI) of size 250 × 120× 20 mm collected from M/S Cresmac Foundry Pvt. Ltd., Kolkata. The base plate was grit blasted on the front side to remove any grease, embedded particles and contaminants. The typical chemical composition and mechanical properties of the base metal are given in **Table 4.3** and **Table 4.4** respectively.

Table 4.3 Typical chemical composition of as-cast DI

Element	C	Si	Mn	S	Cr	Mg	P
wt. %	3.60	2.92	0.22	0.019	0.028	0.041	0.01

Table 4.4 Mechanical properties as-cast DI

Sample Name	UTS (MPa)	YS (MPa)	El (%)	Hardness (BHN)
DI	445.40	275.6	18	153

4.3 Development of chemical pad

Chemical pad was prepared for chemical analysis of weld deposits without dilution. For the present work, chemical pad was prepared by depositing all the trial coated electrodes marked as Trial 1 to Trial 9 on DI base plate of 20 mm thick. Eight layers of beads (**Fig. 4.8**) were simultaneously deposited using each trial electrode with current (150A) and voltage (24V) in SMAW process. After completion of the chemical pad, surface of the weld deposits was ground to a smooth surface. The chemical composition of all the weld deposits was analyzed using optical emission spectrometer (OES).

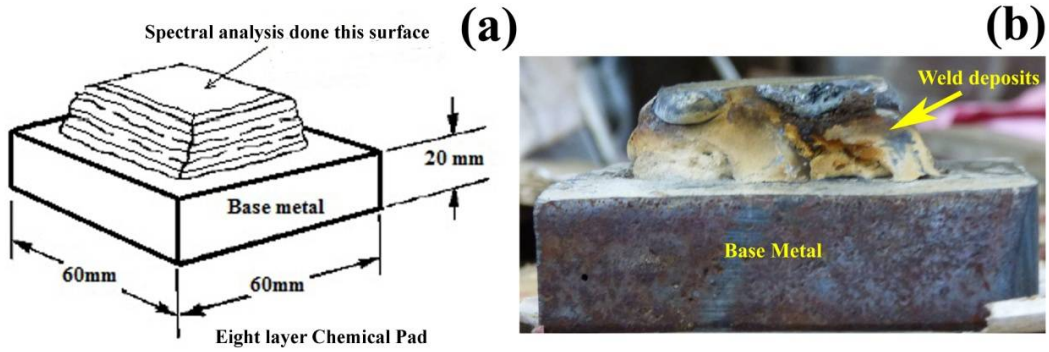

Fig.4.8: Chemical pad (a) schematic (b) deposited

4.4 Establishment of weld procedure using bead-on-plate

For the establishment of weld procedure single-pass bead-on-plate weld was deposited on DI base plate (150 × 50 × 20) in flat position using all the selected electrodes (without and with Ce containing) at the same welding parametersin SMAW process. But three different levels of preheating i.e. 200°C, 300°C, and 400°C for 1 h and PWHT which was maintained at the same preheat temperature for 1h holding time were tried. However, the quality of the welds as per standardAWS(D11) **[3]** for all the selected electrodes were obtained only at preheat of 300°C for 1 h and PWHT immediately after welding at 300°C for 1 h. The details welding parameters for the establishment of weld procedure are given in **Table 4.5** and the schematic view of the bead-on plate is shown in **Fig.4.9**.

Table 4.5 Parameters for establishment of weld procedure

Parameters	Units	Values
Preheat Temperature (1h)	°C	300
PWHT (1h)	°C	300
Welding Current	A	150
Arc voltage	V	24 ±1
Welding Speed	mm/sec	1.70 ± 0.2
Heat input	KJ/mm	1.58± 0.2

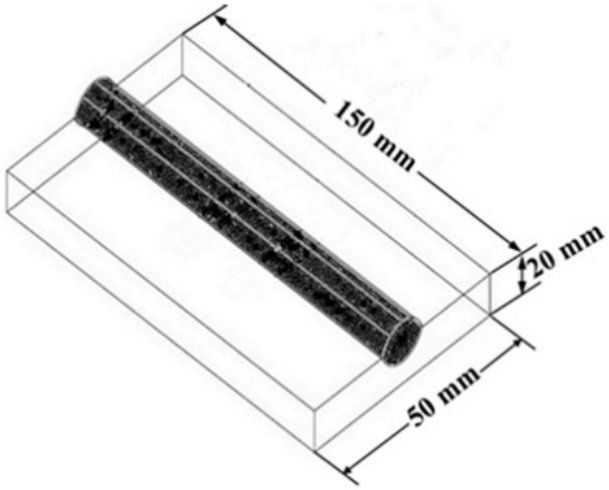

Fig. 4.9: Schematic view of single pass bead-on-plate

4.5 Modified groove design

After establishing the weld procedure for welding DI plate using bead-on-plate study, further establishment of procedure for a groove weld of 20 mm thick DI plate was required in order to extract metallography, transverse tensile, charpy impact and fatigue test specimens. After several trials, the weld procedure for groove weld of 20 mm thick DI plate was possible to establish by optimizing the U groove design **[3]** even after using the established weld procedure for bead-on-plate test. The modified U-groove design is shown schematically in **Fig.4.10**.

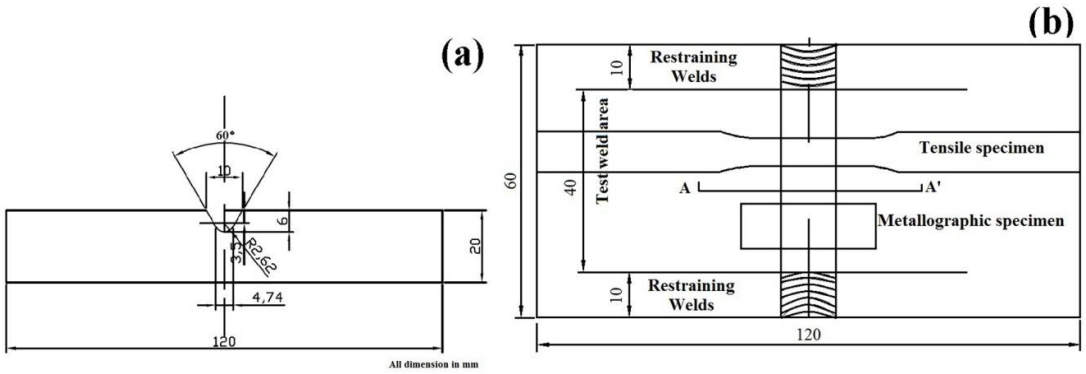

Fig.4.10: (a) Modified grove design, (b) schematic view of extracting samples from weld metals

4.6 Isothermal heat treatment

After completion of groove welding of DI plates, isothermal heat treatments of the DI welded plates containing weld metal, HAZ and base metal were done for converting ADI. The heat treatment was performed in two step heat treatment process, i.e austenitization and austempering. Austenitization was done at 900°C for 2 h holding time at box type furnace **(Fig.4.5)** and austempering was done at 300°C and 350°C for 1.5 h, 2 h and 2.5 h holding time for each temperature at salt bath furnace **(Fig.4.11)** and finally air cooled to room temperature. The typical heat treatment cycle is given in **Fig. 4.12**.

Fig. 4.11: Salt bath furnace

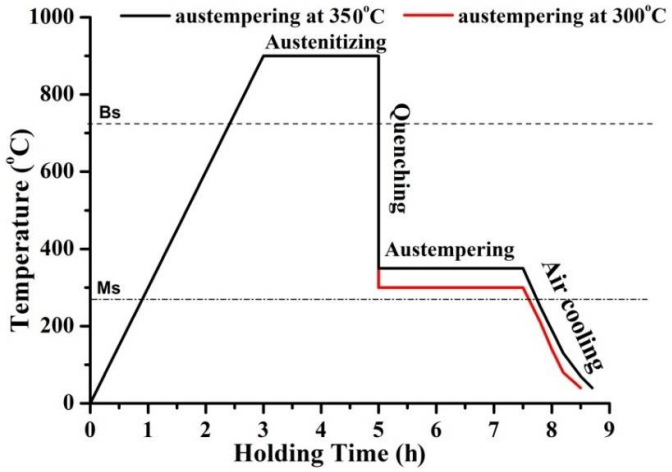

Fig.4.12: Typical isothermal heat treatment cycle

4.7 Characterization of welded joints

Several techniques were used to characterize the weldments including weld metals, PMZ, HAZ and base metal for evaluating the performance of each zone in welded joints as well as understanding the metallurgical phenomenon involved in each zone.

4.7.1 Metallographic study

For metallographic study the samples before and after austempering were cut from the DI welded joints and grounded flat for removing the carburised skins and finally mounted at room temperature. The samples were then polished systematically in different grades of silicon carbide paper containing 120, 240, 320, 400, 600, 800 and 1200 followed by cloth polishing using fine 0.05 μm alumina solutions. After that, the samples were cleaned with running water followed by alcohol and dried in hot air. After polishing and drying the samples were etched with 5% nital solution.

4.7.2 Optical microscopy

The etched samples were observed under an optical microscope (Carl Zeiss made: Axio Image A1m). The monochromatic light beam illuminated the sample and the magnification is obtained by the multiplication of objective lens and eyepiece. The magnification of eyepiece was fixed (10X). The observed magnification is specified by selecting the suitable objective lens from the set of objective lenses provided with the microscope. The images were captured at different magnification (100X, 200X, 500X) using a CCD camera mounted on top of the microscope and attached to the computer. For nodularity calculation at each condition (before and after austempering) four samples were

taken in un-etched conditions and averages of the four values were considered as representative one.

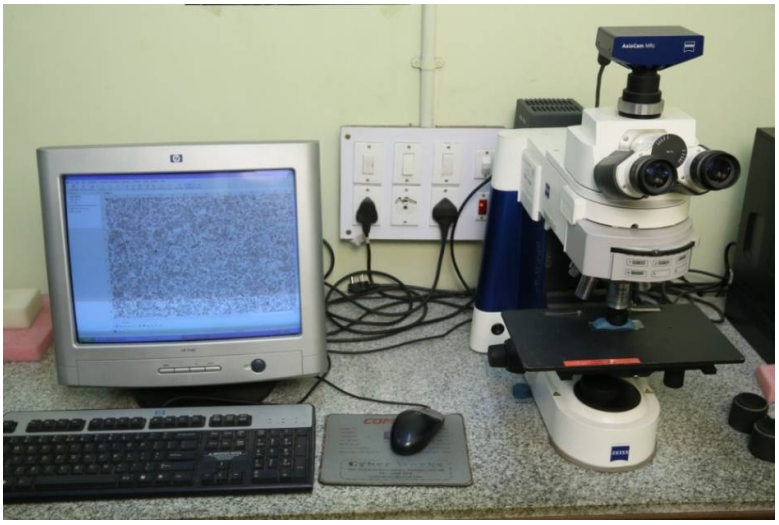

Fig.4.13: Optical microscope

4.7.3 Nodularity calculation

Nodularity, nodule count and nodule size of base metal (DI) and weld metals using all the selected electrodes have been determined using the following steps **[4]**:

a. At first total number of nodules in the image were counted (Nodule count K).

b. Then the exact round shape of the nodules is decided by the roundness metric given by the expression,

$$\text{Roundness metric} = 4 \times \pi \times \frac{\text{area}}{\text{perimeter}^2} \quad \text{..... (4.1)}$$

A threshold value of 0.8 is set as roundness metric to check the roundness of nodule. The nodules having a metric value greater than the threshold are counted as exact round nodules as per standard.

c. Nodularity has been determined from the ratio of exact round shaped nodules to the total number of nodules.

d. Nodule size is then calculated from the diameter of nodules

Area of nodule = πr^2,

$$r^2 = \frac{\text{area of nodule}}{\pi} \quad \text{.....(4.2)}$$

Diameter, $d = 2r$,

All the calculations have been done using Auto Cad 2007.

4.7.4 SEM and EDS analysis study

The scanning electron microscope (SEM) with EDS system is one of the most versatile instruments available for the examination and analysis of the microstructure morphology, chemical composition, fractography etc. For better clarity the microstructures of weld metals were evaluated using scanning electron microscope (JEOL JSM -5510) with link INKA software EDS system using an ultra-thin window detector **(Fig.4.14)**. Also fracture surfaces of the freshly broken charpy impact and fatigue test specimens were examined under SEM to understand the mode of fracture and photographs were taken at different magnifications. EDS analysis was also done on the matrix phase and graphite nodules of the weld metals before and after austempering in order to understand the presence of alloying elements specially Ce content in ADI weld metals.

Fig.4.14: Scanning electron microscopy with EDS system

4.7.5 TEM studies

For detailed microstructural analysis of the weld metals, thin foil specimens for TEM were first prepared by mechanical means having less than 100 μm thick and then 3 mm diameter cylinder disc was extracted by punching from the middle region of each thinned weld metal. The 3 mm diameter cylinder disc was then polished down to a thickness of 20

µm using a dimple grinder and diamond pastes. The final thin foil was carried out by ion milling in a Philips CM-12 ion mill. Thin foils were examined in JEOL 2100 at 80-200 kV **(Fig. 4.15)** and structures were taken from the different positions at different magnification.

Fig.4.15: Transmission electron microscopy

4.7.6 XRD analysis

X-ray diffraction of weld metals and base metal were recorded using an X-ray Diffractometer (Bruker D8 ADVANCE A25 with Texture Cradle) **(Fig.4.16)** using Co-Kα radiation. The range of angle scanned varies from 30° to 110° with a step speed of 0.2°/min. The diffraction peak was finally analyzed with the help of standard JCPDS software.

Fig.4.16: X-ray diffractometer (Bruker D8 ADVANCE A25)

4.7.6.1 Calculation of retained austenite, bainitic ferrite and carbon content of austenite

X-ray diffraction (XRD) analysis was performed to estimate the volume fraction of retained austenite and its carbon content using anode Co–K_α radiation in 1.79026 targets with 24 kV and tube current was 40 mA. The specified 2θ range was varied from 30º to 110º with a step size of 0.2º/min. Detailed XRD analysis was performed using integrated intensities of the positions and the integrated intensities for the {1 1 1}, {2 2 0} and {3 1 1} planes of FCC austenite as well as the {1 1 0} and {2 1 1} planes of BCC ferrite. The volume fraction of retained austenite was calculated using the following empirical formula **[5]**:

$$X_\gamma = \frac{I_\gamma / R_\gamma}{(I_\gamma / R\gamma) + (I_\alpha / R_\alpha)} \quad \text{..... (4.3)}$$

Where I_γ and I_α are the integrated intensities and R_γ and R_α are the theoretical relative intensity for the austenite and ferrite, respectively, and Bainitic ferrite was calculated by using the formula:

$$X_\gamma + X_\alpha + X_g = 1 \text{..... (4.4)}$$

Where, X_γ , X_α and X_g represents the volume percentage of retained austenite, volume percentage of bainitic ferrite and the volume percentage of graphite. The carbon concentration of the austenite was determined using the equation **[5]**:

$$a_\gamma = 0.3548 + 0.0044C_\gamma \quad \text{..... (4.5)}$$

Where a_γ is the lattice parameter of austenite (in nm) and C_γ is the carbon content of austenite (in wt. %). The {111}, {220} and {311} planes of austenite were used to estimate the lattice parameter.

4.8 Mechanical testing

4.8.1 Microhardness

Vickers microhardness test of traverse welded samples across the weldment (before and after austempering) was performed at room temperature using Leco microhardness tester (Model LM 248SAT) (**Fig.4.17)** with 100 gf load at 10s holding. The average microhardness values of the entire as-welded and heat treated samples were calculated. In each conditions hardness were taken at the six different positions of the weld metal and an average of six hardness values have been reported.

Fig.4.17: Vickers microhardness tester

4.8.2 Tensile test

Tensile properties of the welded joints using with and without Ce containing electrodes, with respect to their ultimate tensile strength (UTS), yield strength (YS) and percentage of elongation (%El) were evaluated using transverse flat tensile test specimens as per ASTM E8M standard **[6] (Fig.4.18)**. The tensile test was performed using a Universal

Tensile Testing Machine (Instron 8862) of 100 kN capacities at a crosshead speed of 5 mm/min shown in **Fig.4.19**. The transverse tensile specimens were held in the grip and a monotonically increasing displacement and load were applied by the actuators. The load and displacement histories were simultaneously recorded during the test. Tests were terminated when two components of the specimen were completely separated. At each conditions 3 no's of samples were tested and average of the three was considered as representative one.

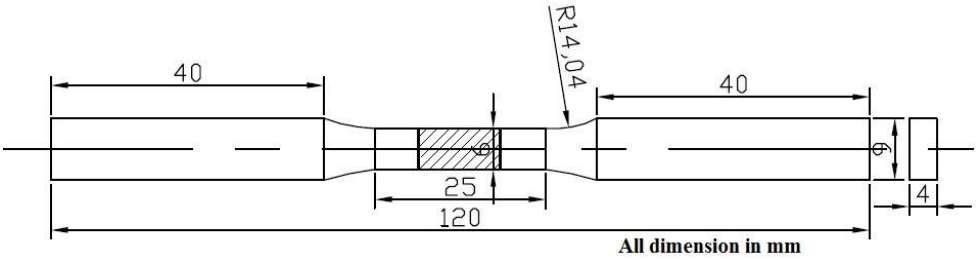

Fig.4.18: Schematic of transverse tensile test sample as per ASTM E8M **[6]**

Fig.4.19: Servo-electric Instron 8862 M/C

4.8.3 Charpy impact test

Transverse sub-size (55 x 10 x 3.3mm) charpy impact specimen without notch as shown schematically in **Fig.4.20** from ADI welded joints was tested at room temperature as

per ASTM E-237 M **[7]**. Four samples were tested at each austempering temperature and an average of four toughness values has been reported.

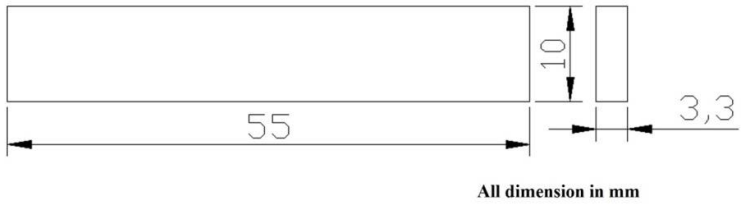

Fig.4.20: Schematic of sub size without notch transverse charpy impact sample as per ASTM E 237M **[7]**

4.8.4 Fatigue test

High cycle fatigue (HCF) test of traverse welded samples as shown schematically in Fig. **4.21** were performed as per ASTM E466-15 **[8]** using a Rumul resonant testing machine (**Fig. 4.22**) to determine the S-N curve. The tests were run to failure up to 10^7 cycles at constant stress control mode and the number of cycles of failure was recorded with keeping the load ratio R=0.1. The stress levels were varied from 30% to 80% of the yield strength to obtain the endurance limit and S-N curve was plotted by stress amplitude and the number of cycles in log-log scale.

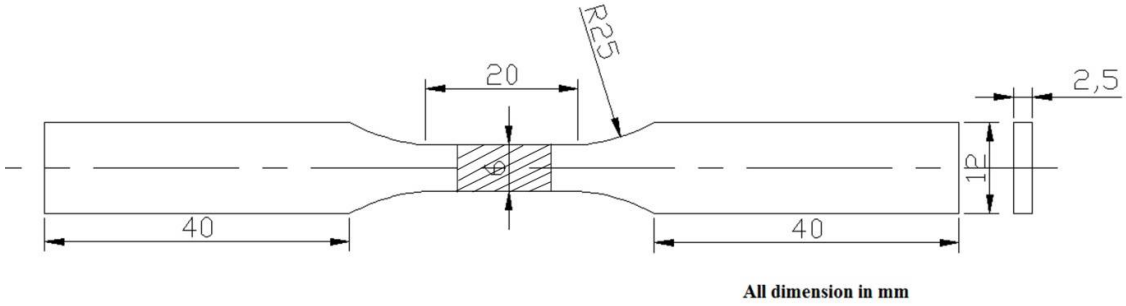

Fig.4.21: Schematic of transverse high cycle fatigue sample as per ASTM 606**[8]**

Fig.4.22: RUMUL resonant testing machine

References

1. D. Sun, Z. Zhou, Z. Zhao, "Development of a New Electrode for Arc Welding of Austempered Ductile Iron (ADI)", Chin Met Sci Technol, (1992) 401-405
2. D. Q. Sun, W. Q. Wang, Z. Z. Xuan, Z. A. Ren, D. X. Sun, "Transformation characteristics, microstructure and mechanical properties of austempered ductile iron welds", Materials Science and Technology, 23(1) (2007) 92-96
3. Guide for Welding Iron Castings: "ANSI/AWS D11.2-89 (R2006)", An American National Standard Institute, (1988) 52-54
4. B. I. Imasogie, U. Wendt, "Characterization of graphite particle shape in spheroidal graphite iron using a computer-based image analyzer", Journal of Minerals and Materials Characterization and Engineering, 3(1) (2004)1-12
5. B. D. Cullity, "Elements of X-ray Diffraction", Addison-Wesley Publishing Company Reading MA, (1978) 32-106
6. ASTM E8/E8M-13, "Standard Test Methods for Tension Testing of Metallic Materials", ASTM International, West Conshohocken, PA, (2013), www.astm.org
7. ASTM E327M, "Annual Book of ASTM Standards", vol. 01.02, (1991)138–139.
8. ASTM E466-15, "Standard Practice for Conducting Force Controlled Constant Amplitude Axial Fatigue Tests of Metallic Materials", ASTM International, West Conshohocken, PA, (2015), www.astm.org

Results & Discussion

Chapter 5

Study on as-welded and austempered microstructures and mechanical properties of ductile iron weldment using developed electrode

5.0 Introduction

In this chapter, results of weld deposits using trial electrodes have been discussed followed by as-welded microstructures of groove weld DI joint which was made using one selected electrode among the six different developed electrodes based on deposit chemistry (close to the target composition). Finally influences of austempering temperature and time on microstructure of each zone of the weldment i.e. weld metal, PMZ, HAZ and base metal and mechanical properties have been discussed. It is to be noted that for successful utilization of ADI as- welded structures/components, in addition to the development of suitable electrode, more understanding about the effect of austempering heat treatment on the microstructures and properties of all the three zones i.e. weld metal, HAZ (PMZ could not be distinguished from HAZ) and base metal of the ADI weldment as composite material, is of utmost important for integrity of the ADI joint.

The groove weld DI joints were made using established weld procedure as per standard AWS (D11) and then weldments were first austenitized at 900°C for 2 h holding time, followed by austempering heat treatment at two different temperatures, i.e. 300°C and 350°C for three different holding time i.e. 1.5 h, 2 h and 2.5 h. Detail microstructural characterization, phase analysis, microhardness and mechanical properties of ADI welded joints have been performed. Microstructural analysis was done by optical microscopy (OM) and scanning electron microscope (SEM), phase analysis was done by XRD and EDS analysis and mechanical properties of the welded joints were evaluated by hardness, transverse tensile testing and charpy impact toughness.

5.1 Results and Discussion

5.1.1 Approach towards development of coated electrode for DI

It is well established that two factors play an important role in controlling the microstructure at the eutectic and eutectoid transformation during DI welding **[1]**. Thus to control the microstructure of DI weld two approaches are being emerged when developing electrode for DI. One approach is to the formation of sufficient amount of graphite nodules in the weld zone with carbide free matrix structure with the addition of graphitizing and nodularizing agent in the flux composition. The second approach is to produce a tough, relatively soft austenite based weld metal. However, the second approach which aims to form a fully austenitic structure, is not suitable to fulfil the objective of the present work i.e. response of austempering heat treatment, as austenite which is stable at room temperature,

could not be transformed to any other structure. Therefore, in the present investigation, the first approach has been followed to develop coated electrode for DI. It is worth mentioning here that the weldability of DI depends on its original matrix microstructure **[2-3]**, chemical composition of the filler metal **[3-4]**, mechanical properties, welding process, preheat and post weld heat treatment **[3, 5]**.

5.1.2 Chemical composition of weld deposits using developed electrodes

The flux composition (coating) of developed electrodes has been formulated with a view to achieve the target chemical composition of the weld deposits as the core wire contains very lower amount of carbon, silicon and other elements. Accordingly, alloying elements and other ingredients were added in the coating in the form of ferro-alloys or metallic powders. For example, graphite powder was added to the flux composition to increase carbon content in weld deposit and Fe-Si was added to stabilize the function of graphite and also to prevent the formation of carbide in the weld metal. Al powder and Fe-Ti were added as a strong deoxidiser to react with oxygen. The purpose of adding Fe-Mo, Cu and Ni powders is to increase the austemperability and hardenability of weld metal.

The chemical compositions of weld deposits (from chemical pad) using six no.s of developed electrodes are given in **Table 5.1**. Among all the six developed electrodes, only Trial 4 electrode was selected for further study due to very closeness of the target chemical composition (3.7%C, 3.4%Si, 0.4% Mn, 0.23% Cu, 0.7% Ni, 0.5% Al) **[6-7]**.

Table 5.1 Chemical composition of weld deposits using different developedcoated electrodes

Element wt. %	C	Si	Mn	S	P	Ni	Mo	Cu	Al	Bi	Mg	Ca	Ti
Trial 1	2.61	2.79	0.41	0.007	0.13	0.12	0.05	1.32	0.29	0.03	0.002	0.5	0.05
Trial 2	1.80	3.34	0.44	0.003	0.009	0.85	0.42	0.37	0.64	0.002	0.001	0.008	0.18
Trial 3	3.1	2.45	0.43	0.005	0.017	0.61	0.26	0.25	0.49	0.02	0.005	0.008	0.005
Trial 4	**3.08**	**2.60**	**0.40**	**0.006**	**0.039**	**0.5**	**0.19**	**0.24**	**0.62**	**0.03**	**0.004**	**0.015**	**0.09**
Trial 5	1.77	3.40	0.44	0.004	0.007	0.61	0.27	0.30	0.44	0.025	0.018	0.007	0.13
Trial 6	1.99	3.65	0.44	0.008	0.017	0.66	0.19	0.17	0.30	0.004	0.0005	0.004	0.24

The final chemical composition of weld deposits obtained from coated electrode is mainly determined by the slag-metal reactions that occur in the weld pool **[8-11]**. The recovery of alloying elements in the weld deposits mainly depends on the extent of losses in slag metal reactions or to the welding fume. In fact, the available oxygen is one of the ingredients acting

to reduce alloy recovery in the weld deposits. The important concept related to the various chemical reactions that occur during welding with coating (flux) of the electrode is the 'basicity of the slag' or 'basicity index' **[12-13]**. Basicity index is an empirical index developed to describe the metallurgical behaviour of the slag. Higher basicity fluxes generally results in welds of lower oxygen content.

In a basic coated electrode, calcite decomposition results in the atmosphere consisting predominantly of carbon monoxide and carbon dioxide, which cause extensive absorption of carbon and oxygen in the weld deposit. Since carbon is a much stronger deoxidant than silicon and aluminum **[14]**, it can control oxygen levels as per the following reaction:

$$[C] + [O] = CO\ (gas) \ldots\ldots\ldots\ldots\ldots\ldots \textbf{(5.1)}$$

However, carbon oxidation gradually becomes suppressed during cooling, and the deoxidation capacity of silicon and aluminum increases rapidly with decreasing temperature. It is apparent from **Table 5.1** that, manganese content of the weld deposits produced from all the six trial electrodes is more uniform. This is expected as manganese has been transferred from core wire only, not from the coating (flux). In case of silicon, it can be stated that silicon content in the weld deposit increased **(Table 5.1)** with increasing addition of ferrosilicon in the flux **(Table 4.1)**. However, the silicon content in the weld deposit has been reported to be affected not only by the basicity of the flux but also by the aluminum content of the electrode. The silicon content in the weld deposit can increase due to the following reaction **[9]**.

$$4Al + 3SiO_2 = 3Si + 2Al_2O_3 \ldots\ldots\ldots\ldots\ldots\ldots \textbf{(5.2)}$$

Generally, very little nickel or copper is lost to the slag during welding since these metals are less prone to oxidation than iron, silicon, and aluminum. Addition of nickel powder in coating from 0.5% (Trial 1) to 3.5% increases nickel content in the weld deposits. Except Trial 2 electrode nickel content is more or less close to weld deposits of other electrodes. Similarly copper in weld deposits is shown to decrease with decreasing copper powder addition from 5% to 1.5% in the coating. But in case of molybdenum, Trial 1 electrode where maximum amount of Mo powder (0.4%) has been added in coating shows very low Mo content (0.05%) in the weld deposit. Since molybdenum has got high affinity for oxygen, more loss due to oxidation took place probably due to presence of insufficient amount of strong deoxidizer such as Al (4%). However, the flux complexicity of the welding environment, non-equilibrium behaviour of the reactions as well as competitive reactions occurring in the weld pool, make difficult to justify the variation of each alloying element of weld deposits produced from six different developed electrodes.

5.1.3 Base metal microstructure

The optical and SEM microstructures of the as-received DI are shown in **Fig.5.1 (a) & (b)** respectively. Microstructure consists of graphite nodules surrounded by ferrite matrix. The average measured graphite nodularity is approximately 90%. There are 130 nodules per unit area (mm^2) and the average nodule size (r) = 18.43µm. The recommended minimum nodule count and nodularity for ductile iron to be austempered are as follows: Nodule Count $100/mm^2$ (with uniform distribution) Nodularity 85% **[15]**. Thus base metal fulfilled the minimum requirement towards responding isothermal heat treatment.

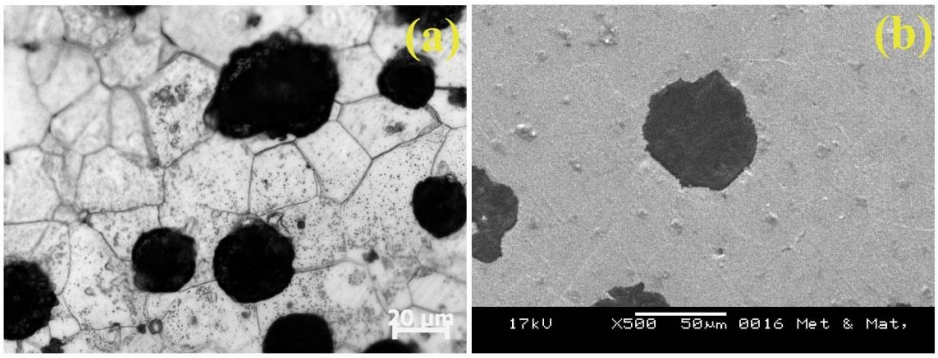

Fig.5.1: Microstructure of as-cast DI by (a) optical and (b) scanning electron microscopy

5.1.4 Microstructure of weldment before austempering

The microstructures of different zones of the as-welded DI weldment have been represented schematically in **Fig.5.2** with the help of iron-carbon phase diagram **[16]**. Typical microstructure of weldment (weld metal, PMZand HAZ) of groove weld using developed electrode (Trial 4) is shown in **Fig.5.3 (a, b)**. The microstructure of weld metal **(Fig.5.3a)** shows ledeburitic carbide, alloyed pearlite (alloyed pearlite is formed when the alloy addition usually do not effect first stage graphitization but serve as carbide stablllzers during the eutectoid range or subeutectold tempering treatment) and graphite nodules. **Fig.5.3b** shows microstructures of PMZ and HAZ. PMZ forms next to the weld metal (WM) as a boundary to HAZ. Microstructures formed in PMZ are similar to weld metal, e.g. ledeburitic carbide and alloyed pearlite with graphite nodules. However, ledeburitic carbides are coarser as well as lesser in amount and graphite nodules are larger in size. In PMZ, the portion of the matrix of the base metal near the primary graphite nodules melted during welding, while the remainder of the matrix transformed to austenite. Both the liquid and austenite were enriched with carbon by partial solution of graphite leading to structure close to weld metal. Similarly the

microstructures of HAZ exhibited pearlite, cementite delineating the prior austenite grain boundary along with graphite nodules. Some portion of HAZ experienced temperature above the critical temperature forming austenite and simultaneously some amount of carbon from graphite nodules may dissolve in austenite. During faster cooling of weld thermal cycle carbon enriched austenite transforms to pearlite and excess carbon precipitated as cementite on the prior austenite grain boundary.

Essentially microstructure of weld metal shows higher amount of ledeburitic carbide with some alloyed pearlite in the matrix. As far as graphite morphology is concerned maximum number of graphite nodules per unit area (280 nodules per mm^2) with smaller graphite size (r = 6.72 µm) and graphite nodularity of 72% are obtained in weld metal compare to HAZ (95 nodules per mm^2 with 78% nodularity with larger graphite size r =16.92 µm) and base metal (130 nodules per mm^2 with 90% nodularity with larger graphite size r = 18.43 µm). The differences in graphite size, no.s per mm^2 and nodularity among weld metal, HAZ and base metal are mainly due to differences in cooling rate. Faster cooling rate due to weld thermal cycle attributed finer and more no's of graphite nodules and lower nodularity compare to base metal which experienced slower cooling during casting. Whereas, in HAZ which is basically the base metal experienced weld thermal cycle above Ac1 during welding, it is reasonable to consider that some amount of carbon from graphite has been dissolved resulting in smaller graphite size, increased the gap between two nodules and lesser nodularity compared to a base metal due to relatively faster cooling than base metal.

Since the carbon content of the weld metal is well below the eutectic carbon content, solidification begins by the formation of austenite and as the temperature falls as shown in **Fig. 5.2** primary austenite will solidify and its composition moves down towards the solidus line. At the eutectic temperature, the alloy will consist of austenite dendrites containing about 2% C and remaining liquid will contain 4.3% C. The liquid thus undergoes the eutectic reaction isothermally appeared as a coarse mixture rather than the fine mixture typical of many eutectics. It is not unusual for ledeburite to be separated completely, with the eutectic austenite added to the primary austenite dendrites, leaving behind a layer of massive, free cementite as shown in **Fig.5.3a**. As the temperature falls, the solubility of carbon in austenite decreases. This causes precipitation of pro-eutectoid cementite, most of which is deposited upon the cementite already present. At the eutectoid temperature, the remaining austenite undergoes the eutectoid reaction to form pearlite.

Since silicon shifts the graphite eutectic line upwards **[17]** Trial 4 electrode having higher Si content should shift the austenitic eutectic line more upwards. Thus, during cooling from the

liquid state, a large degree of under cooling is possible with greater chances to form austenite, before cementite formation becomes feasible.

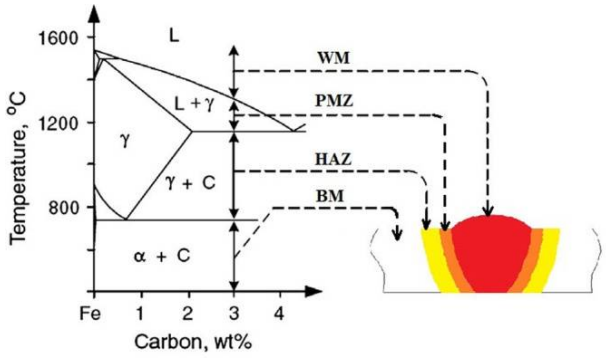

Fig.5.2: Schematic diagram of the various microstructural zones of the DI weldment **[16]**

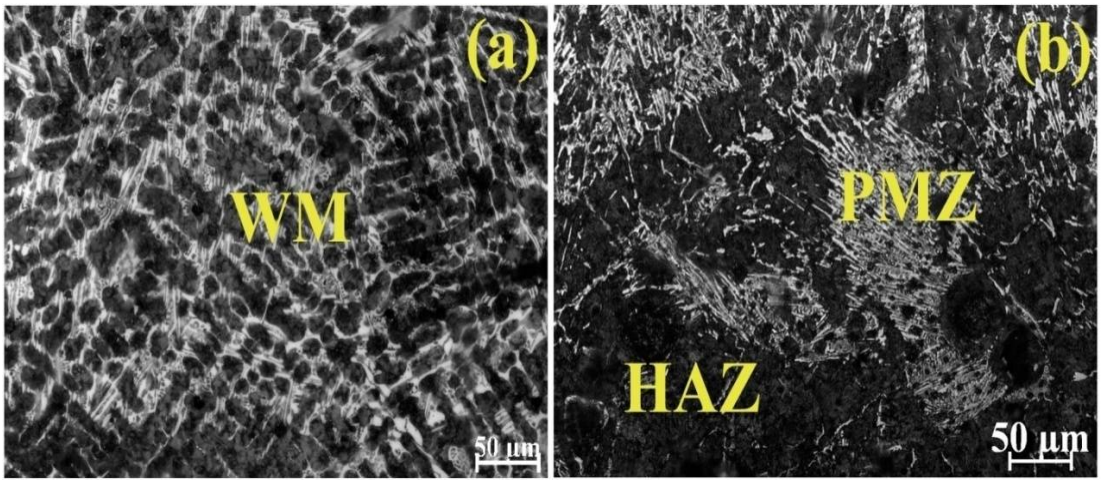

Fig.5.3: Optical microstructures of PWHT DI weldment (a) weld metal (b) PMZ with HAZ using Trial 4 electrode

5.1.5 Microstructure of weldment after austenitization

During isothermal heat treatment carbon content of austenite is the driving force for stage I reaction **[18]** and thus understanding the effect of initial matrix structure as well as graphite nodules in each zone (weld metal, HAZ and base metal) of weldment on characteristic of austenite during austenitization is important. Accordingly, as-welded DI weldment was austenitized at 900°C for 2 h holding time and quenched into ice water. The optical microstructures of different zones in weldment after austenitization are given in **Fig.5.4**. Microstructures of all the three zones (weld metal, HAZ and base metal) in weldment show martensite, retained austenite with graphite nodules. The amount of retained austenite in weld metal and base metal after ice water quenching was evaluated from X-ray diffraction analysis **(Fig. 5.5)** and the results are given in **Table 5.2**.

The microstructure of weld metal **(Fig.5.4c)** shows very finer martensite with higher amount of retained austenite (26.38%), whereas the base metal microstructure (**Fig.5.4a**) shows coarser martensite with lesser amount of retained austenite (18.29%). The microstructure of HAZ (**Fig.5.4b**) shows more or less similar microstructure as base metal. However, the amount of retained austenite could not be evaluated from XRD in HAZ. The microhardness was taken on all the three zones (base metal, HAZ and weld metal) of weldment after ice water quenching from austenitizing temperature in order to confirm about the microstructural features. The results of microhardness of all the three zones i.e. base metal (avg. 691.58 Hv), HAZ (avg. 669.02 Hv) and weld metal (avg. 565.96 Hv) clearly reflect the matrix structure of different zones. For example, higher hardness of base metal compare to weld metal is due to more amount of martensite and lesser amount retained austenite compare to weld metal (18.29% in base metal and 26.38% in weld metal). Since hardness of HAZ is lower than base metal, it could be stated that amount of retained austenite is higher in HAZ than base metal.

During austenitization, the nucleation of austenite occurs at the ferrite/graphite or ferrite/cementite interface **[19]**. The base metal having fully ferrite matrix structure, only ferrite/graphite interface is available for nucleation of austenite. Whereas, in case of weld metal with finer ledeburitic carbide and alloyed pearlite matrix structure both pearlite/ graphite or pearlite/cementite interfaces are available for nucleation of austenite. This probably has caused not only finer austenite in weld metal due to increased no. of sites for nucleation, but also higher rate of transformation due to lesser diffusion distance compared to only ferritic matrix in base metal **[20]**. This has ultimately caused quick transformation to austenite as well as enrichment of carbon in austenite in weld metal than base metal leading to the formation of relatively more amount of retained austenite in weld metal.

As far as graphite morphology is concerned, a significant change after austenitization for all the three zones of weldment has been noted. From **Table 5.3**, it is clearly apparent that graphite size (r = 6.72 μm) decreased and number of graphite nodules per mm^2 (280) and nodularity (72%) in weld metal have increased from the initial state of weld metal (average graphite size r = 5.35μm, 293 nodules per mm^2, and nodularity 77%). Similar is the case for base metal. That means both graphite nodule size (r =16.8 in μm), nodules per mm^2 (100) and nodularity (83%) in base metal have decreased from the initial state of base metal (nodule size r =18.43, 130 nodules per mm^2 and nodularity 90%). This clearly indicates that carbon has diffused into austenite from the graphite nodules in both weld metal and base metal resulting in decrease in nodules size. However, the changes in size and no.s of graphite after austenitization is relatively more in base metal probably due to the fact that graphite is the

only source of carbon in base metal; whereas in weld metal both graphite and ledeburitic carbide contributed carbon during austenitizing. This is not unexpected as retained austenite content is more in weld metal than base metal which indicates more carbon has been diffused into austenite from the two microstructural constituents of initial weld metal and probably reached to an equilibrium stage. Improved nodularity in weld metal and decrease nodularity in base metal after austenitizing reflects the carbon saturation in austenite in case of weld metal. On the other hand, HAZ reveals very little change in graphite morphology which shows nodule size of r = 16.6 μm, 88 nodules per mm^2 and 76% nodularity after austenitization.

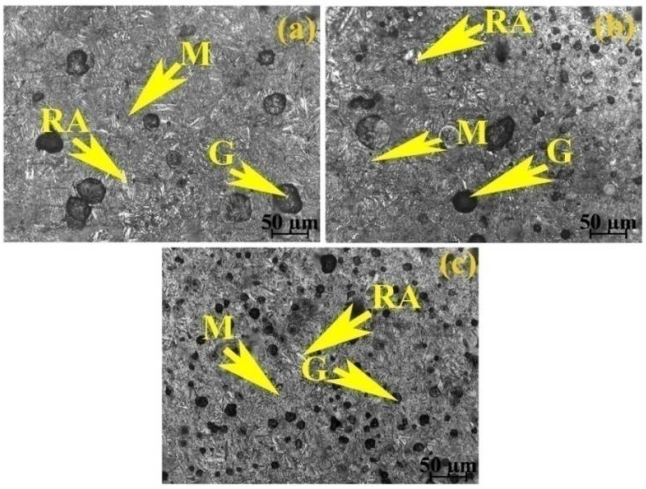

Fig.5.4: Optical microstructures of austenitized weldment (900°C for 2 h) (a) base metal (b) HAZ and (c) weld metal

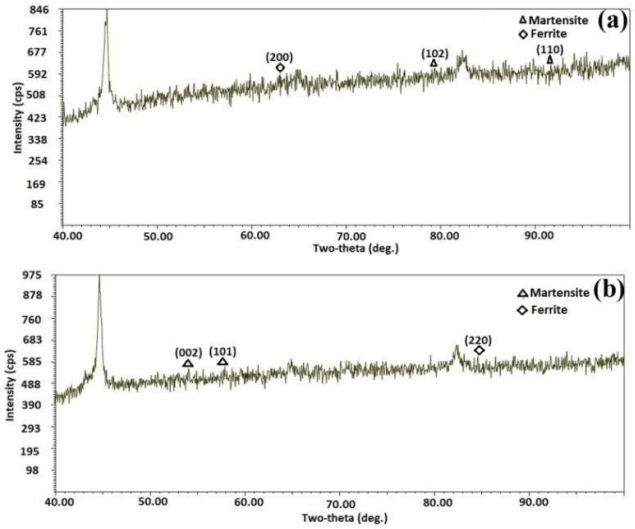

Fig. 5.5: Typical X-ray diffraction pattern after austenitization at 900°C for 2 h holding time (a) weld metal, (b) base metal

Table 5.2 Microstructural constituents of weldment after austenitization

Weld metal			Base metal		
Retained austenite (vol %)	**Martensite (vol %)**	**Microhardness (Hv)**	**Retained austenite (vol %)**	**Martensite (vol %)**	**Microhardness (Hv)**
26.38	73.62	565.96	18.29	81.71	691.58

Table 5.3 Nodularity, nodule size and no.s of nodules per unit area of different zones of weldment before and after austenitization

	Before Austenitization			After Austenitization		
	Nodularity %	Nodule size (r) μm	Nodules per unit area (mm^2)	Nodularity %	Nodule size (r) μm	Nodules per unit area (mm^2)
Weld metal	72	6.72	280	77	5.35	293
Base metal	90	18.43	130	83	16.80	100
HAZ	78	16.92	95	76	16.60	88

5.1.6 Microstructure of weldments after austempering

The microstructures of weld metals after austempering at 300°C and 350°C for 1.5 h, 2 h and 2.5 h holding time are shown in **Fig.5.6**. **Fig.s 5.6 a1, a2, a3** represent the microstructures of weld metals austempering at 300°C for 1.5 h, 2 h and 2.5 h respectively. Similarly, the microstructures of weld metals austempering at 350°C at 1.5 h, 2 h and 2.5 h are presented in **Fig.s 5.6 b1, b2, b3** respectively. For better clarification, the microstructures of weld metals were observed under SEM and are shown in **Fig. 5.9**. After austempering microstructures of the weld metals show bainitic ferrite, retained austenite and graphite nodules. However, significant variation in morphology and amount of the phases as well as morphology of graphite including graphite nodule size and nodularity has been noted with austempering temperature and holding time for a given temperature. At lower austempering temperature (300°C) microstructure shows lower (needle shape) bainitic ferrite and higher austempering temperature (350°C) microstructure shows upper (feathery shape) bainitic ferrite. Also at 350°C volume fraction of bainitic ferrite decreased and volume fraction of retained austenite and nodule count increased. Whereas, opposite effect is observed at 300°C i.e. volume fraction of bainitic ferrite increased and volume fraction of retained austenite and nodule count decreased. Again, at a given austempering temperature, the proportion of microstructural constituents changed with holding time. Interestingly, the trend in changing the proportion of microstructural constituents with holding time is identicalfor both 300°C and 350°C, i.e. bainitic ferrite first decreases from 1.5 h to 2 h and then increases from 2 h to

2.5 h. Also, for both the austempering temperatures (300°C and 350°C) the carbon enrichment in austenite is maximum at 2 h holding time **(Fig.5.13)** and thus higher carbon content at 2 h holding time has attributed to stabilize more amount of retained austenite **(Fig.5.12)** after cooling to room temperature. However, beyond 2 h holding time i.e. at 2.5 h the carbon enrichment in austenite has decreased. This has caused decreasing the stability of austenite leading to lower amount of retained austenite at 2.5 h. The unstable austenite latter transformed to bainitic ferrite and carbide (ε carbide) as shown in the microstructure **(Fig. 5.6 a3, b3**).

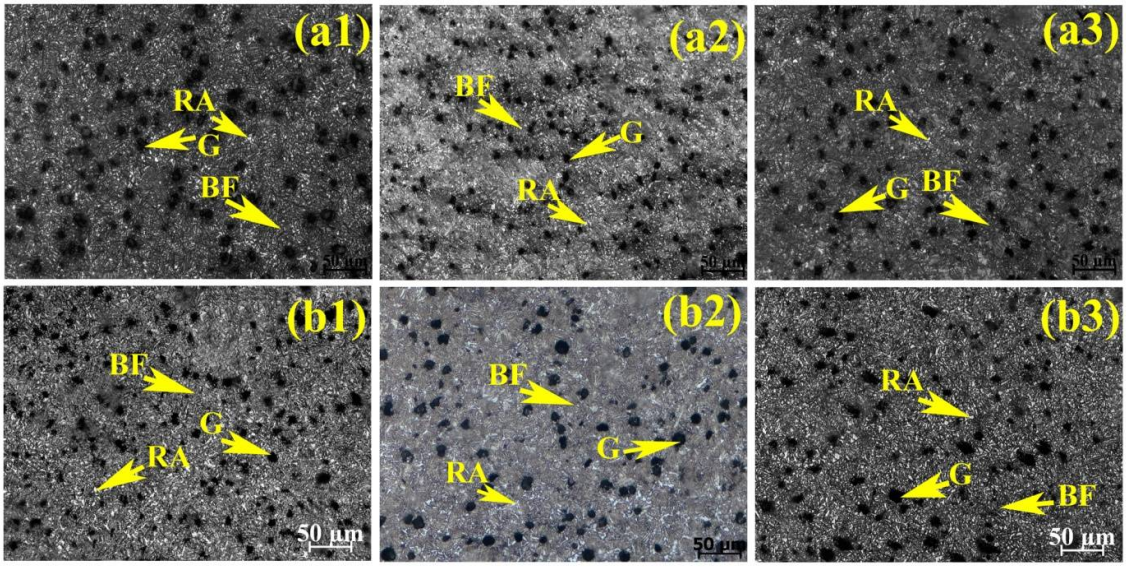

Fig.5.6: Optical microstructures of weld metals after austempering at 300°C for (a1)1.5 h, (a2) 2 h, (a3) 2.5 h and 350°C for (b1) 1.5 h, (b2) 2 h, (b3) 2.5 h holding time

Like weld metal, HAZ and base metal also responded austempering heat treatment at both austempering temperatures (300°C and 350°C for 1.5, 2 and 2.5 h holding time). **Fig. 5.7** and **Fig. 5.8** show the austempered microstructures of HAZ and base metal at 300°C and 350°C respectively for 1.5, 2 and 2.5 h holding time respectively. The microstructures of both HAZ and base metal show bainitic ferrite with retained austenite and graphite nodules similar to weld metal. However, the microstructure of base metal shows coarser bainitic ferrite and retained austenite than HAZ. Also difference in shape and size of bainitic ferrite and morphology of graphite nodules has been observed. With changing austempering temperature from 300°C to 350°C the size of the graphite nodules as well as graphite nodularity change in both HAZ and base metal. Compared to weld metal, the size of graphite has increased, but graphite nodularity has decreased in HAZ [at 300°C for 2 h shows graphite size r =16.6 µm with 74% nodularity and 74 nodules per unit area (mm^2), at 350°C for 2 h shows size r =

16.10 µm with 74% nodularity and 78 nodules per unit area (mm^2)]; where as in base metal the graphite size is largest and graphite nodularity is higher than weld metal and HAZ [at 300°C for 2 h shows r =16.6 µm with 82% nodularity and 91 nodules per unit area (mm^2); at 350°C for 2 h shows r =16.50 µm with 85% nodularity and 100 nodules per unit area (mm^2)].

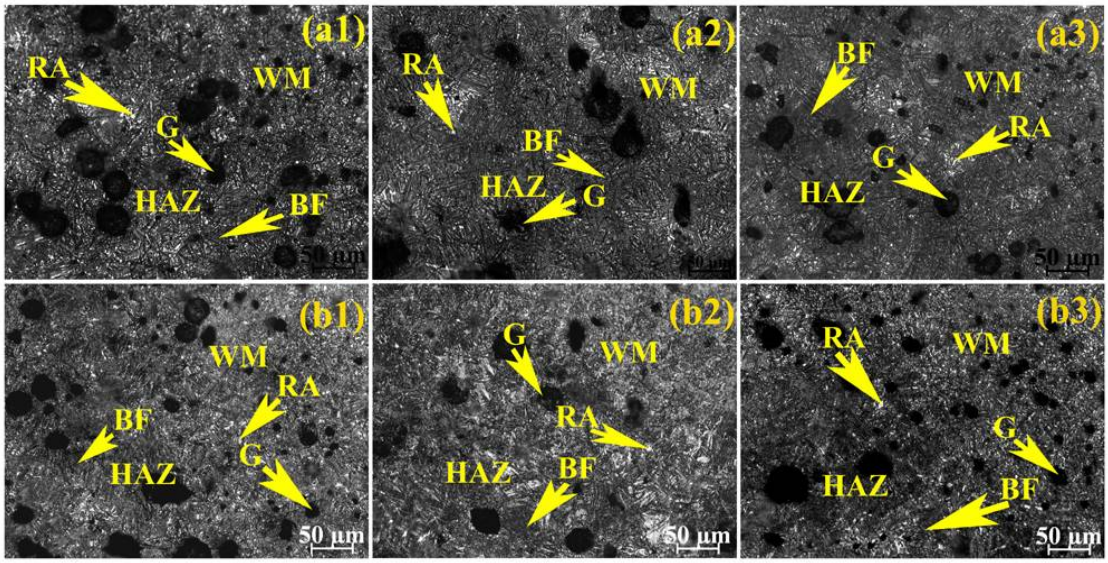

Fig.5.7: Optical microstructures of HAZ after austempering at 300°C for (a1)1.5 h, (a2) 2 h, (a3) 2.5 h and 350°C for (b1) 1.5 h, (b2) 2 h, (b3) 2.5 h holding time

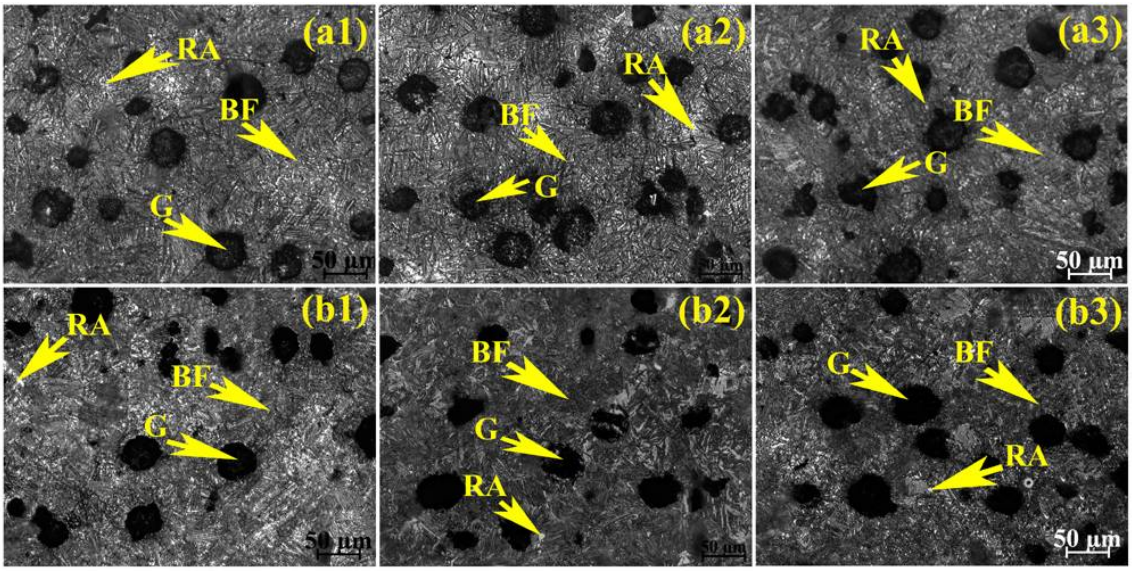

Fig.5.8: Optical Microstructures of base metal after austempering at 300°C for (a1)1.5 h, (a2) 2 h, (a3) 2.5 h and 350°C for (b1) 1.5 h, (b2) 2 h, (b3) 2.5 h holding time

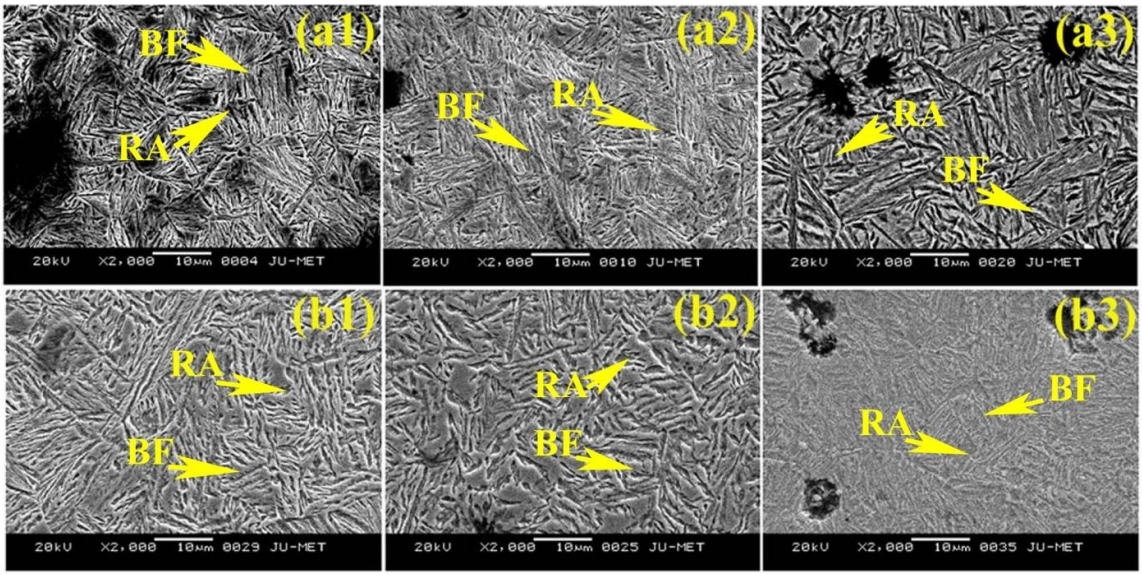

Fig.5.9: Scanning electron micrographs of weld metals after austempering at 300°C for (a1)1.5 h, (a2) 2 h, (a3) 2.5 h and 350°C for (b1) 1.5 h, (b2) 2 h, (b3) 2.5 h holding time

It is well established that austempering is a two stage heat treatment process **[18]**. At stage I austenite (residual austenite) decomposes into bainitic ferrite and high carbon austenite (retained austenite). Increasing holding time the stage II reaction starts and high carbon austenite further decomposesinto bainitic ferrite and carbide **[18]**.

Since the driving force for stage I of austempering increases with decrease of carbon content in initial austenite **[18-19]**, base metal containing lesser amount of carbon content (0.74 wt. %) in initial austenite will attribute more bainitic ferrite by rejecting carbon to the residual austenite and thus consume more amount of residual austenite. However, remaining less residual austenite will be enriched with carbon and will be stable at room temperature as retained austenite. Whereas weld metal having more carbon (1.01wt. %) will form lesser bainitic ferrite due to lower driving force and thus lesser amount of residual austenite will be consumed. Although lesser bainitic ferrite transformation will reject relatively lesser amount of carbon in residual austenite; but because of higher carbon content in initial austenite of weld metal, total rejection of carbon by the ferrite is most likely to be sufficient to stable the remaining higherresidual austenite as retained austenite. Thus at the end of stage I i.e. at 2 h the amount of retained austenite (42.8% at 2 h at 350°C) in weld metal will be higher than that of base metal (31.1% at 2 h at 350°C). As expected, during stage II the high carbon residual austenite will decompose into bainitic ferrite and carbide **(Fig.5.6 a3, b3)** leading to decrease in amount of retained austenite.

In addition to carbon content of initial austenite, the rate of transformation to bainitic ferrite also depends on the austempering temperature, holding time and rate of super cooling **[20]**. Lower austempering temperature will result in large supercooling of austenite and at the same time the diffusion rate of carbon will be slower at lower austempering temperature. Hence, at lower austempering temperatures, the nucleation of the bainitic ferrite platelets will be favoured and will result more amount of bainitic ferrite. However, because of lower diffusion rate of carbon the bainitic ferrite will be finer. Whereas, at higher austempering temperature, the carbon diffusion rate is faster and, consequently the growth rate of bainitic ferrite is rapid. But due to small supercooling, volume fraction of bainitic ferrite will be lower and bainitic ferrite platelets will be rather large or coarse in nature. As a result lower austempering temperature (300°C) will attribute higher bainitic ferrite (53.2% at 2 h for weld metal) and lower amount of retained austenite (40.8%at 2 h for weld metal) with finer in nature (**Fig.5.6 a2**). Opposite is the case for higher austempering temperature (350°C) i.e. lower amount of bainitic ferrite (48.2% at 2 h for weld metal) and higher amount of retained austenite (42.8% at 2 h for weld metal) with coarser in nature **(Fig.5.6 b2) [22]**.

At 1.5 h holding time for a given austempering temperature, as usual transformation of bainitic ferrite will start from residual austenite and carbon will be rejected from the bainitic ferrite leading to enrichment of carbon in remaining residual austenite. If the degree of carbon enrichment of remaining residual austenite reaches to the level of its stability, residual austenite will be stable as retained austenite at room temperature. However, formation of martensite along with bainitic ferrite and retained austenite **(Fig. 5.5a)** at 1.5 h holding time indicates that bainitic ferrite transformation could not be completed resulting in lesser carbon enriched austenite which partially transforms to martensite during air cooling. This has caused lower amount of retained austenite. With increasing holding time i.e. at 2 h, the microstructure shows bainitic ferrite and higher amount of retained austenite (40.8% at 300°C and 42.8% at 350°C). This is expected as sufficient bainitic ferrite has been formed with increasing holding time and this has caused residual austenite more enriched with carbon resulting in higher amount of stable austenite. Further increasing holding time i.e. at 2.5 h amount of bainitic ferrite has increased and amount of retained austenite has decreased compare to 2 h holding time. This is only possible when austenite will partly decompose into ferrite. Actually austenite has decomposed partially into ferrite and and carbide. Similar results of decomposition of austenite into ferrite and carbide have been reported by previous investigator **[23]**.

As far as graphite morphology is concerned, the nodularity of graphite and size of graphite nodule in weld metal first increased from 1.5 h to 2 h. With further increasing holding time from 2 h to 2.5 h, graphite becomes coarser and non-spherical in shape as presented in **Table 5.4**. It is well established that the graphite nodules are nucleated on small inclusion during the solidification. In fact, during solidification graphite nodules are surrounded by austenite and growth takes place by diffusion of carbon from the austenitic cell **[24]**. Presence of alloying elements such as Ni, Mo and Mg act as nodularizing element in ADI. The results of the graphite morphology with holding time indicate that carbon has got sufficient time to diffuse and thus increased nodularity as well as size of graphite nodule from 1.5 h to 2 h. Further increasing holding time from 2 to 2.5 h diffusion of more carbon will make the graphite coarser significantly resulting in bonding only between two nearest graphite nodules which is similar to Ostwald ripening effect. However, non-spherical shape of the graphite observed at 2.5 h indicates that precipitation of carbide has taken place on the exiting graphite making the graphite shape non-spherical. It is worth mentioning here that the size, uniformity and distribution of the nodular graphite influence the strength and elongation of ADI.

EDS analysis at nodular graphite and matrix of weld metal austempered at 350°C for 2 h holding time has been performed and is given in **Fig.5.10**. The nodular graphite shows presence of Si, S, O, Mg, Cr and trace amount of Ca **(Fig.5.10b)**. Whereas, the matrix shows higher amount of Fe and Si with trace amount of S, Cr and Ca as shown in **Fig.5.10a**. Thus it is clear that Mg, as expected facilitated the nodular graphite formation by elimination of excess sulphur and oxygen.

Table 5.4 Nodularity, nodule size and no.s of nodules per unit area of different zones of Trial 4 weld metal after austempering

Austempering Temp.(°C)	Holding Time (h)	Nodularity (%)	Nodule Size (r) (µm)	Nodule per unit area (mm^2)
300	1.5	75	5.90	317
	2	78	5.82	324
	2.5	75	6.14	314
350	1.5	75	5.9	328
	2	80	5.7	330
	2.5	77	6.10	309

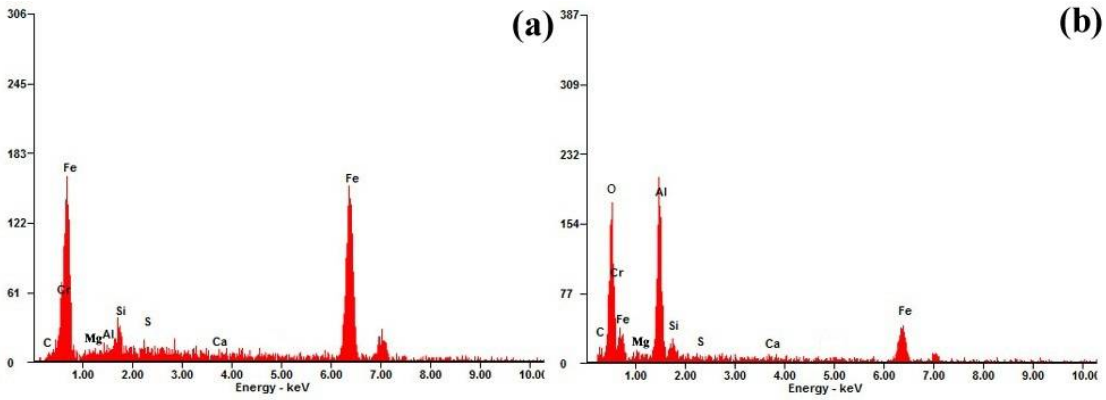

Fig.5.10: EDS analysis of weld metal (a) matrix (bainitic ferrite) and (b) nodule graphite after austempering at 350℃ for 2 h holding time

5.1.7 Retained austenite and it's carbon content

The volume percentage of retained austenite (X_γ) in weld metals and base metal after austempering and its carbon content was determined by X-ray diffraction analysis as shown in **Fig.5.11**. The effect of three different holding times (1.5 h, 2 h and 2.5 h) at two austempering temperatures (300°C and 350°C) on the volume fraction of retained austenite in weld metal has been presented in **Fig.5.12**. It is observed from **Fig.5.12** that with increasing holding time up to 2 h results in an increase in the amount of retained austenite (vol %) with simultaneous decrease in bainitic ferrite (vol %). With further increasing holding time up to 2.5 h the amount of retained austenite (vol %) decreases. This trend in changing the amount of retained austenite (vol %) with holding time is prevalent for both the austempering temperatures (300°C and 350°C) studied. However, compare to 300ºC, the amount of retained austenite (vol %) in the weld metals is higher at 350°C. This could be due to higher diffusion rate of carbon from graphite nodules at higher austempering temperature resulting in higher amount of retained austenite (vol %). Under same austempering condition base metal shows lesser amount of retained austenite (26.73% at 300°C and 31.13% at 350°C for 2 h holding time). This could be due to lower carbon content in austenite of base metal during austenitizing compare to the weld metal **[18-19]**. Also, in case of 300°C austempering temperature, higher amount of bainitic ferrite with fine needle shape microstructure was obtained compared to 350ºC austempering temperatures. This is probably due to higher supercooling and lower diffusion rate of carbon in ferrite. Whereas, relatively lower supercooling and higher carbon diffusion at 350ºCaustempering temperature, has caused higher volume fraction of retained austenite at the expense of bainitic ferrite **[25]**. It is worth mentioning here that high volume fraction of retained austenite in ADI is the desirable

microstructure for achieving optimum combination of mechanical properties **[26]**. However, it is to be noted that during cooling from austenitization to austempering temperature, transformation of austenite to pearlite has been prevented due to the presence of alloying elements such as Cu, Ni, Mn and Mo **[27]**.

Since stability of austenite depends on carbon content, the carbon content of retained austenite at different holding time has been determined from equation **(4.5)**. The measured values of carbon content in retained austenite in weld metals at two austempered conditions (both temperature and time) have been shown in **Fig.5.13**. Interestingly, the trend in variation of carbon content of retained austenite with holding time shown in **Fig.5.13** matches well with the variation of the amount of retained austenite with holding time **(Fig.5.12)**. Also, increasing the austempering temperature, the carbon content was increased. During austempering process, bainitic ferrite needles are nucleated out of residual austenite, which have lower carbon content. The remaining residual austenite absorbs the carbon and becomes sable as retained austenite with higher in amount. The maximum carbon content in retained austenite of weld metal however was achieved for 2 h holding time irrespective of austempering temperature. Therefore, it can be postulated that the change of carbon content in retained austenite is proportional to the change in amount of retained austenite (vol %) at different holding time and austempering temperatures for weld metal as well. Thus in the present investigation, it can be stated that the stability of retained austenite is higher at 2 h holding time irrespective of austempering temperature.

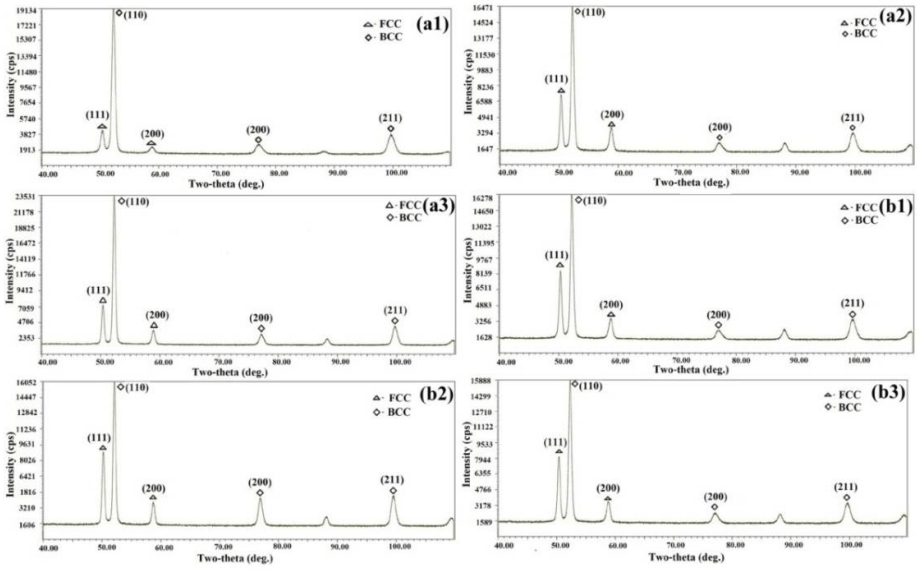

Fig. 5.11: Typical X-ray diffraction patterns of Trial 4 weld metals after austempering at 300°C for (a1) 1.5 h, (a2) 2 h, (a3) 2.5 h and 350°C for (b1) 1.5 h, (b2) 2 h, (b3) 2.5 h holding time

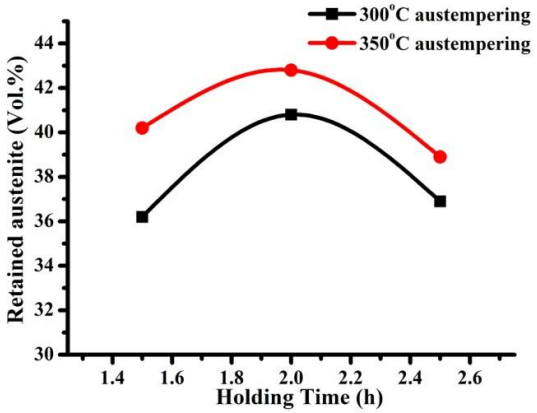

Fig.5.12: Variation of retained austenite volume percentage with different holding time at 300°C and 350°C austempering temperature for weld metal.

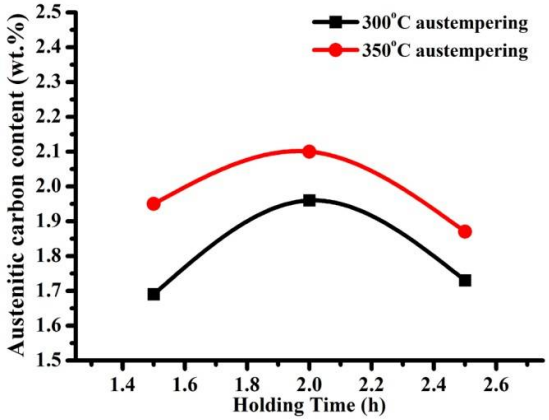

Fig.5.13: Variation of austenitic carbon content with different holding time at 300°C and 350°C austempering temperature for weld metal

5.1.8 Microhardness of weldments

Like any other welded joints hardness measurement across the weldment is one of the most common and useful method for predicting the overall performance of the weldment as composite material. Because hardness mismatch among different microstructural zones significantly affects the fracture behaviour of weldment and obviously ADI weldment is not exceptional **[28-29]**. In order to compare the hardness of each zone of ADI weldment before and after austempering, the microhardness values across the as- welded DI weldment were taken and have been presented in **Fig. 5.14(a)**. Also the microhardness values across the ADI weldment, after two austempering conditions (300°C and 350°C for 2 h holding time) are presented in **Fig. 5.14(b)**. It is clearly apparent from **Fig. 5.14(a)** that before austempering i.e.in as-welded DI weldment; weld metal shows highest hardness value and hardness values

of PMZ, HAZ and base metal are in descending order. Hardness values of different zones in weldment could be correlated with the microstructure of the respective zone. Weld metal consisting of ledeburitic carbide with some amount of alloyed pearlite based microstructure have attributed higher hardness than PMZ and HAZ which show lesser amount of coarser ledeburitic carbide and higher amount of pearlite and only pearlite respectively. The base metal being fully ferritic structure shows lowest hardness value compare to the other three zones (WM, PMZ and HAZ).

Interestingly, after austempering heat treatment opposite trend in microhardness values across the weldment has been realized. This is true for both the austempering temperatures (300°C and 350°C). The hardness of the weld metal is lowest and maximum hardness is achieved in base metal. The hardness of HAZ is in between weld metal and base metal. However, PMZ could not be distinguished from HAZ after austempering and thus it is marged with the HAZ. After austempering heat treatment, all the zones in the weldment show banitic ferrite and retained austenite. Thus relative amount of those two phases will ultimately determine the hardness value. Essentially austenite being softer phase than ferrite, higher amount of retained austenite will provide lower hardness. It is to be mentioned here that the increase in carbon content in austenite has little effect on hardness **[26]**. Thus hardness of different zones of weldments inversely correlates with the amount of retained austenite present. Weld metal having higher amount of retained austenite attributed lower hardness than base metal which shows higher amount of banitic ferrite. However, each zone of weldment austempering at 350°C reveals relatively higher amount of retained austenite and lesser amount of bainitic ferrite compare to austempering at 300°C. This has caused lower hardness of all the three zones at 350°C compare to 300°C **(Fig. 5.14 b)**.

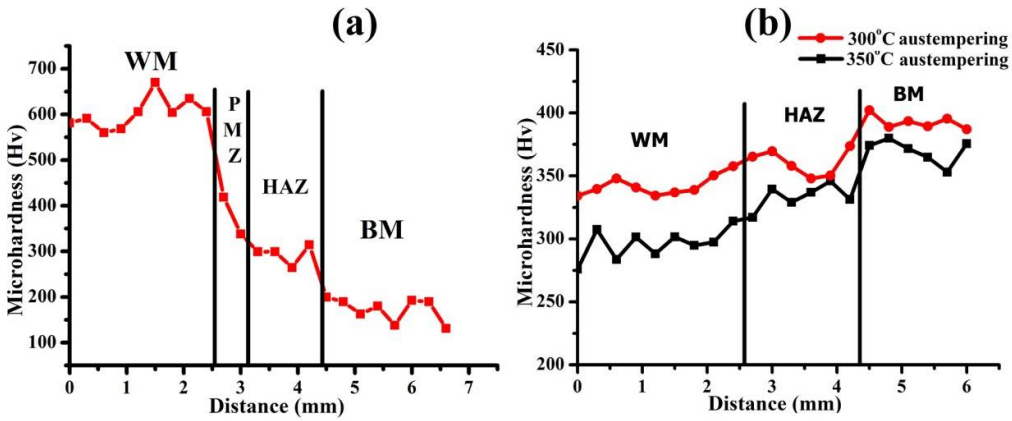

Fig. 5.14: Traverse microhardness value of the weldment (a) before austempering, (b) after austempering at 300°C and 350°C for 2 h holding time

5.1.9 Tensile properties

The transverse tensile tests were carried out for the ADI joints austempering at 300°C and 350°C for 2 h holding time. For both the austempering conditions, failure of the test samples took place from the base metal as shown in **Fig.5.15**, indicating that weld metal and even HAZ is stronger than base metal. Thus the transverse tensile results show 100% joint efficiency of ADI weld metals indicating successful development of coated electrode and establishment of a weld procedure which could be applied commercially. It has been observed that, the tensile property of the ADI depends on the ratio of retained austenite and its carbon content along with the shape of bainitic ferrite **[26]** as well as nodule size and numbers of nodule per unit area **[30]**. For the two austempering temperature studied the amount of retained austenite and its carbon content is higher and the shape and size of bainitic ferrite and size of graphite nodules are finer in weld metal compare to the base metal. Presence of higher nodularity with smaller size and higher amount of retained austenite with higher carbon content in weld metals attributed comparatively higher strength compare to the HAZ and base metal. Higher strength of higher amount of retained austenite and its carbon content is derived from higher strain hardening capacity **[26, 31]**. Interestingly, though all the failure of transverse tensile of ADI joint specimen took place from base metals, it is seen from **Table 5.5** and **Fig. 5.16** that the average YS and UTS decreased and % elongation increased with increasing the austempering temperature from 300°C and 350°C. Obviously variation of tensile properties with variation of austempering temperature is due to change in microstructure of base metal only. From the microstructure of base metal, it clearly indicates that unlike weld metal bainitic ferrite mainly controls the strength of base metal. Change from needle shaped ferrite to feathery shaped ferrite along with a relatively higher amount of retained austenite **(Fig.5.12)** with change in austempering temperature from 300°C to 350°C is largely responsible for decreasing strength and increasing % elongation **[31]**.

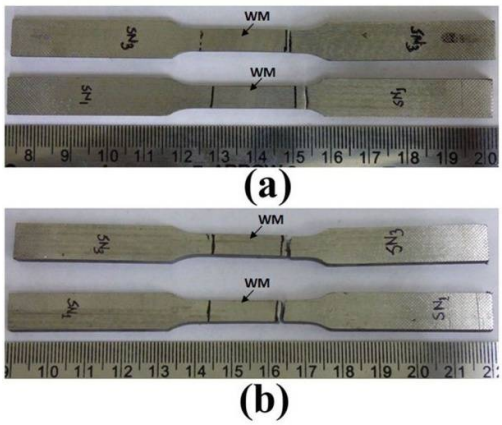

Fig.5.15: Failure location in transverse tensile weld samples austempering at (a) 300°C and (b) 350°C for 2 h holding time

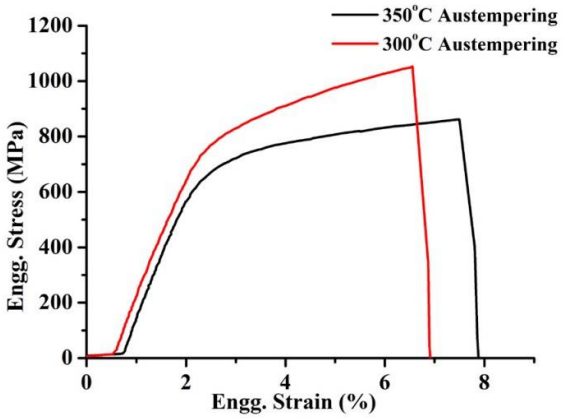

Fig.5.16: Engg. stress vs Engg. strain plot of ADI joints austempering at 300°C and 350°C for 2 h holding time

Table 5.5 Average tensile testing results of ADI joints

Austempering Temp (°C)	Holding Time (h)	Trial 4		
		UTS (MPa)	YS (MPa)	El (%)
300	2	913	700	4.32
350		857	663	6.42

5.1.10 Charpy impact toughness

The average sub-size charpy impact values of two weldments austempered at 300°C and 350°C for 2 h holding time are 20J and 26J respectively. The entire specimen brooke from weld metals which was at the middle portion of the test specimen. The results clearly show improved impact toughness of the weld metal at a higher austempering temperature. The charpy impact values are directly related to austempered microstructure of the

weldmetals. The impact toughness of ADI depends on the amount of retained austenite, austenitic carbon content, nodule size as well as nodularity and shape of the bainitic ferrite **[27]**. The presence of higher carbon content in austenite increases the strain hardening rate of austenite and consequently more energy is being absorbed leading to increase in impact toughness **[26, 31]**. Also the higher nodularity could suppress crack initiation due to lower stress concentration and increase in amount of graphite nodules could act as crack arrester during impact testing. At 350°C with 2 h, weld metal shows the maximum amount of retained austenite (42.5%) along with higher carbon content (2.1%) and smaller nodule size (r =5.7 µm) as well as higher nodularity which contributed the maximum charpy impact value compare to weld metal at 300°C for 2 h (retained austenite 39.2%) .

The freshly broken charpy impact samples were examined under SEM and the fractographs of weld metals are shown in **Fig.5.17 (a, b**, **c, d)**. In general, a typical mixture of quasi-cleavage and dimples are evident for both the weld metals. Zone of brittle fracture by intergranular decohesion is also visible (**Fig. 5.17 a, c)**. On the application of load, the matrix around the graphite deforms plastically, resulting in decohesion at the graphite/matrix and graphite/wrapped graphite interface **[27, 31]**, as shown in **Fig. 5.17 (b, d)**. It seems certain that micro crack first forms at the graphite nodules/matrix interface and may later spreads into the matrix adjacent to the graphite nodules. Besides the graphite/matrix interfacial cracking, graphite in ADI might crack. The crack, which normally initiates near the graphite nodule, propagates through the matrix to reach the adjoining nodules. Crack progation in the matrix depends on various factors, the most relevant of which being the matrix structure.

At 300°C, because of relatively small volume fraction of retainedaustenite, plastic deformation is limited primarily tothe regions near the graphite nodule. There is verylittle deformation in the intercellular regions, and small dimples are observed near the graphite nodule. Whereas at 350°C, the austempered with are relatively higher volume fraction of retained austenite, the plasticde formation has spread over the matrix, and the dimple has increased **[31-32]**.

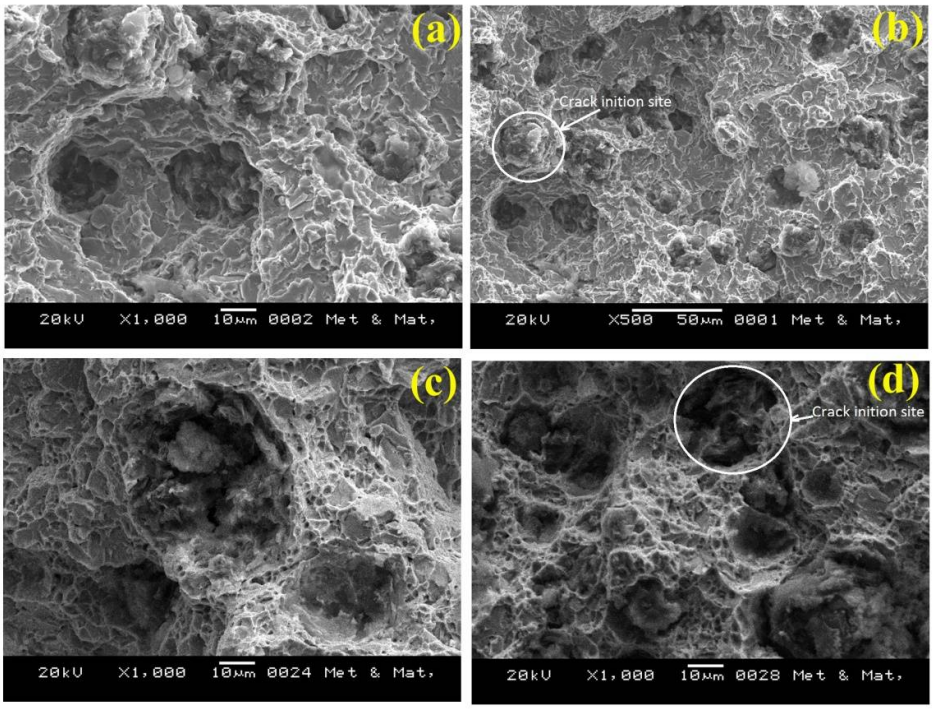

Fig.5.17: (a) fracture surfaces, (b) decohesion or crack initiation path of ADI charpy impact sample after austempering at 300°C and (c) fracture surface, (d) decohesion or crack initiation path after austempering at 350°C for 2 h holding time

5.2 Conclusions

The results obtained in this chapter lead to the following conclusions:

- It has been possible to successfully develop basic coated electrode as well as weld procedure for groove welding DI plate of 20 mm thick with modified U groove as per AWS(D11) standard. Also the weld metal responded well to isothermal heat treatment.
- The microstructure of as-welded weld metal shows ledeburitic carbide, alloyed pearlite and graphite nodules. Though PMZ shows the similar structure like weld metal, ledeburitic carbides are coarser as well as lesser in amount and graphite nodules are larger in size. HAZ exhibited pearlite, cementite delineating the prior austenite grain boundary along with graphite nodules.
- All the zones of DI weldment e.g. base metal, weld metal and HAZ responded isothermal heat treatment which consists of austenitization at 900°C for 2 h holding time and austempering at 300°C and 350°C for 1.5 h, 2 h and 2.5 h holding time.
- At 300°C austempering temperature microstructures of base metal, weld metal and HAZ shows needle like bainitic ferrite with lower amount of retained austenite and

lower nodule count; whereas feathery shape bainitic ferrite microstructure with higher amount of retained austenite and higher nodule count is observed at 350°C in all the three zones of the weldment. However, weld metal always shows finer microstructure with smaller nodule size at both 300°C and 350°C compare to base metal, which show coarser structure with larger nodule size. The microstructure of HAZ is between i.e., comparatively finer matrix structure than base metal, but coarser than weld metal with larger nodule size compare to weld metal.

- The amount of retained austenite in weld metal varies with both austempering temperatures (300°C and 350°C) and holding time. Maximum amount of retained austenite was obtained for 2 h holding time at 350°C. The carbon content of retained austenite is directly related to the amount of retained austenite. Compare to weld metal, base metal always shows lesser amount of retained austenite along with lower carbon content of austenitic at the same austempering temperature and time.
- The microhardness values of weld metal before austempering show higher than base metal due to presence of ledeburitic carbide in the weld metal. After austempering just opposite behaviour of hardness is observed, i.e. weld metal shows minimum hardness compared to base metal. The change in microhardness values with austempering temperature and time correlated well with volume percentage of retained austenite. In general, weld metal austempering at 350°C attributed lower hardness value compared to 300°C and showing minimum hardness value at 2 h holding time in both the cases.
- Transverse tensile testing of the welded joints shows failure from base metal indicating that weld metal and even HAZ are stronger than base metal and achievement of 100% joint efficiency. Charpy impact values of weld metals show higher at 350°C for 2 h compare to 300°C for 2 h and the values correlated well with retained austenite volume percentage along with its carbon content as well as shape and size of the bainitic ferrite. Thus 350°C and 2 h holding time could be considered as an optimum austempering condition in the present study. Also results of the mechanical properties of ADI joints indicate successful development of coated electrode for DI and establishment of weld procedure which could be used for commercial applications.

References

1. D. Q. Sun, X. Y. Gu, W. H. Lui, Z. Z. Xuan, "Welding consumable research for austempered ductile iron (ADI), Material Science and Engineering A", 402(1-2) (2005) 9-15
2. S. D. Kiser, B. Irving, "Unravelling the mysteries of welding cast iron", Welding J, (1993) 39–44
3. G. R. Pease, "The welding of ductile iron", Welding J, 39 (1960) 15–95
4. S. K. Ya, C. R. Loper Jr, "The effect of molybdenum, copper and nickel on the perlitic and martensitic hardenability of ductile cast iron", AFS Trans, (1988) 811–822
5. E. M. El-Banna, "Effect of preheat on welding of ductile cast iron", Material Letters, 41 (1) (1999) 20-26
6. D. Q. Sun, W. Q. Wang, Z. Z. Xuan, Z. A. Ren, D. X. Sun, "Transformation characteristics, microstructure and mechanical properties of austempered ductile iron welds", Materials Science and Technology, 23(1) (2007) 92-96
7. D. Q. Sun, Z. Zhou, Z. Zhao, "Development of a New Electrode for Arc Welding of Austempered Ductile Iron (ADI)", Chin Met Sci Technol., 8(6) (1992) 401-405
8. U. Mitra, T. W. Eagar, "Slag-metal reactions during welding: Part II. Theory", Metallurgical and Materials Transactions B, 22(1) (1991) 73-81
9. U. Mitra, T. W. Eagar, "Slag metal reactions during submerged arc welding of alloy steels", Metallurgical Transactions A, 15(1) (1984) 217-227
10. G. R. Belton, T. J. Moore, E. S. Tankins, "Slag-metal reactions in submerged arc welding", Welding journal, 42(7) (1963) 289-297
11. J. E. Indacochea, M. Blander, N. Christensen, D. L. Olson, "Chemical reactions during submerged arc welding with FeO-MnO-SiO_2 fluxes", Metallurgical Transactions B, 16(2) (1985) 237-247
12. T. W. Egar, "Source of Weld metal oxygen contamination during submerged arc welding", Welding journal research supplements, 1978
13. C. S.Chai,T. W. Eagar, "Slag-metal equilibrium during submerged arc welding", Metallurgical Transactions B, 12(3) (1981) 539-547
14. N. D. Pandey, A. Bharti, S. R. Gupta, "Effect of submerged arc welding parameters and fluxes on element transfer behaviour and weld-metal chemistry", Journal of Materials Processing Technology, 40(1-2) (1994)195-221

15. K. L. Hayrynen, K. R. Brandenberg, J. R. Keough, "Applications of austempered cast irons", Transactions-american Aoundrymens Society, 2 (2002) 929-938
16. S. Kou, "Welding metallurgy 2nd Ed", New Jersey John Wiley and Sons, 2003
17. J. Lacaze, "Solidification of spheroidal graphite cast irons: III. Microsegregation related effects", Acta materialia, 47(14) (1999) 3779-3792
18. S. K. Putatunda, "Development of austempered ductile cast iron (ADI) with simultaneous high yield strength and fracture toughness by a novel two-step austempering process", Materials Science and Engineering A, 315(1-2) (2001)70–80
19. U. M. Batra, P. Tandon, K. Kaur, "A study of austenitization of SG iron", Bull Mater Sci, 23(5) (2000) 393–398
20. N. Darwish, R. Elliott, "Austempering of low manganese ductile irons", Materials Science and Technology, 9(7) (1993) 572-585
21. P. P. Rao, S. K. Putatunda, "Influence of microstructure on fracture toughness of austempered ductile iron", Metallurgical and Materials transactions A, 28(7) (1997) 1457-1470
22. B. Bosnjak, B. Radulovic, K. P. Tone, V. Asanovic, "Microstructural and Mechanical Characteristics of Low Alloyed Ni–Mo–Cu Austempered Ductile Iron", ISIJ International, 40(12) (2000) 1246–1252
23. J. Aranzabal, J. Gutierrez, J. M. Rodriguez-Ibabe, J. J. Urcola, "Influence of the amount and morphology of retained Austenite on the mechanical properties of an austempered ductile iron", Metallurgical and Materials Transactions A, 28(1997) 1143-1156
24. G. I. Rees, H. K. D. H. Bhadeshia, "Bainite transformation kinetics Part 2 non uniform distribution of carbon", Materials Science and Technology, 8(11) (1992) 994-1003
25. H. K. D. H. Bhadeshia, "The bainite transformation: unresolved issues", Materials Science and Engineering A, 273(1999) 58–66
26. P. P. Rao, S. K. Putatunda, "Dependence of fracture toughness of austempered ductile iron on austempering temperature", Metallurg Mater Trans A, 29(12) (1998) 3005-3016
27. U. Batra, S. Ray, S. R. Prabhakar, "The influence of Nickel and Copper on the Austempering of Ductile iron", JMEPEG,13(1) (2004) 64-68
28. H. Cetinel, "Fracture behaviour of overmatched ductile iron weldment", Int J Mater Res, 98(2) (2007)128-136

29. H. Cetinel, B. Uyulgan, T. Aksoy, “The effect of yield strength mismatch on the fracture behaviour of welded nodular cast iron”, Mater Sci Eng A, 387 (2004) 357-360
30. Y. Tanaka, H. kage, “Development and Application of austempered spheroidal graphite cast iron overview”, Materials Transaction JIM, 33(6) (1992) 543-557
31. S. K. Putatunda, P. K. Gadicherla, “Influence of austenitizing temperature on fracture toughness of a low manganese austempered ductile iron (ADI) with ferritic as cast structure”, Materials Science and Engineering A, 268(1-2) (1999)15-31
32. U. Batra, “Fracture behaviour and mechanism in austempered ductile iron”, JFAPBC, 5(5) (2005) 75-81

Chapter 6

Study on the effect of Cerium on as-deposited and ADI weld metal microstructures for optimum Cerium content

6.0 Introduction

Cerium (Ce) is one of the most successful nodulizing agents for DI casting and addition of Ce in DI shows beneficial or detrimental effects on the microstructure and properties of DI **[1]**. Small amount of Ce is frequently used to restore the graphite nodule count and nodularity in DI containing subversive elements such as antimony, lead, and titanium **[2, 3]**. However, there is no published literature available on the effect of Ce on DI weld metal. Thus study on the effect of cerium content on microstructures of DI weld metal for optimum cerium content which will attribute beneficial effect, is of great significance. In the present investigation, three different level of nano size (90-150 nm) CeO_2 was added to the coating (flux formulation) of selected (Trial 4) electrode in order to introduce Ce in DI weld metals. The optimum amount of Ce was found out by comparing microstructures of DI weld metals followed by microhardness studies. Finally response of isothermal heat treatment of Ce containing DI weld metal has been studied.

6.1 Results and Discussion

6.1.1 Chemical composition of the cerium containing developed electrodes

The chemical compositions of the three Ce containing weld deposits (eight layers chemical pad) were analyzed using optical emission spectrometer (OES). The details chemical compositions of the developed electrodes are given in **Table 6.1**.

Table 6.1 Typical chemical composition of the weld deposits using developed electrodes

Elements (wt. %)	C	Si	Mn	S	P	Ni	Mo	Cu	Al	Bi	Mg	Ca	Ti	Ce
Trial 4	3.08	2.60	0.40	0.006	0.039	0.5	0.19	0.24	0.62	0.03	0.004	0.015	0.09	-
Trial 7	3.28	2.76	0.43	0.008	0.02	0.66	0.31	0.29	0.48	0.03	0.003	0.003	0.14	0.10
Trial 8	3.15	2.6	0.46	0.005	0.001	0.63	0.30	0.28	0.14	0.003	0.01	0.002	0.11	0.05
Trial 9	3.22	3.06	0.46	0.006	0.001	0.74	0.37	0.33	0.14	0.003	0.01	0.004	0.013	0.2

6.1.2 Microstructure of as-deposited DI weld metal

The optical microstructures of as-deposited weld metals using without (Trial 4) and with three different levels of Ce containing developed electrode such as Trial 7 (0.1%), Trial 8 (0.05%) and Trial 9 (0.2%) are shown in **Fig.6.1 (a, b, c, d)**. All the weld metals show almost similar microstructural features containing ledeburitic carbide, alloyed pearlite and lower amount as well as smaller size of graphite nodules because of higher cooling rate. The microstructure of weld metal containing 0.05% Ce is finer and reveals higher amount of

ledeburitic carbide with a small amount of alloyed pearlite (**Fig. 6.1c**) compare to weld metal without Ce content (**Fig. 6.1a**). Increasing Ce content from 0.05 to 0.1% (**Fig. 6.1b**) the weld microstructure becomes finer than 0.05% Ce content. Interestingly, the amount of ledeburitic carbide decreased and the amount of alloyed pearlite increased. However, further increasing Ce content (0.2%) the weld microstructure becomes finest and shows almost fully ledeburitic carbide with very lesser amount of alloyed pearlite.

The size of the graphite nodules, nodularity and number of nodules per unit area (mm^2) were changed with addition of Ce content and the results were varied with varying the Ce content in weld metal. Addition of Ce content (0.05%) size of graphite nodule (r = 5.90 μm) and nodularity (70%) decreased from nodule size (r = 6.72) and nodularity (72%) of weld metal without Ce. But the numbers of nodule per mm^2 (325) increased in Ce containing weld metal compared to weld metal without Ce (numbers of nodule per mm^2: 280). Increasing Ce content (0.1%) the size of the nodule (r = 6.29), graphite nodularity (74%) and numbers of nodule per mm^2 (359) increased. Further increasing Ce content (0.2%) the graphite's become non-spherical in shape and larger in size (r = 6.63μm). Thus the graphite nodularity (65%) and the no.s of nodules per mm^2 (223) both decreased.

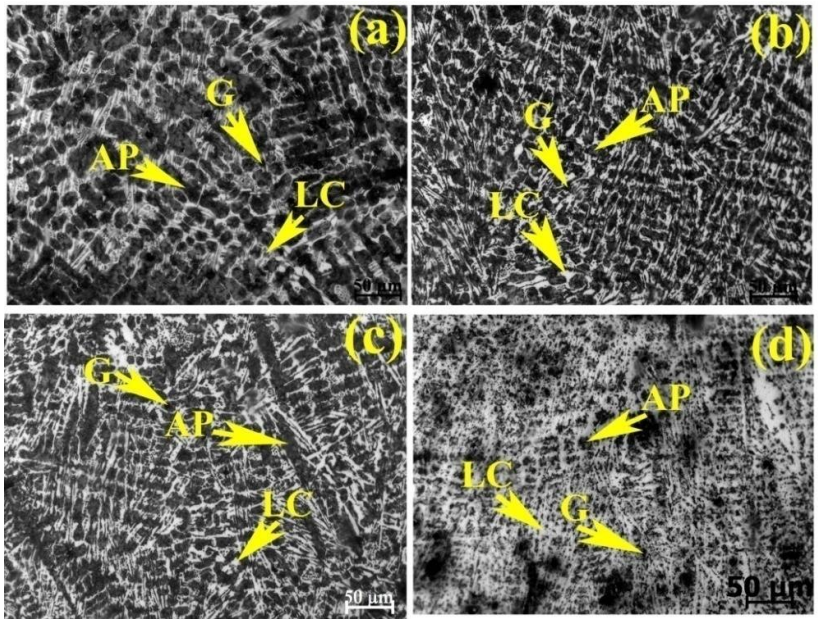

Fig. 6.1: Optical microstructures of as- deposited weld metal containing (a) without Ce, (b) 0.1% Ce, (c) 0.05% Ce, and (d) 0.2% Ce content

Rare earth (RE) elements (Ce) have a strong ability of deoxidization and desulphurization with the results of forming the high melting point RE_xO_y, RE_xS_y, $RE_xO_yS_z$ **[4]**. The Gibb's

free energies of these compounds at high temperatures are so low that RE elements can combine readily with O and S when added to liquid metal **[5- 6]**. The Gibb's free energy, melting point, molecular wt. and size of inclusion as well as calculated misfit value are given in **Table 6.2 [7-9]**.

Table 6.2 Gibb's free energy, melting point, molecular wt. and size of inclusion **[7-9]**

Inclusion type	Gives free energy (Δ°G) (J/mol)	Melting Temp (°C)	Molecular wt. g/mol	Inclusion Size (μm)	Calculated Lattice misfit (δ)
Ce_2O_3	-714380+179.79T	1690	328.229	2-4	6.86
Ce_2O_2S	-675700+165.50T	1950	704.641	>7	6.65
Ce_2S_3	-536420+163.50T	1887	376.412	4-7	4.54

According to the theory of heterogeneous nucleation by Turnbull and Vonnegut **[10]**, whether the nucleating agent could promote nucleation of liquid metal depends on the following two conditions:

(a) There must be high melting point phase particles, which provide an interface of the heterogeneous nucleation, and

(b) The lattice misfit of low-index surfaces between high-melting phase particles and matrix metal must be low.

One dimensional lattice misfit has been estimated from the following equation **[11-13]**:

$$\delta = (a_C - a_N)/ a_N \ldots\ldots\ldots\ldots\ldots\ldots\ldots \textbf{(6.1)}$$

Where, δ is the lattice misfit, a_C is the atomic spacing of low index crystal face of the crystallizing phase, $a_N$is the atomic spacing of low index crystal face of the nuclei.

The calculated misfit value of Ce_2O_3, Ce_2S_3 and Ce_2O_2S of the three inclusions are 6.86%, 6.65% and 4.54% respectively as given in **Table 6.2**.

As per the theory proposed by Bramfitt **[12]** during heterogeneous nucleation, the nuclei with δ<6% are the most effective, while those with δ between 6% and 12% are medium effective and those with δ>12% are ineffective. Also the melting point can be used as an estimate of the measure of the stability of that compound **[3]**. Thus among the three particles oxy sulphide particles as presented in **Table 6.2** having higher melting point and close matching with the carbide (matrix) lattice spacing creates the possibility of most favoured substrate for graphite nuclei.

It can be seen from XRD spectra **(Fig.6.2)** that addition of Ce attributes the formation of Ce_2O_3 and Ce_2S_3 at 0.05% Ce. Whereas at 0.1% Ce all the three compounds i.e. Ce_2O_3, Ce_2S_3 and Ce_2O_2S are formed. With further increasing Ce, i.e.at 0.2% both Ce_2S_3 and Ce_2O_2S

are formed. However, from the intensity of the XRD spectra it can be stated that more oxy-sulphite particles has been formed at 0.1% Ce and this has caused increased the numbers of nodules per mm^2 in weld metal containing 0.1%Ce. Increased numbers of nodules per mm^2 is only possible when a large number of eutectic cells are being formed during solidification. Thus the eutectic solidification of such a weld metal containing more numbers of nuclei proceeds more rapidly within the graphite solidification temperature range leading to decreased amount of ledeburitic carbide after solidification. Also increasing the numbers of nodules per mm^2 in DI weld metal was reported to a reducing the chilling tendency of cast iron **[14-15]**.

It is well known that the chilling tendency of cast iron has a significant effect on the formation of ledeburitic carbide. Thus reducing the chilling tendency of cast iron will decrease the amount of ledeburitic carbide. However, with further increasing Ce content (0.2%) in weld metal the numbers of nodules per mm^2 decreased. This is not unexpected as the less oxy-sulphite have been formed as evident from the intensity of XRD analysis. Hence, eutectic solidification in such weld metal proceeds slowly due to less number of nuclei leading to formation of more ledeburitic carbide after solidification. Also it has been reported that an excessive amount of RE is known to promote the formation non-spherical graphite **[1]**. Weld metal containing 0.2% Ce as shown in **Fig. 6.1d** reveals non-spherical graphite indicating excessive amount of Ce in the present study.

The graphitizing elements present in DI are expected to influence nodule count in the weld metal. The graphitizing elements such as C and Si present in each weld metal (with and without Ce) have been represented by the carbon equivalent (CE) using the following formula **[16]**.

$$CE=C\%+0.31\ Si\% \quad \textbf{(6.2)}$$

The CE values of each weld metal have been plotted against nodule count of each weld metal (with and without cerium) and are shown in **Fig. 6.3**. It is shown that nodule count (numbers of nodules per mm^2) is strongly dependent on CE and increases in proportion to the CE of weld metal. However, nodule count decreases sharply even with further increase in CE **(4.16)** indicating the dominating effect of chilling effect over CE when excessive amount of Ce (0.2%) is present.

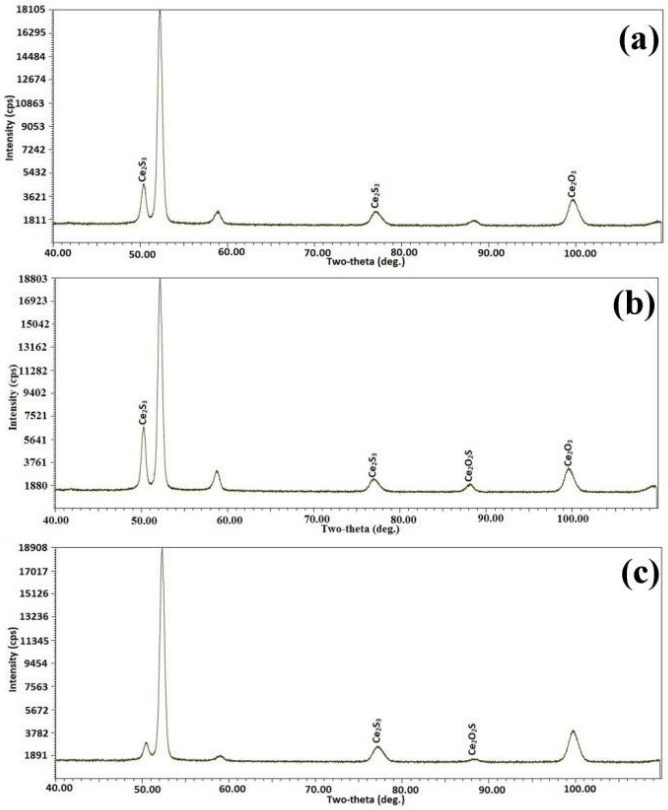

Fig. 6.2: Typical X-ray diffraction pattern of as-deposited weld metal containing (a) 0.05% Ce, (b) 0.1% Ce, (c) 0.2% Ce

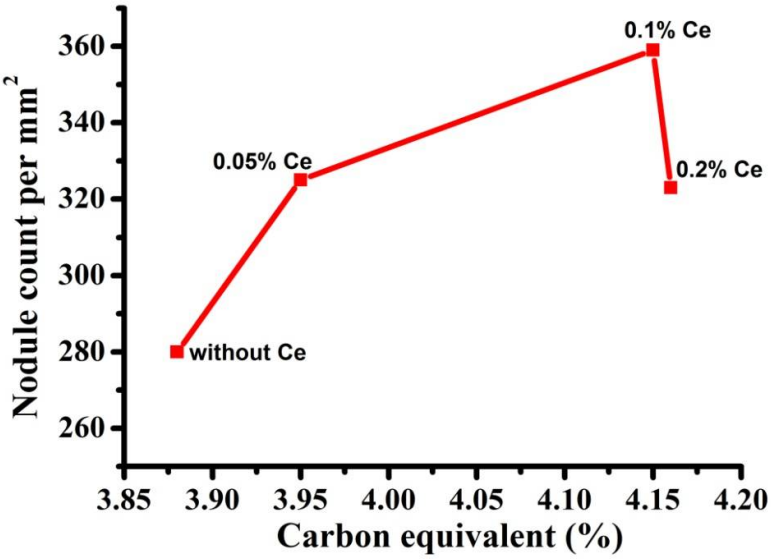

Fig.6.3: Relation between carbon equivalent and nodule count of without and different Ce containing weld metals

It is well established that the graphite nodules are separated from the liquid iron of DI at the eutectic temperature during solidification and are subsequently enveloped by austenite phase, forming eutectic cells **[16]**. Each eutectic cell consists of graphite nodules and austenite. The growth of eutectic cell proceeds by the diffusion of carbon from the liquid iron on the graphite nodules through the austenitic shell. The diffusion of carbon through the austenite and austenite/graphite interface plays an important role at this stage. Increasing nodule count from 325 to 359 with increasing Ce content from 0.05% to 0.1% indicates that more no.s of graphite nuclei has been formed. Also increase in nodule size from 5.9 to 6.25µm indicates that sufficient carbon has been diffused. This is only possible when longer period of time for diffusion of carbon is available at a given temperature. Thus it is apparent that the chilling effect has been minimized with increasing Ce level at 0.1%. Similar behaviour of Ce addition in DI was reported by previous investigators **[16-17]**. However, with further increasing Ce (0.2%), nodule count decreases (223 nodules per mm^2) but nodule size increased and nodule shape became non- spherical.

The results of EDS analysis of as-deposited weld metal containing optimum Ce content (0.1% Ce) are shown in **Fig.6.4**. SEM structure (**Fig.6.4 a)** clearly revealed the different phases of the weld metal and **Fig.6.4 b, c** represents the EDS analysis results of the two different phases i.e. graphite and matrix respectively. The results show the presence of Ce along with other elements like Si, S, O, C, Mg, Cr and trace amount of Ca in the graphite nodules of weld metal containing Ce. This indicates that graphite nucleated from Ce_2O_3, Ce_2O_2S and Ce_2S_3 after reacting Ce with O & S and also facilitated Mg to nucleate the graphite nodules as well. However, the matrix of weld deposits is composed of Al, Si, Ca, Cr and C and Ce.

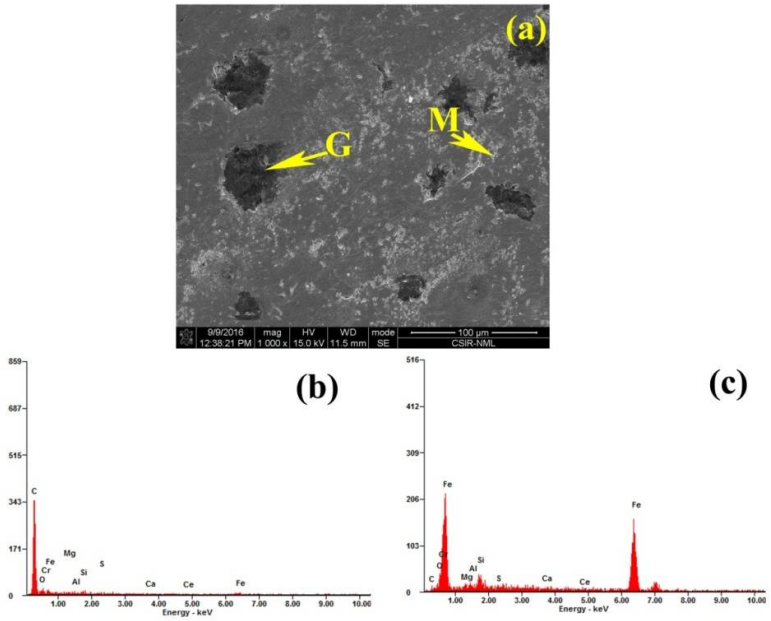

Fig.6.4: (a) SEM structure of as-deposited weld metal containing 0.1% Ce shows different phase and EDS analysis of (c) graphite, (b) matrix

6.1.3 Microstructures of austempered weld metals

Fig.s (6.5, 6.6, 6.7, 6.8) show the austempered microstructures of deposited weld metals without and with Ce (0.1% , 0.05% and 0.2%) austempered at 300°C and 350°C for 1.5, 2 and 2.5 h holding time respectively. For better clarity, the microstructures (with and without Ce contents) at both 300°C and 350°C for different holding time were studied under SEM and the structures are shown in **Fig. 6.9, 6.10, 6.11** and **6.12**.

After austempering, the microstructures of weld metals in general consist of bainitic ferrite (dark), retained austenite (white) and graphite nodules. However, the proportion of microstructural constituents varies with changing the austempering temperature and holding time. At 300°C austempering temperature microstructure shows needle-shaped bainitic ferrite with a small amount of film shaped retained austenite and graphite nodules. Whereas, at 350°C austempering temperature microstructure shows feathery shaped bainitic ferrite with a higher amount of blocky shaped retained austenite and graphite nodules. With changing the austempering holding time (for both the temperatures and varying Ce content), the microstructures varied with respect to shape, size and amount of the constituents. Increasing holding time from 1.5 to 2 h the size of bainitic ferrite as well as the amount of retained austenite content increased. Further increasing holding time from 2 to 2.5 h the sizeof the bainitic increased further, but the amount of retained austenite decreased.

It is well established that during austempering process, the bainitic ferrite is formed out of the austenite (residual austenite). The growth of bainitic ferrite takes place through diffusion of carbon into the surrounding austenite and thus austenite enriched with carbon and becomes stable as retained austenite **[18-19]**.

Addition of Ce in weld metals has shown significant effect on austempered microstructure. Initially, at 0.05% Ce content (**Fig.6.7**) the microstructures at both the austempering temperatures show coarser bainitic ferrite and lower amount of retained austenite compared to without Ce content (**Fig.6.5**). Interestingly with increasing Ce content (0.1%) the structure becomes finer and homogeneous (**Fig.6.6)**. Also bainitic ferrite decreased and retained austenite increased compare to without Ce and 0.0.5% Ce at both the temperature and holding time. Further increasing Ce content (0.2%) both bainitic ferrite and retained austenite become coarser and higher amount of bainitic ferrite and lower amount of retained austenite are observed (**Fig.6.8)**.

ADI undergoes a two-stage process **[18]**. In stage I, austenite decomposes into bainitic ferrite and high carbon retained austenite. In stage II retained austenite transformed to ferrite and carbide **[18]**. The driving force for stage I of austempering depends on carbon content of initial austenite and increases with the decrease of carbon content of initial austenite **[20]**. Since austenitizing temperature and time was same for all the four weld metals (three with Ce and one without Ce), the carbon content of initial austenite depends on as- deposited microstructure. As expected microstructure containing higher amount of fine ledeburitic carbide will contribute more carbon to the initial austenite. In that respect weld metal containing 0.2% Ce should posse's highest carbon content of initial austenite followed by 0.05% Ce and 0.1% Ce. Thus the driving force for stage I of austempering is highest in weld metal containing 0.1% Ce and lowest in 0.2% Ce. Obviously higher driving force will increase the rate of formation of bainitic ferrite and simultaneously remaining austenite will be enriched with more carbon partitioned from ferrite leading to more amount of high carbon stable retained austenite. Thus addition of 0.1% Ce in weld metal attributed maximum amount of retained austenite **(Table 6.4)**. However, weld metal containing 0.05% Ce having relatively lower driving force for stage I of austempering than 0.1% Ce containing weld metal shows more bainitic ferrite **(Table 6.4)**. This should not happen; actually weld metal containing 0.05% Ce provided lesser bainitic ferrite and thus less carbon partitioned from ferrite to residual austenite which will result more amount of retained austenite with lesser carbon. But lower amount of retained austenite and more amount of bainitic ferrite obtained from XRD results probably indicates portion of low carbon austenite transformed to

martensite. This is not unjustified as the hardness of weld metal containing 0.05% Ce (380 Hv) is significantly higher than 0.1% Ce containing weld metal (326 Hv). Similarly 0.2% Ce containing weld metal can be justified with lesser amount of retained austenite than 0.05% Ce containing weld metal. But only exception is that portion of low carbon austenite in 0.2% Ce weld metal has been transformed into ferrite and carbide **[18]**.

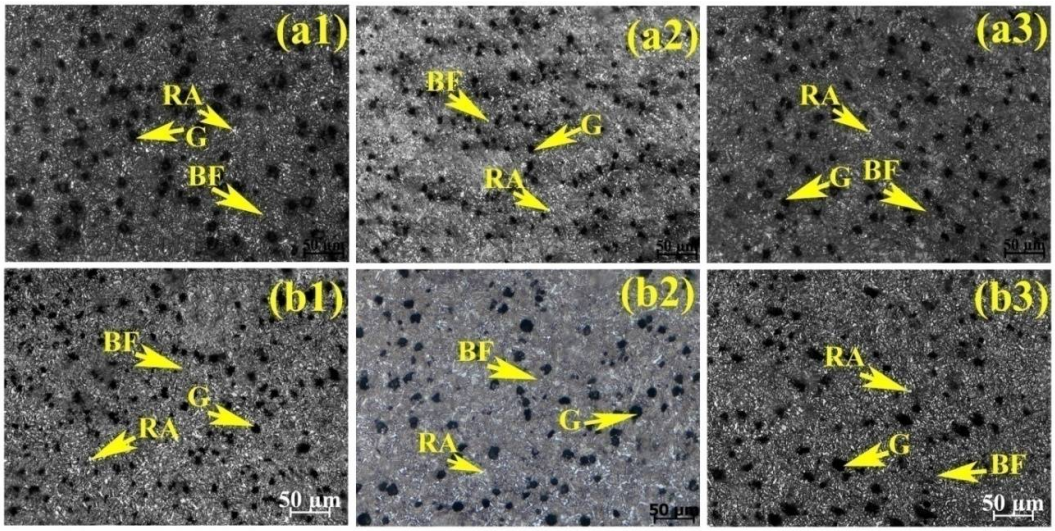

Fig. 6.5: Optical microstructures of weld metal after austempering at 300°C for (a1) 1.5 h, (a2) 2 h, (a3) 2.5 h and 350°C for (b1) 1.5 h, (b2) 2 h, (b3) 2.5 h holding time using without Ce content electrode

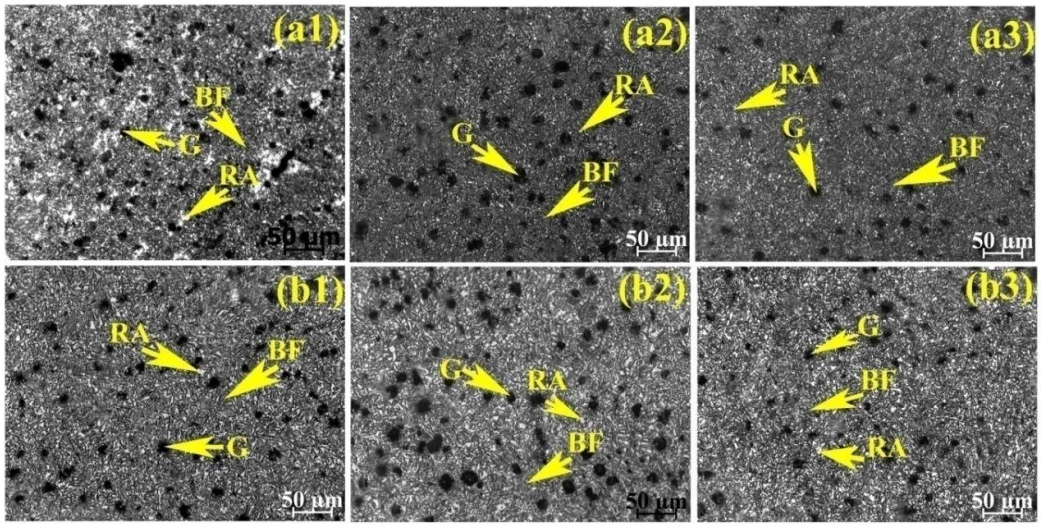

Fig. 6.6: Optical microstructures of weld metal after austempering at 300°C for (a1) 1.5 h, (a2) 2 h, (a3) 2.5 h and 350°C for (b1) 1.5 h, (b2) 2 h, (b3) 2.5 h holding time using 0.1% Ce content electrode

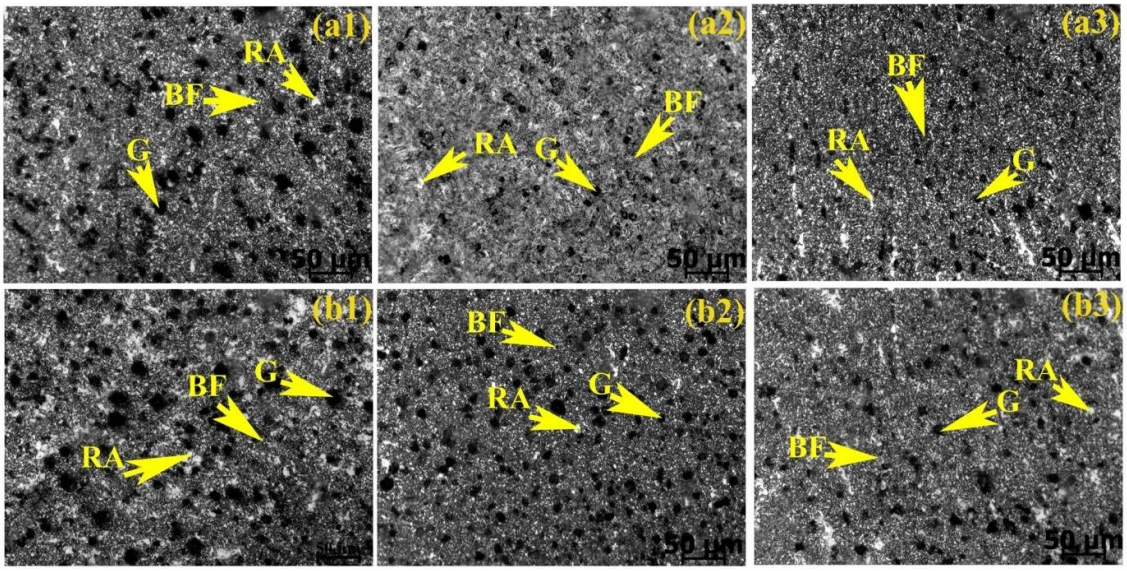

Fig. 6.7: Optical microstructures of weld metal after austempering at 300°C for (a1) 1.5 h, (a2) 2 h, (a3) 2.5 h and 350°C for (b1) 1.5 h, (b2) 2 h, (b3) 2.5 h holding time using 0.05% Ce content electrode

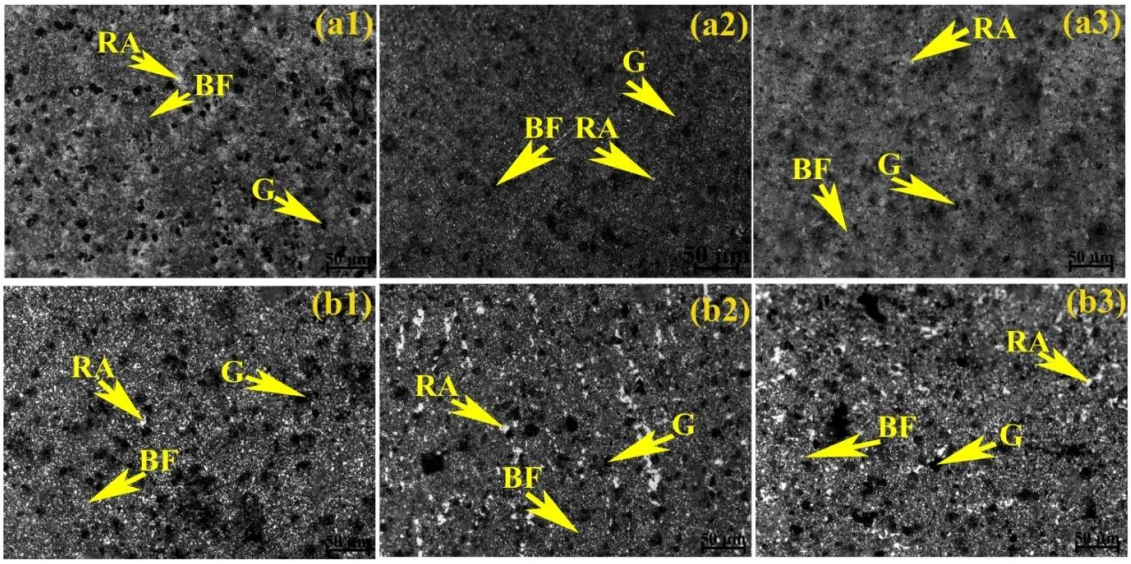

Fig. 6.8: Optical microstructures of weld metal after austempering at 300°C for (a1) 1.5 h, (a2) 2 h, (a3) 2.5 h and 350°C for (b1) 1.5 h, (b2) 2 h, (b3) 2.5 h holding time using 0.2% Ce content electrode

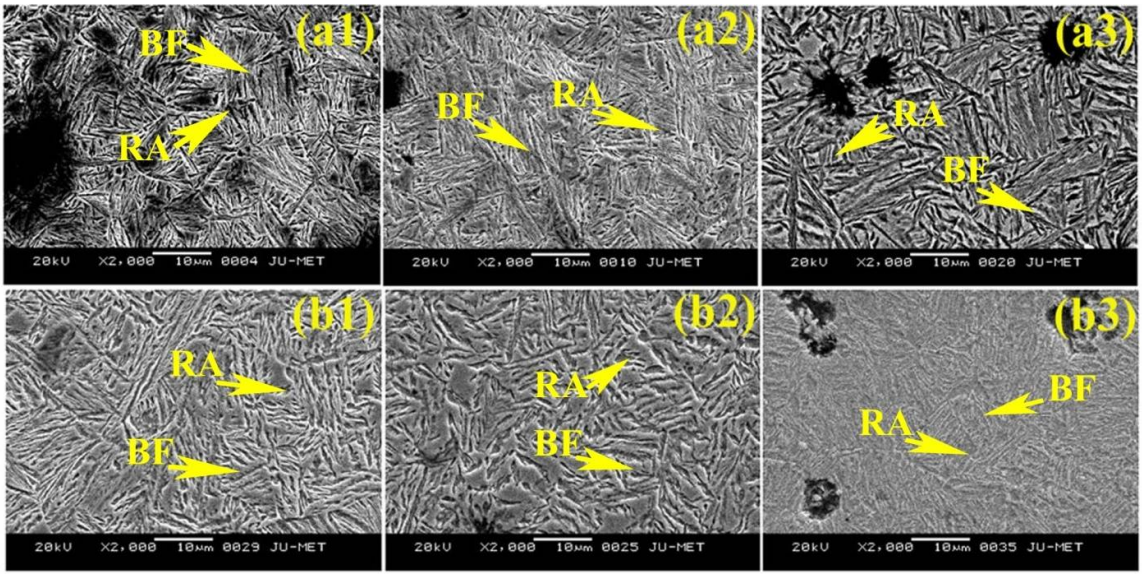

Fig. 6.9: SEM structures of weld metal after austempering at 300°C for (a1) 1.5 h, (a2) 2 h, (a3) 2.5 h and 350°C for (b1) 1.5 h, (b2) 2 h, (b3) 2.5 h holding time using without Ce content electrode

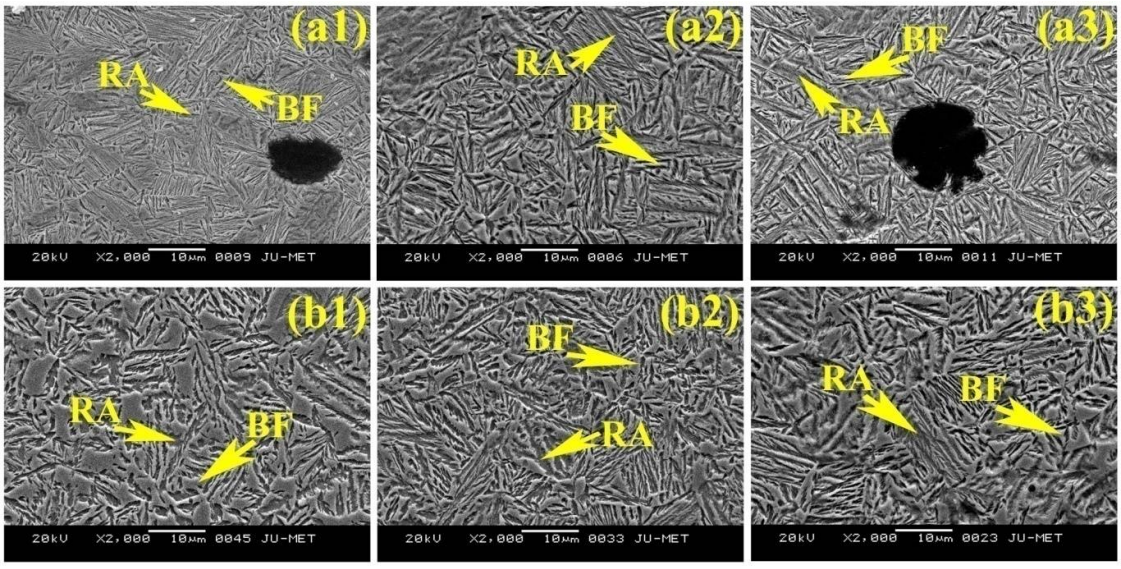

Fig. 6.10: SEM structures of weld metal after austempering at 300°C for (a1) 1.5 h, (a2) 2 h, (a3) 2.5 h and 350°C for (b1) 1.5 h, (b2) 2 h, (b3) 2.5 h holding time using 0.1% Ce content electrode

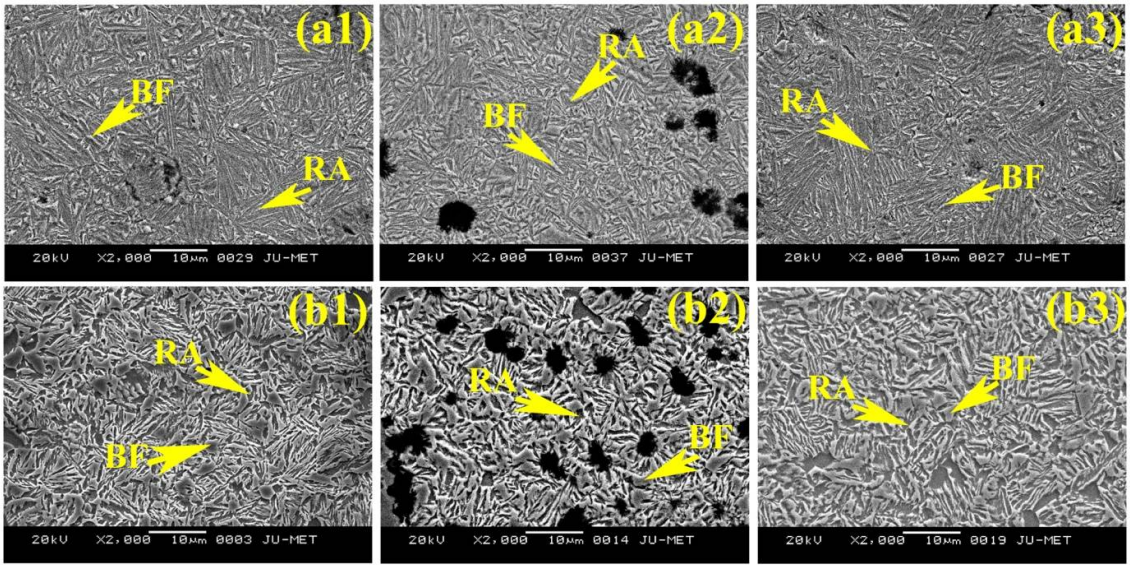

Fig. 6.11: SEM structures of weld metal after austempering at 300°C for (a1) 1.5 h, (a2) 2 h, (a3) 2.5 h and 350°C for (b1) 1.5 h, (b2) 2 h, (b3) 2.5 h holding time using 0.05% Ce content electrode

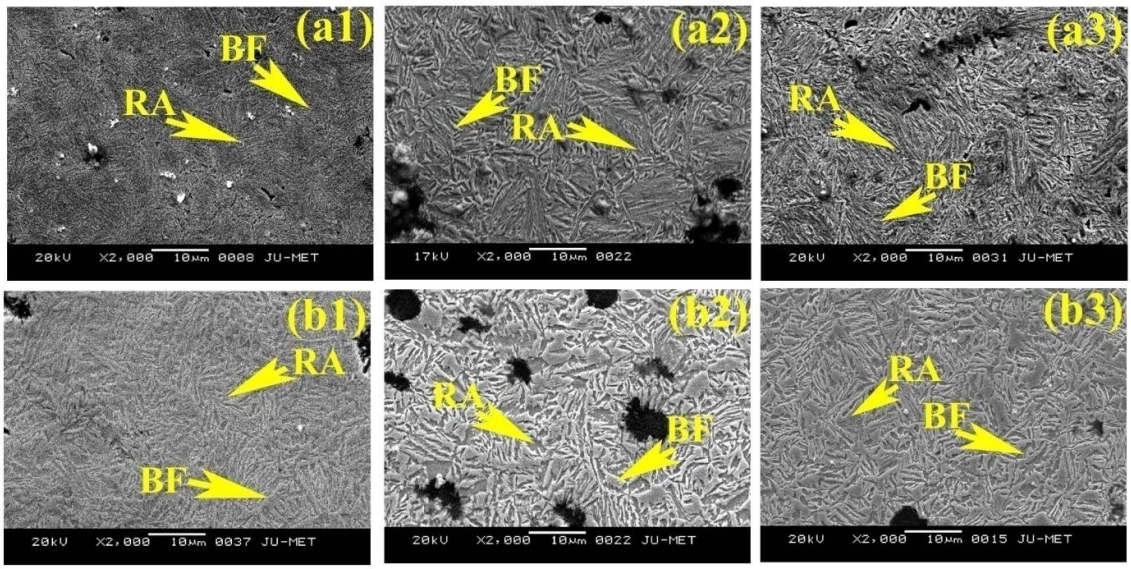

Fig. 6.12: SEM structures of weld metal after austempering at 300°C for (a1) 1.5 h, (a2) 2 h, (a3) 2.5 h and 350°C for (b1) 1.5 h, (b2) 2 h, (b3) 2.5 h holding time using 0.2% Ce content electrode

Apart from matrix structure, graphite nodularity and its size of weld metals also changed with changing the austempering temperature and holding time and the quantitative values are given in **Tables 6.3**. With addition of Ce (0.05%) in weld metals, graphite nodularity improves and size of graphite decreases. Increasing Ce content at 0.1%, there is little change in the size of nodule **(Table 6.3)**, but graphite nodularity improves further.

However, the nodules become non-spherical in shape and the nodularity is degraded in weld metals containing 0.2% Ce.

Table 6.3 Nodularity and the average size of the nodules of all without and with Ce contening weld metals

Austempering Temp.	Holding Time	Without Ce		0.1% Ce		0.05% Ce		0.2% Ce	
(°C)		Nodularity	Nodule size (r)(µm)	Nodularity	Nodule size (r)(µm)	Nodularity	Nodule size (r)(µm)	Nodularity	Nodule size (r)(µm)
As deposited		72	6.72	74	6.29	70	5.90	65	6.90
300	1.5	76	5.90	74	5. 79	72	5.60	68	6.35
	2	78	5.86	82	5.98	76	5.68	72	6.30
	2.5	76	6.34	81	5.72	76	5.89	69	6.65
350	1.5	78	6.10	78	5.60	72	5.49	70	6.28
	2	80	5.90	84	5.68	80	5.60	76	6.10
	2.5	80	6.67	76	6.20	74	6.00	72	6.81

Fig. 6.13(a1, b1) shows a transmission electron micrograph typical of the isothermal transformation heat treated microstructure austempered at 300°C for 2 h containing without and 0.1% Ce weld metal. The microstructure consists of carbide free bainitic ferrite laths and interlath film of retained austenite. This structure is considered as “lower bainite” in which the precipitation of interlath cementite has been prevented by the presence of high silicon. At 300°C thin film of retained austenite is the predominant austenite morphology. The microstructure changes from lower to upper bainite as the austempering temperature increases to 350°C (**Fig.6.13 a2, b2**). The bainitic ferrite lath becomes wider and the retained austenite present between the bainitic ferrite laths become thicker and appears as blocky form **[21]**; also there is no carbide present here.

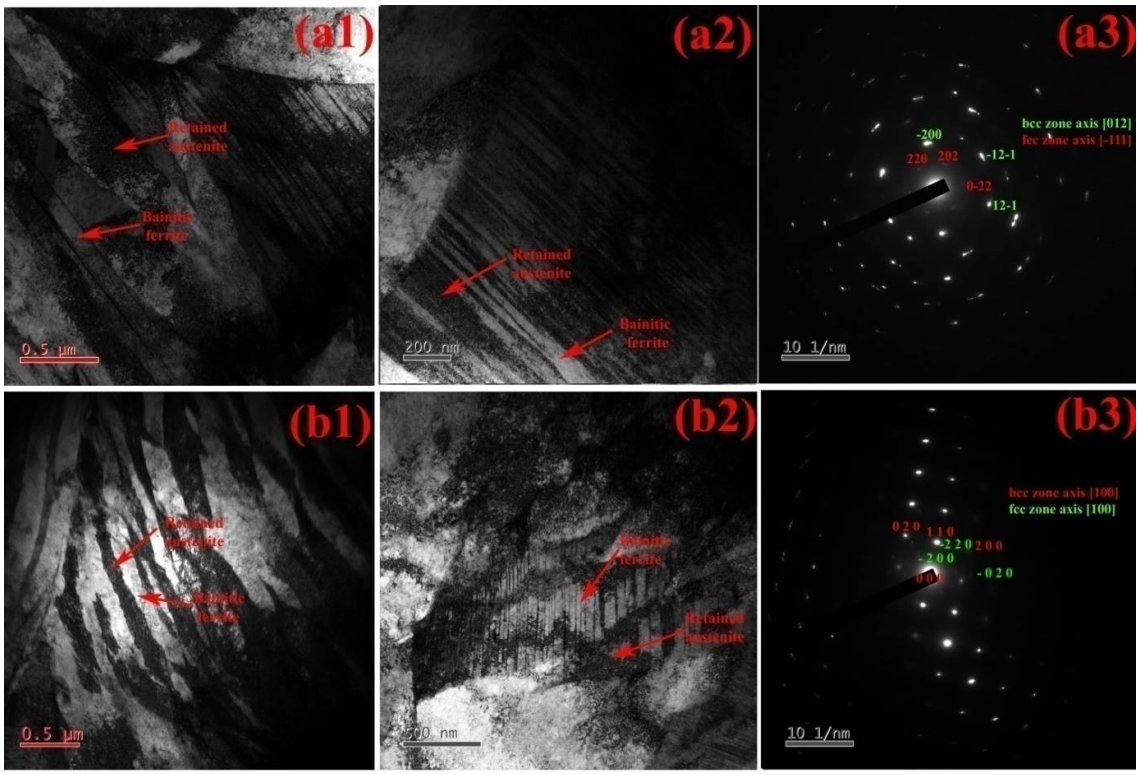

Fig. 6.13: TEM images of weld metals austempered at (a1)300°C (a2) 350°C, (a3) related SAD pattern in without Ce content and (b1) 300°C (b2) 350°C, (b3) related SAD with Ce content for 2 h holding time.

6.1.4 Volume percentage of retained austenite and it's carbon content

The volume percentage of retained austenite (vol % RA) in different weld metals after austempering was determined by XRD analysis and the typical X-ray diffraction patterns of different Ce containing weld metals are given in **Fig.6.14**to**Fig.6.16** respectively and the calculated results are given in **Table 6.4**.The calculated values have been plotted with respect to austempering holding time (1.5, 2 and 2.5 h) for two austempering temperatures (300°C and 350°C) and are shown in **Fig. 6.17** and **Fig. 6.18** respectively. For both the austempering temperatures (300 and 350°C), vol % of RA increases with holding time from 1.5 h to 2 h and then decreased with further increasing holding time (2h). However, vol % RA is always higher at 350°C than 300°C for each holding time and thus maximum percentage of RA is obtained at 350°C for 2 h. As expected percentage of bainitic ferrite will vary just opposite manner of vol % of RA as the austempered structure consists of two microstructural constituents along with graphite nodules.

Lower amount of retained austenite at 1.5 h holding time is due to shorter austempering time which causes incomplete transformation of bainitic ferrite. Increasing the

holding time from 1.5 to 2 h, transform of bainitic ferrite will approach to completion resulting with diffusion of more carbon to the surrounding austenite and thus more austenite will be stable as retained austenite. However, further increasing holding time from 2 to 2.5 h the volume percentage of retained austenite was decreased. This decrease is probably due to start of second stage reaction in which the high carbon austenite starts to decompose into ferrite and carbide **[20]**.

However, Ce content influences the amount of retained austenite (vol %) in weld metals at both austempering temperatures (300 and 350°C). The variation of Ce content in weld metal amount of retained austenite was varied. Initially, addition of Ce content (0.05 %) the amount of retained austenite decreased with increasing the amount of bainite ferrite at each austempering temperature compared to the without Ce content weld metal. With increasing Ce content from 0.05 to 0.1.%, the amount of retained austenite increased and shows maximum amount of retained austenite at both the temperatures compared to without and 0.05% Ce. However, further increasing Ce content from 0.2 wt. %, the amount of retained austenite was decreased further with increasing the amount bainitic ferrite.

The carbon content of retained austenite at different holding time was determined using the equation **(4.5)**. The calculated results of the austenitic carbon content of all the weld metals (without and with three different level Ce content) at both the austempering temperatures are plotted with respect to the holding time as shown in **Fig.6.19 (a, b)**. Interestingly, at both the austempering temperatures, the variation of austenitic carbon content with holding time exactly follows the same pattern with vol % RA content **(Fig.6.17)**. Like retained austenite the carbon content of retained austenite was varied with varying the austempering temperature and shows higher at 350°C than 300°C for all the weld metals. It is to be noted that maximum carbon content as high as 2.2 wt. % in retained austenite (46.7%) was obtained in weld metal containing 0.1% Ce at 350°C for 2 hour holding time.

At 1.5 h holding time the amount of carbon content is less, because at short time the growth of bainitic ferrite cannot be completed. As a result less amount of carbon diffused to the surrounding austenite. Increasing holding time from 1.5 to 2 h the amount of carbon content was increased because more carbon diffused into austenite. However, further increasing the austempering holding time from 2 to 2.5 h the carbon content decreased due to decrease the amount of retained austenite (vol %).

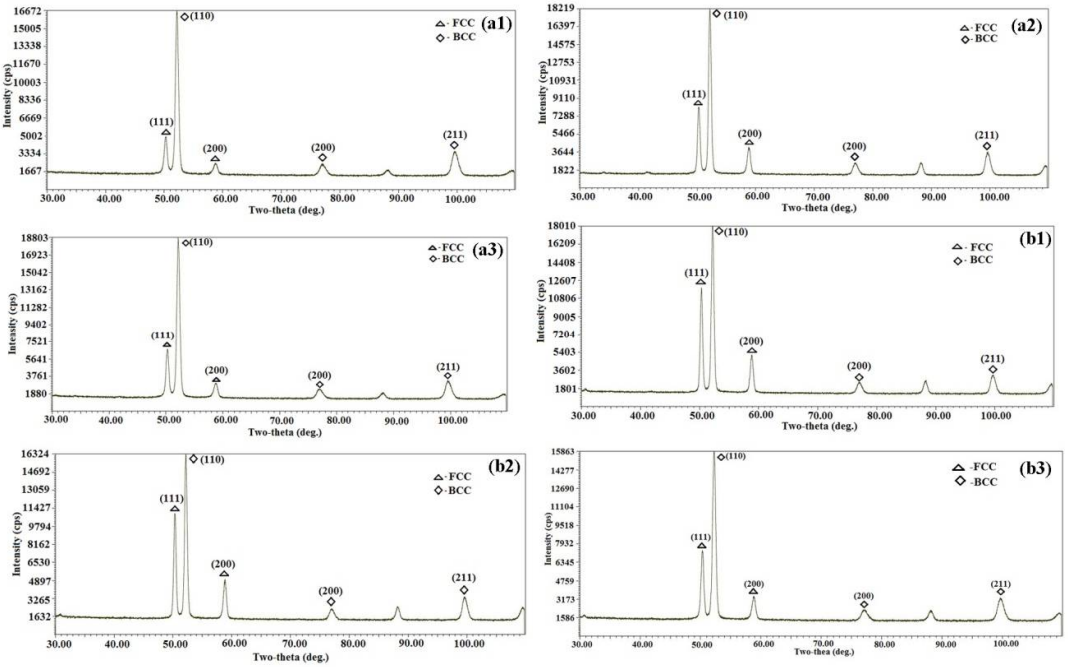

Fig. 6.14: Typical X-ray diffraction patterns of 0.1% Ce containing weld metals after austempering at 300°C for (a1) 1.5 h, (a2) 2 h & (a3) 2.5 h and 350°C for (b1) 1.5 h, (b2) 2 h & (b3) 2.5 h holding time

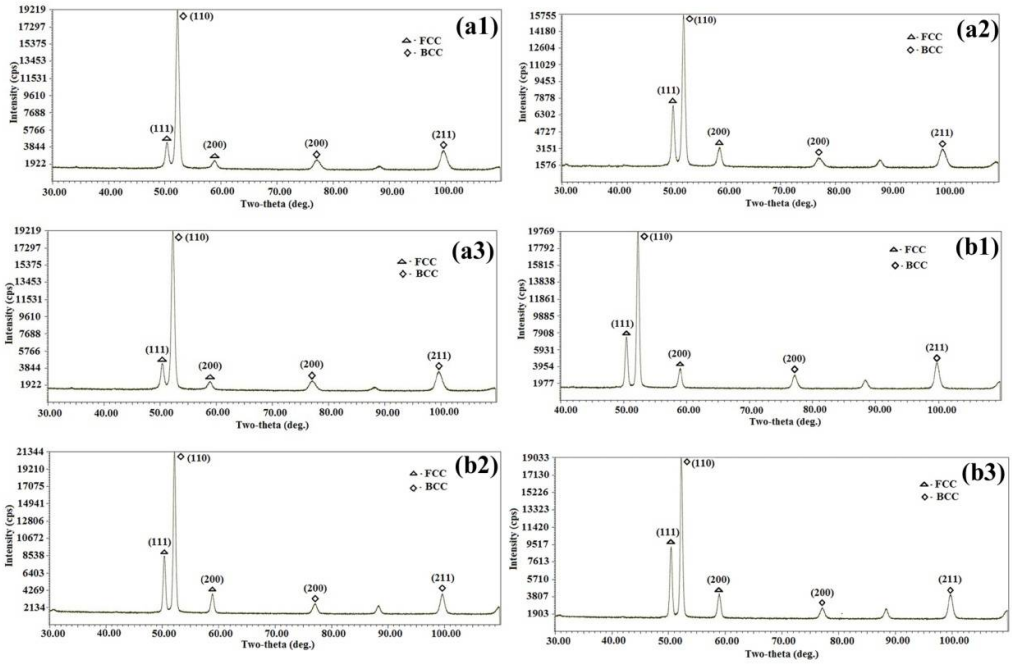

Fig. 6.15: Typical X-ray diffraction patterns of 0.05% Ce containingweld metals after austempering at 300°C for (a1) 1.5 h, (a2) 2 h & (a3) 2.5 h and 350°C for (b1) 1.5 h, (b2) 2 h & (b3) 2.5 h holding time

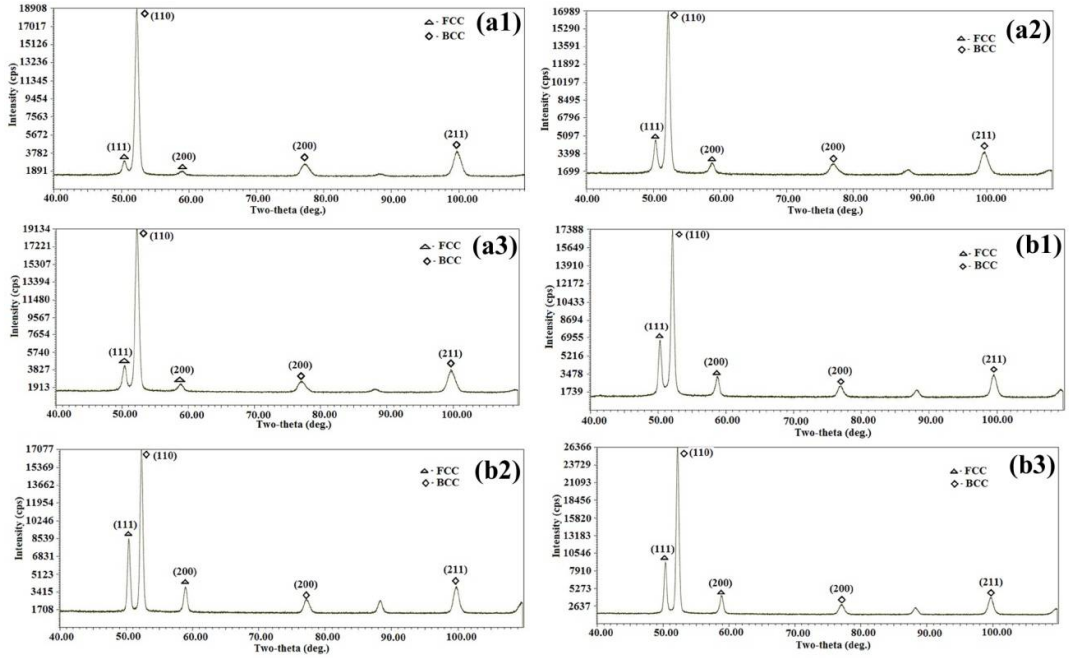

Fig. 6.16: Typical X-ray diffraction patterns of 0.2% Ce containing weld metals after austempering at 300°C for (a1) 1.5h, (a2) 2h & (a3) 2.5 h and 350°C for (b1) 1.5 h, (b2) 2 h & (b3) 2.5 h holding time

Table 6.4 Quantitative micorstructural constituents and corresponding microhardness of ADI weld metals containing with and without cerium

Austempering Temp (°C)	Holding Time (h)	Without Ce			0.05% Ce			0.1% Ce			0.2% Ce		
		Retained austenite (vol %)	Bainitic ferrite (vol %)	Micro hardness	Retained austenite (vol %)	Bainitic ferrite (vol %)	Micro Hardness (Hv)	Retained austenite (vol %)	Bainitic ferrite (vol %)	Micro Hardness (Hv)	Retained austenite (vol %)	Bainitic ferrite (vol %)	Micro Hardness (Hv)
300	1.5	36.2	59.7	369	34.89	61.1	380	36.81	57.1	326	33.8	59.2	398
	2	40.8	53.1	327	37.6	55.4	340	42.7	47.3	394	38.6	57.4	349
	2.5	36.9	56	358	34.48	59.2	383	38.12	55.8	338	36.83	59.1	372
350	1.5	40.2	51.7	289	39.8	53.2	309	42.55	53.4	280	39.82	56.1	315
	2	42.5	48.1	280	40.83	51.1	290	46.71	46.2	273	42.81	52.4	292
	2.5	38.9	55	308	36.9	55.1	355	39.27	54.7	287	36.02	57.7	358

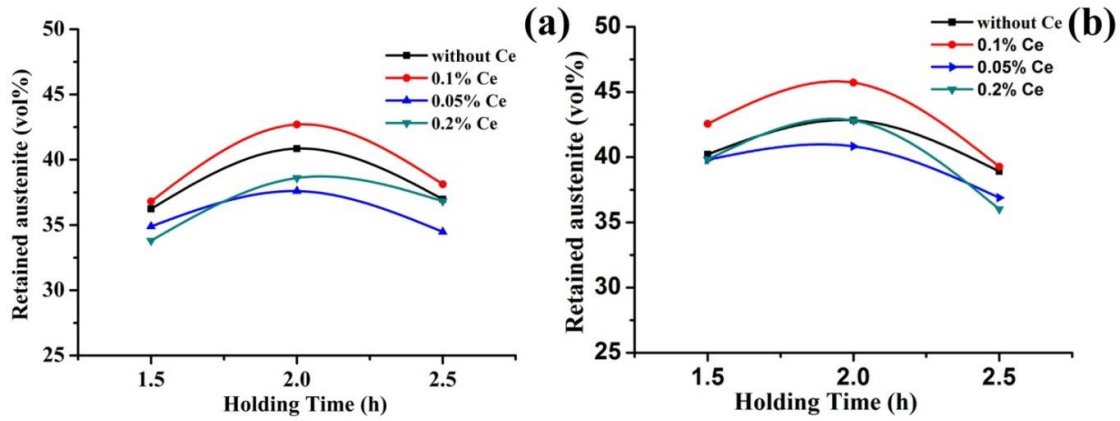

Fig.6.17: Volume percentage of retained austenite of without and with Ce containing weld metals after austempering at (a) 300°C and (b) 350°C for 350°C for 1.5 h, 2 h, and 2.5 h holding times

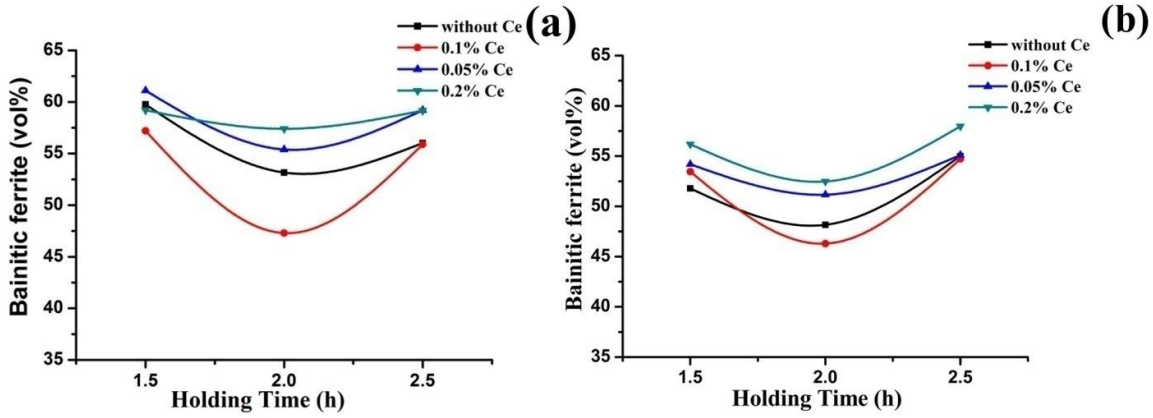

Fig.6.18: Volume percentage of bainitic ferrite of without and with Ce containing weld metals after austempering at (a) 300°C and (b) 350°C for 1.5 h, 2 h, and 2.5 h holding times

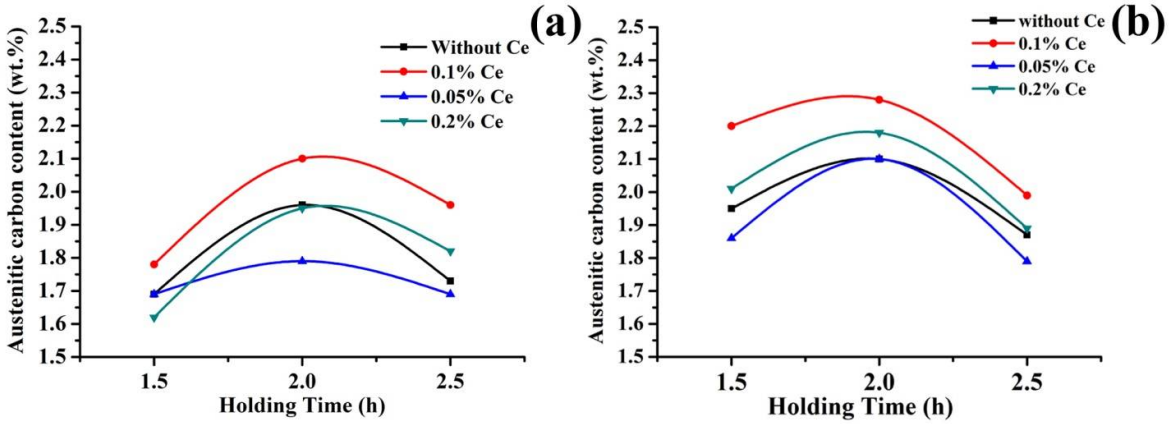

Fig.6.19: Austenitic carbon content of without and with Ce containing weld metals after austempering at (a) 300°C and (b) 350°C for 350°C for 1.5 h, 2 h, and 2.5 h holding times

6.1.5 Microhardness

The average microhardness value of as-deposited weld metals and weld metals after austempering at 300°C and 350°C for 1.5, 2 and 2.5 h holding time using without and with Ce content are shown in **Fig. 6.20** and **Fig.6.21 (a, b)**. In **Fig. 6.20** all the as-deposited weld metals show higher hardness value due to the presence of hard ledeburitic phase in the microstructure. With addition of Ce content in weld metals the hardness values varied due to the variation of microstructural constituents in weld deposits. Initially at 0.05% Ce content, the hardness shows higher value (706 Hv) than without Ce content (545 Hv) due to presence of higher amount of finer ledeburitic carbide in the weld metal. With increasing Ce content from 0.05 to 0.1% the hardness value decreased (568 Hv) than 0.05% Ce content, because of lower amount of ledeburitic carbide in weld structure. However, increasing Ce content (0.2%) the hardness shows the highest value (820 Hv) compared to others welds due to the presence of fully ledeburitic carbide in weld metal.

After austempering, the hardness shows lower value in all the weld metals compared to as-deposited weld metals. The average microhardness value of all the weld metals after austempering at 300°C and 350°C for different holding times are shown in **Fig.6.21 (a, b)**. The microhardness values of all the weld metals are lower at 350°C compared to 300°C; because of higher retained austenite content in weld metal at 350°C.

The micrhardness values also varied with varying the austempering holding time for both the temperatures. For all the weld metals, with varying holding time from 1.5 to 2 h the hardness values decreased, because of increasing the amount of retained austenite in weld metals. However, further increasing holding time from 2 to 2.5 h the hardness values increased to a great extent which indicates that some amount of austenite further transformed to bainitic ferrite and carbide to make the weld metals hard **[18]**.

The microhardness value in Ce containing weld metals after austempering at both 300°C and 350°C has been changed compare to without cerium containing weld metals. The extent of variation depends on the amount of Ce. For example, weld metal with Ce content in 0.05% the hardness shows comparatively higher than without Ce content. The presence of a lower amount of retained austenite content and higher bainitic ferrite compare to weld metal without Ce content has caused higher hardness. Increasing Ce content (0.1%) the hardness shows lower value compared to other weld metals (with and without Ce) because of the presence highest amount of retained austenite (46%) content in weld metal at both the temperature. Further, increasing Ce content to 0.2% the hardness shows higher value at both temperature due to presence of higher amount of bainitic ferrite and lower amount of retained

austenite content. Since bainitic ferrite is harder phase compared to retained austenite, hardness of weld metals will govern by the relative proportion of these two phases as the hardness of graphite is very low.

Since maximum amount of retained austenite (46%), which is obtained in weld metal containing 0.1% Ce, is the desirable microstructure after austempering heat treatment **[22]**. Thus, it can be concluded that austempering at 350°C for 2 h holding time is optimum austempering condition and 0.1% Ce is optimum one for DI weld metal studied.

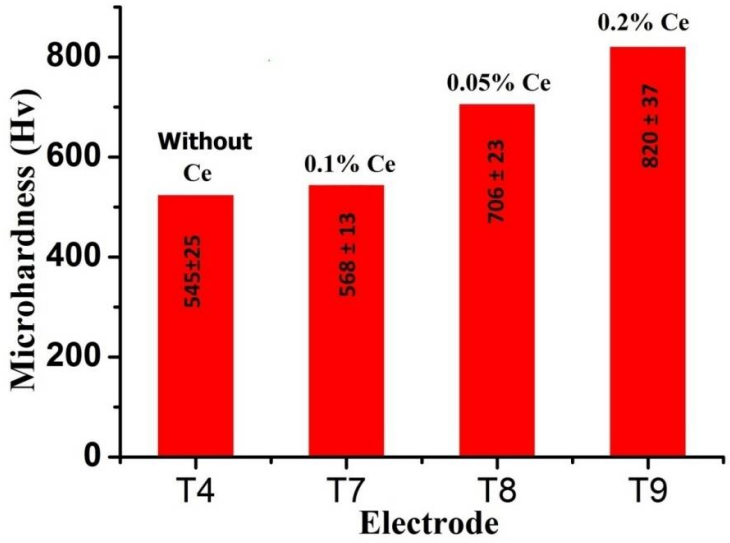

Fig.6.20: Average microhardness value of as-deposited without and with Ce containing weld metal

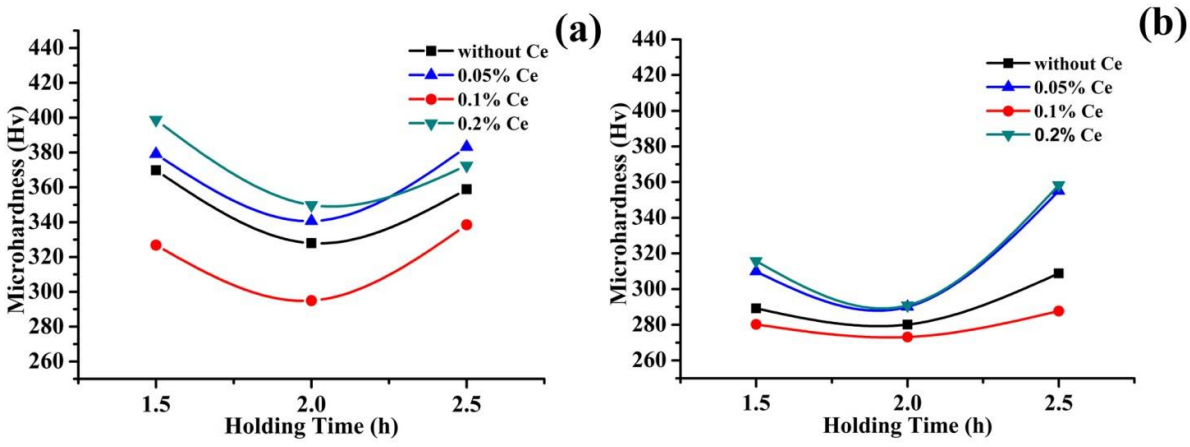

Fig.6. 21: Average microhardness value of without and with different Ce containing weld metals after austempering at (b) 300°C, (b) 350°C for three different holding times

6.2 Conclusions

The results obtained in this chapter leads to the following conclusions:

- Addition of Ce in DI weld metals has exerted significant effect on microstructures in as-welded as well as after isothermal heat treatment conditions.
- All the Ce containing as-welded weld microstructures in general show ledeburitic carbide, alloyed pearlite and graphite nodules; but varied significantly with Ce content. At 0.05% Ce, microstructure of weld metal shows finer with increased amount of ledeburitic carbide and lesser alloyed pearlite. Increasing Ce content (0.1%) the structure becomes more refined with decreased amount of ledeburitic carbide and higher amount of alloyed pearlite. At 0.2% Ce the structure of weld shows almost fully finer ledeburitic carbide and very small amount of alloyed pearlite.
- Ce containing weld metals well responded isothermal heat treatment performed at 300°C and 350°C for 1.5, 2 and 2.5 h holding time. At 300°C microstructure shows needle-shaped bainitic ferrite with film shape austenite and graphite nodules. However, at 350°C shows feathery shape bainitic ferrite with blocky shaped retained austenite. Addition of Ce content (0.05%) the shape and size of bainitic ferrite become coarser; whereas at 0.1% Ce content microstructure shows finer and homogeneous. Addition of higher Ce content (0.2%) structure of weld metal again becomes coarser and non-homogeneous.
- With addition of Ce content (0.05%) the amount of retained austenite was initially decreased and then increased with increasing Ce content (0.1%). The amount of retained austenite again decreased with further increasing Ce content at 0.2%. Similar trend of varying retained austenite with holding time at both the austempering temperature observed in case of without Ce also persists with Ce containing weld metal. Thus the maximum amount of retained austenite was obtained at 0.1% Ce containing weld metal at 350°C for 2 h holding time.
- As-welded weld metals show higher hardness which varied with varying the Ce content in the weld metal. After austempering the microhardness decreased significantly than the as-welded weld metals and also varied with varying the austempering conditions and amount of Ce present in weld metals. Weld metals containing 0.1% Ce shows the lowest hardness value at both the austempering temperature due to presence of maximum amount of retained austenite.

- With respect to the microstructural constituents (maximum amount of retained austenite), 0.1% Ce content in ADI weld metal is considered as the optimum amount of cerium in the present study.

References

1. X. Diao, Z. Ning, F. Cao, J. Sun, "Effect of Ce on Graphite Nodule Count and Size Distribution in Ductile Iron", International Journal of Modern Physics B, 23(2009) 1853-1860
2. Z. Bofan, E. W. Langer, "The Mechanism of Interaction of Lead, Bismuth and Cerium in Ductile Iron", Scand. J. Metall. 13(1) (1984)15-22
3. U. H. Udomon, C. R. Loper Jr, "Comments Concerning the Interaction of Rare Earths With Subversive Elements In Cast Irons", Transactions of the American Foundrymen's Society, 93(1985) 519-522
4. W. Bin, S. Bo, "In Situ Observation of the Evolution of Intragranular Acicular Ferrite at Ce-Containing Inclusions in 16Mn Steel", Steel research international, 83 (2012) 487–495
5. A. Vahed, D. Kay, "Thermodynamics of rare earths in steelmaking", Metallurgical Transactions B 7(1976) 375–383
6. J. Gao, P. Fu, H. Liu, D. Li, "Effects of Rare Earth on the Microstructure and Impact Toughness of H13 Steel", Metals, 5 (2015) 383–394
7. X. Zhi, J. Liu, J. Xing, S.Ma, "Effect of cerium modification on microstructure and properties of hypereutectic high chromium cast iron", Materials Science and Engineering A, 603 (2014) 98-103
8. Y. Jingsheng, Y. Zongsen, W. Chengjian, Rare earths and the mechanical properties off steel, JOM, 40(5)(1988) 26-31
9. Z. Adabavazeh, W. S. Hwang, Y. H. Su, "Effect of adding cerium on microstructure and morphology of Ce-based inclusions formed in low-carbon steel", Scientific reports, 7 (2017) 1-10
10. G. Thewlis, "Effect of cerium sulphide particle dispersions on acicular ferrite microstructure development in steels", Mater. Sci. and Tech., 22(2) (2006) 153-166
11. X. Wu, J. Xing, H. Fu, X. Zhi, "Effect of titanium on the morphology of primary M_7C_3 carbides in hypereutectic high chromium white iron", Materials Science and Engineering A, 457(1-2) (2007)180-185
12. B. L. Bramfitt, "The effect of carbide and nitride additions on the heterogeneous nucleation behavior of liquid iron", Metallurgical Transactions, 1(7) (1970) 1987-1995

13. D. Turnbull, B. Vonnegut, “Nucleation catalysis”, Industrial & Engineering Chemistry, 44(6) (1952) 1292-1298
14. E. Fras, M. Górny, H. F. Lopez, “Chilling Tendency and Nodule Count in Ductile Cast Iron: Part I Theoretical Background”, Transactions of the American Foundry Society 114 (2006) 575-594
15. E. Fraś, M. Górny, H. F Lopez, “Chilling tendency and nodule count in ductile cast iron, Part II Experimental verifi- cation”, AFS Transactions 114 (2006) 595-603
16. H. Horie, T. Kowata, A. Chida, “Effect of Rare Earth Elements on Chill Formation and Nodule Count in Thin-section Spheroidal-Graphite Cast Iron”, Cast Metals, 1(2) (1988) 90-97
17. D. M. Stefanescu, C. R. Loper Jr, “Effect of lanthanum and cerium on the structure of eutectic cast iron”, American Foundrymen's Society Transactions, 89 (1981) 425-436
18. J. Aranzabal, J. Gutierrez, J. M. Rodriguez-Ibabe, J. J. Urcola, “Influence of the amount and morphology of retained Austenite on the mechanical properties of an austempered ductile iron”, Metallurgical and Materials Transactions A, 28 (1997) 1143-1156
19. S. Panneerselvam, S. K. Putatunda, R. Gundlach, J. Boileau, “Influence of intercritical austempering on the microstructure and mechanical properties of austempered ductile cast iron (ADI)”, Materials Science and Engineering A, 694 (2017) 72–80
20. S. K. Putatunda, “Development of austempered ductile cast iron (ADI) with simultaneous high yield strength and fracture toughness by a novel two-step austempering process”, Materials Science and Engineering A, 315(1-2) (2001) 70-80
21. J. Mallia , M. Grech, R. E. Smallman, “Effect of silicon content on transformation kinetics of austempered ductile iron”, Materials science and technology 14 (1998) 452-460
22. M. A. Yescas, H. K. D. H. Bhadeshia, D. J. MacKay, “Estimation of the Amount of Retained Austenite in Austempered Ductile Irons Using Neural Networks”, Mater. Sci. Eng., 311(1-2) (2001) 162-173

Chapter 7

Influence of optimum cerium content on microstructures and mechanical properties of ADI Joints

7.0 Introduction

Optimum Ce content (0.1%) in DI weld metal and response to isothermal heat treatment was established based on microstructure followed by microhardness study as discussed in **Chapter 6**. Obviously the performance of ADI weld metal with optimum Ce content should be evaluated in order to ascertain the reliability of the ADI joints for various applications. Accordingly, mechanical properties such as microhardness, transverse tensile strength, room temperature charpy impact and high cycle fatigue behaviourof the ADI joints have been evaluated and the result of each mechanical property have been discussed and correlated with microstructure. The fracture surfaces of broken charpy impact specimens and fatigue tested specimens have been studied under SEM in order to find out possible micro-mechanism of failure.

7.1 Results and Discussion

7.1.1 As-welded Microstructure

It is to be noted that as-welded microstructures containing 0.1% Ce have been discussed in the previous chapter **(Chapter-6)** when optimum Ce content in weld metal was found out. However, in this chapter only microstructures of PMZ of weld metal containing 0.1% Ce has been discussed and compared first with the structure of weld metal with Ce and then with the PMZ of weld metal without Ce. Microstructure of PMZ is similar to weld metal e.g. ledeburitic carbide and alloyed pearlite with graphite nodules. But ledeburitic carbides are coarser as well as lesser in amount and graphite nodules are larger in size. Since the temperature experienced in PMZ is between the eutectic and liquids temperature of DI base metal, carbon diffuses out of graphite nodules leading to increased concentration of carbon in the surrounding matrix **[1-2]**. This continues until melting takes place and finally leads to eutectic melting. As expected, lesser amount of eutectic formed in PMZ of Ce treated weld metal **(Fig.7.1a)** will attribute lesser amount ofledeburitic carbides after eutectic transformation. Also due to slower cooling rate at PMZ than weld metal, sufficient time was available to grow graphite nodules. When compare with the microstructure of PMZ of weld metal without Ce **(Fig.7.1b)**, lesser and finer ledeburitic carbide has been indentified in PMZ of weld metal with Ce indicating that Ce has been diffused from weld metal and attributed similar effect exerted in weld metal. As expected, HAZ shows the same microstructure in both without and with Ce containing ADI weldments containing pearlite, ferrite and small amount of cementite as well as morphology of graphite nodules.

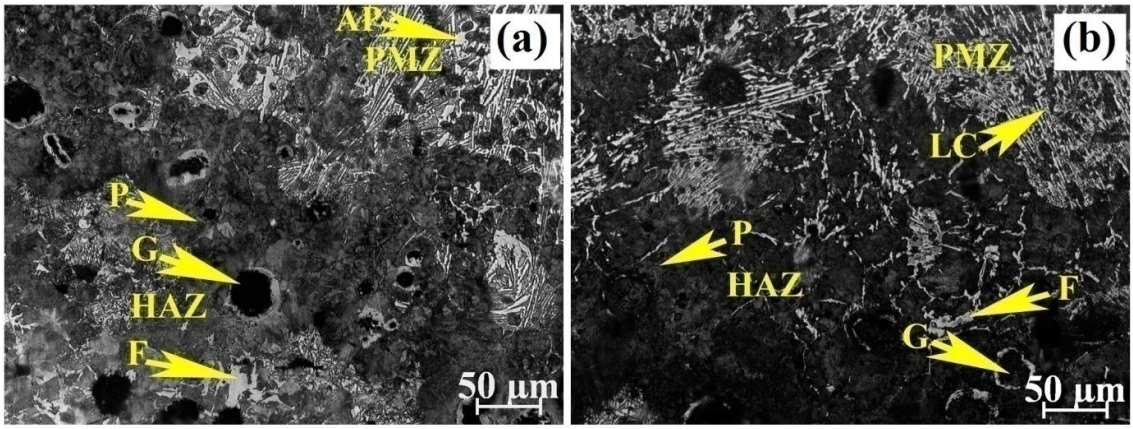

Fig. 7.1: Optical microstructure of HAZ including PMZ using (a) with and (b) without Ce containing coated electrodes

7.1.2 Austempered microstructure

After austempering, the microstructures of both without and with Ce (0.1%) containing weld metals consist of bainitic ferrite (dark), retained austenite (white) and graphite nodules. However, the proportion of microstructural constituents varies with changing the austemperingtemperature and holding time in both cases. Microstructure of Ce containing weld metal shows lower amount of finer bainitic ferrite and higher amount of finer retained austenite (vol %) with smaller nodulesize compare towithout Ce containing weld metal in both the austempering temperatures.

Since it is difficult to distinguish PMZ and HAZ after austempering, it has been marged into HAZ. Thus two zones i.e. weld metal and HAZ have been considered in ADI weldment. However, when compare with HAZ microstructure of without Ce containing weld metal **(Fig.7.2)**, very close to fusion boundary relatively finer bainitic ferrite with smaller graphite nodules in Ce containing weld metal **(Fig. 7.3)** has been noted. Otherwise, microstructures of HAZ in both the weldments (without and with Ce containing) show similar microstructural appearance i.e. bainitic ferrite and retained austenite **(Fig.7.2 and Fig. 7.3)**. In both cases, HAZ shows relatively higher amount (vol %) of coarser bainitic ferrite and lower amount of retained austenite (vol %) than weld metals at both the austempering temperatures.

Base metal shows the similar microstructural appearance like weld metal and HAZ at two austempering temperatures and have been discussed in **Chapter 5**.

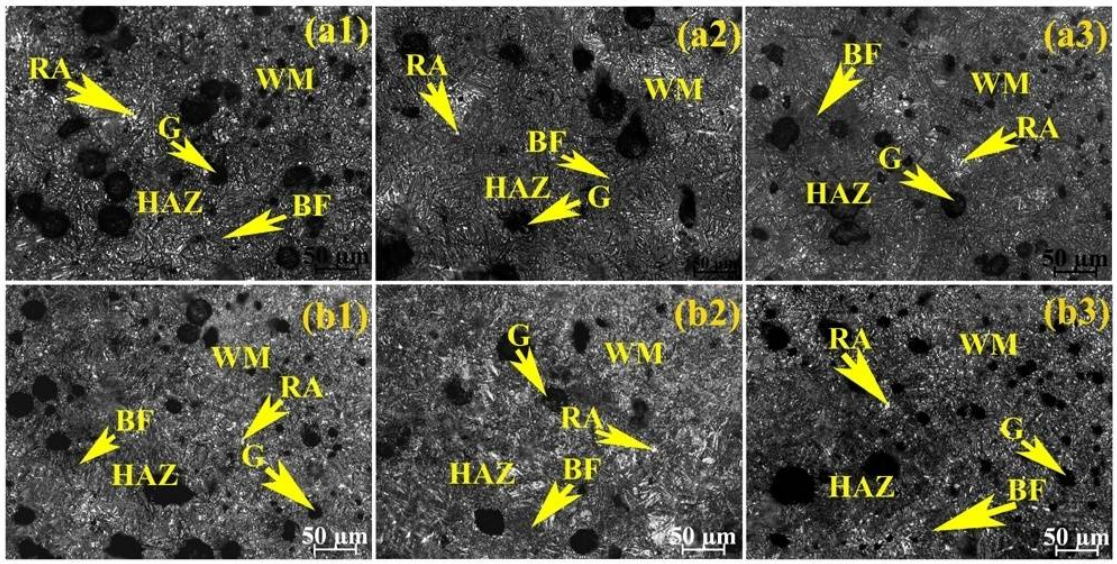

Fig. 7.2: Optical Microstructures of austempered HAZ (including PMZ) at 300°C for (a1) 1.5 h, (a2) 2 h, (a3) 2.5 h and 350°C for (b1) 1.5 h, (b2) 2 h, (b3) 2.5 h holding time using without Ce containing electrode

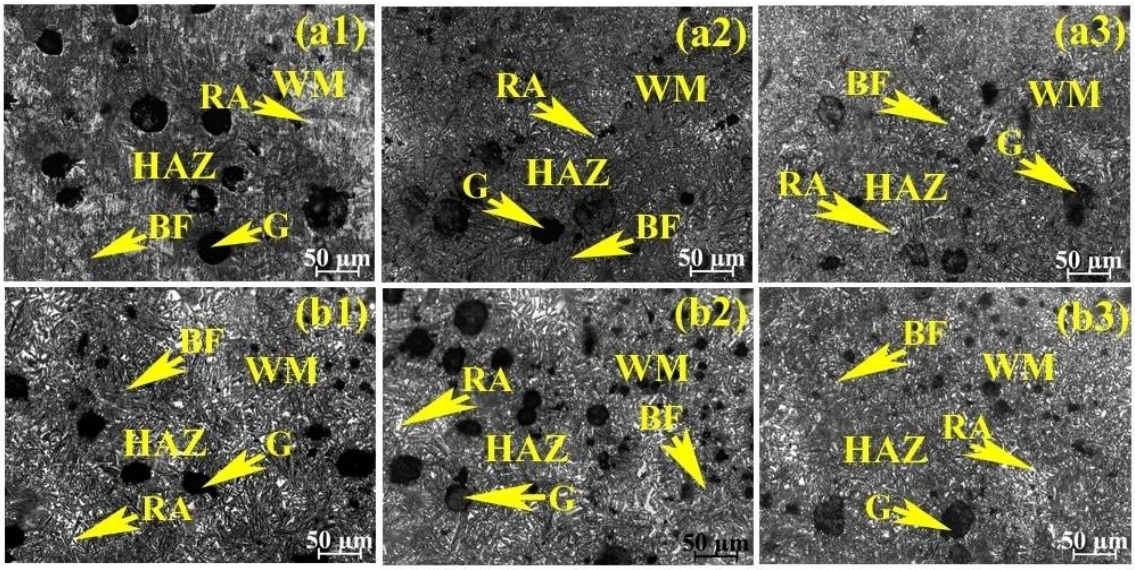

Fig.7.3: Optical Microstructures of austempered HAZ (including PMZ) at 300°C for (a1) 1.5 h, (a2) 2 h, (a3) 2.5 h and 350°C for (b1) 1.5 h, (b2) 2 h, (b3) 2.5 h holding time using with Ce containing electrode

7.1.3 Microhardness

The microhardness were taken across the weldments (without and with Ce content) in as-weld and austempered conditions (at 300°C and 350°C for 1.5, 2 and 2.5 h holding times) and microhardness values have been plotted against distance travel shown in **Fig.7.4** and **Fig.7.5** respectively. In as-weld condition, **Fig. 7.4** shows maximum hardness exhibited in weld metal followed by PMZ, HAZ and base metal. The variation in hardness of different zones of weldment is a reflection of microstructural variation in different zones. Weld metals having more eutectic carbide than PMZ attributed higher hardness. Whereas HAZ showed only pearlite and base metal revealed ferrite. Thus hardness of different zones in weldments is consistent with the result of the microstructural constituent in each zone. Although there is scatter of hardness in both the weld metals indicating microstructural hetroogeneity, weld metals without Ce shows slightly harder than weld metal with Ce. Similarly, PMZ in weld metals without Ce shows slightly harder than PMZ in weld metal with Ce. Higher hardness of both the zones (weld metal and PMZ) in case of without Ce is attributed due to presence of more eutectic carbide. **Fig.7.5** demonstrates microhardness of all the three zones namely weld metal, HAZ and base metal after austempering for different duration at a given temperature in both the ADI weldments. It is evident that hardness gradually increases in ascending manner from weld metal, HAZ and base metal irrespective of holding time and temperature. Also, the lowest hardness in all the zones is exhibited for 2 h duration irrespective of temperature and type of ADI weldment. Interestingly, maximum carbon enriched **(Fig.7.7)** retained austenite was achieved for 2 h duration **(Fig.7.6)** under the austempering conditions studied. In both the weldments weld metal shows the lower hardness value than base metal and HAZ due to presence of higher amount of retained austenite. However base metal shows maximum hardness value due to presence of lower amount of retained austenite and hardness of HAZ is intermediate between weld metal and HAZ indicating the presence of higher RA than basemetal, but lower RA than weld metal. For the same reason, weld metal austempereat at 350°C having higher retained austenite at each holding time show lowest hardness in all the zones.

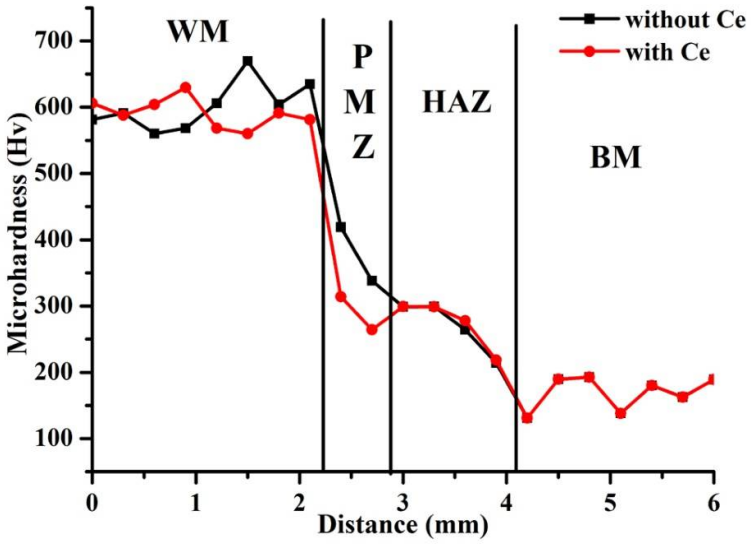

Fig. 7.4: Microhardness of as-welded weldment containing without and with Ce content

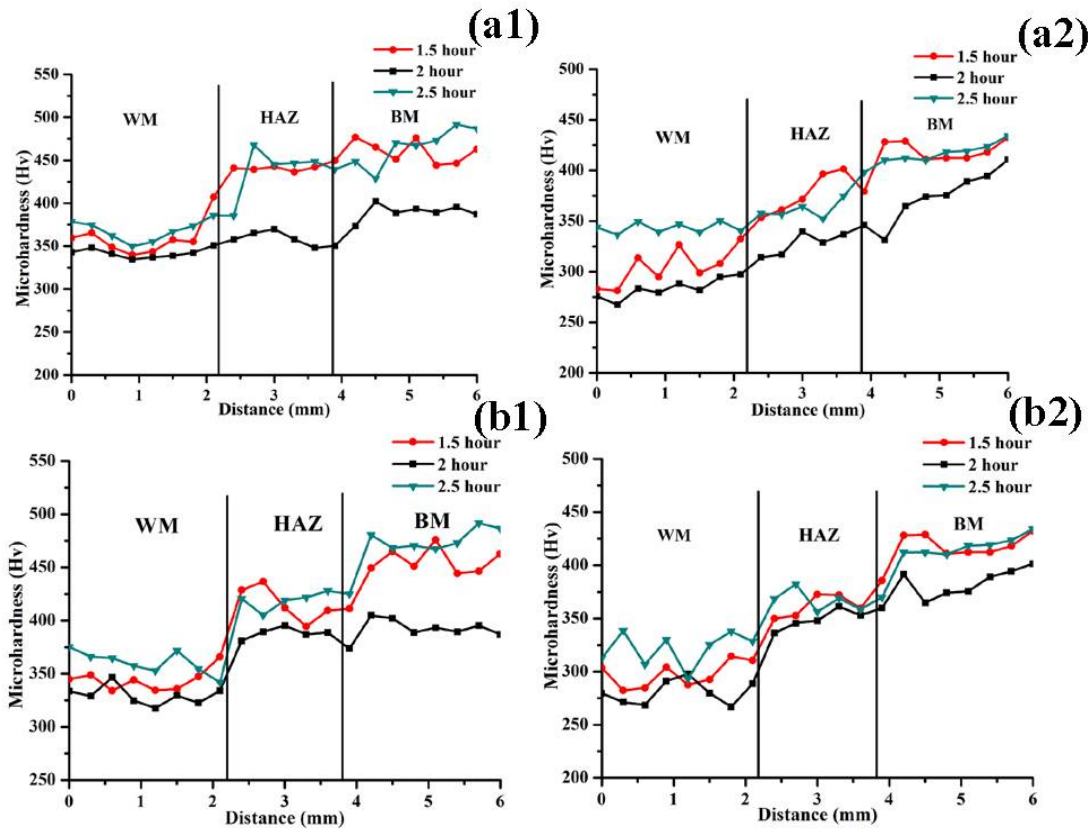

Fig. 7.5: Microhardness of heat treated weld metal, HAZ and base metal austempering at (a1) 300°C, (a2) 350°C for without Ce containing and (b1) 300°C, (b2) 350°C for with Ce containing for different holding times

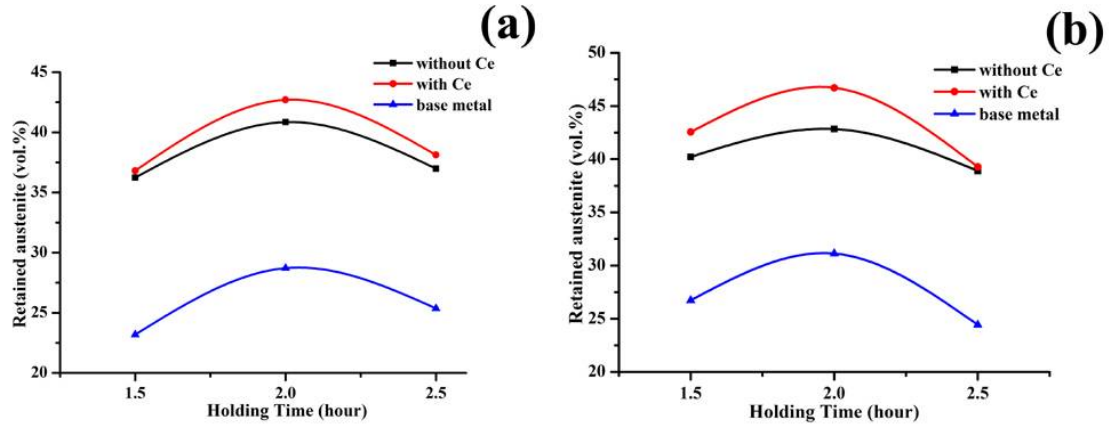

Fig. 7.6: Volume percentage of retained austenite austempering at (a) 300°C and (b) 350°C for different holding times

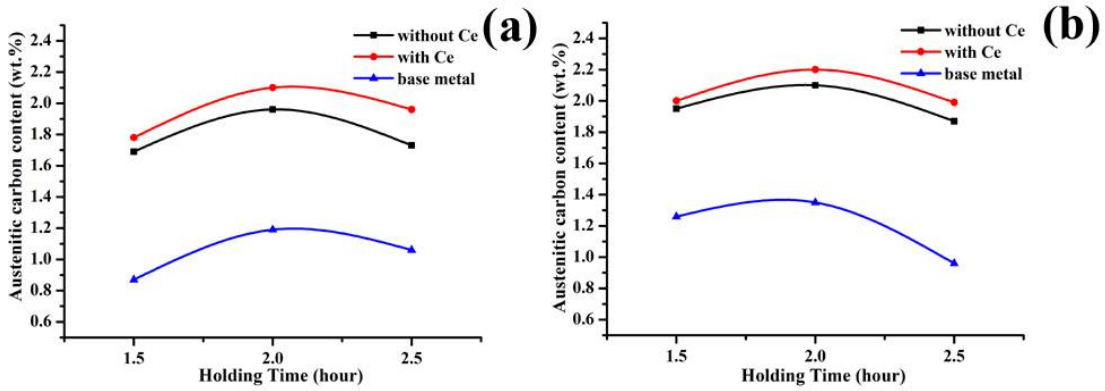

Fig. 7.7: Austenitic carbon content of base metal and weld metals at (a) 300°C and (b) 350°C for different holding times

7.1.4 Tensile properties

The transverse tensile tests of the ADI welded joints (without and with Ce content) were carried out after austempered at 300°C and 350°C for 2 h holding time. For confirmation of the test results, three samples at each condition were tested and average of the three test results was considered as representative one. The failure of the entire tensile test specimen took place from base metals **(Fig.7.8)**. Because all the weld joint samples broke from base metal, tensile results therefore signify that the weld metal and even HAZ are much stronger than base metal. Tensile results also indicate 100% joint efficiency achieved for ADI joining using developed coated electrodes. However, inspite of breaking all the ADI joint samples from base metal, it is clearly apparent from **Table 7.1** that there exists a significant variation in strength between Ce and without Ce containing weld metals as well as between two different austempering temperatures.

The tensile properties of ADI is strongly depended on the amount of retained austenite and its carbon content, the shape and size of bainitic ferrite and the numbers of graphite nodules presence **[3-4]**. At each austempering condition both the weld metals attributed more amount of retained austenite and finer bainic ferrite and smaller size of graphite nodules compare to base metal and HAZ. During tensile testing weld metal is possibly more strain hardened compare to base metal and HAZ due to presence of higher amount of retained austenite **[5]**. It is well known that austenite having FCC structure posses higher strain hardening rate than BCC ferrite (bainitic ferrite) and the strain hardening rate of austenite also increases with carbon content **[5-6]**. However, with increasing tensile load, the strain hardening effect becomes saturated, which facilitates the transmission of load to the adjacent base metal. When the base metal can not bear the load, failure takes place at the base metal. Thus it is more likely, due to more amount of retained austenite along with higher carbon, tensile strength of Ce containing weld metal would be higher than weld metal having without Ce at the same austempering condition. However, for both types of weld metals (with and without Ce), higher strength of austempered sample at 300°C compare to austempered sample at 350°C indicates that morphology of bainitic ferrite has played a dominating role over retained austenite in contributing strength of ADI joint.

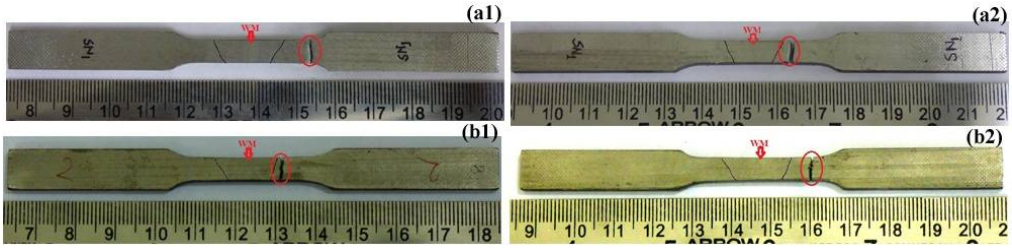

Fig. 7.8: Transverse tensile samples after testing, austempering at (a1) 300°C, (a2) 350°C for without Ce containing and (b1) 300°C, (b2) 350°C for with Ce containing weld metals for 2 h holding time

Table 7.1 Average Tensile test result of without and with Ce containing ADI joints

Austempering Temp (°C)	Holding Time (h)	Trial 4			Trial 7		
		YS (MPa)	UTS (MPa)	El (%)	YS (MPa)	UTS (MPa)	El (%)
300	2	700	913	4.32	727	978	4.98
350		663	857	6.42	713	912	6.8

7.1.5 Charpy Impact Properties

The average sub-size charpy impact values of two weld metals (with and without Ce) austempered at 300°C and 350°C for 1.5, 2 and 2.5 h holding time are shown in **Fig.7.9**. The test results show that the charpy impact value of weld metals increased with increasing austempering temperature (at 350°C). Also, at a given austempering temperatures with increasing holding time from 1.5 to 2 h the impact toughness increased and with further increasing holding time from 2 to 2.5 h the impact toughness are decreased.

The charpy impact values are directly related to austempered microstructure of the weld metals. The impact toughness of weld metals strongly depends on the amount of retained austenite, austenitic carbon content, nodularity, nodule size and shape of the bainitic ferrite. Many research workers have reported that feathery shaped bainitic ferrite microstructure provides higher toughness in unalloyed low manganese ADI; whereas needle-shaped bainitic ferrite microstructure exhibits improved toughness in case of conventional alloyed ADI with higher Mn content **[4-6]**. In the present investigation, feathery shaped bainitic ferrite along with higher carbon and higher amount of retained austenite (at 350°C for 2 h holding time) attributed maximum toughness. The results with ADI weld metals having lower Mn content therefore are in good agreement with the observations of Dorazil and Holtzman **[7]** and others investigators **[4-6]**. This observation is consistent with both the weld metals (with and without Ce). However, maximum toughness achieved with Ce containing weld metal is attributed to higher refinement of graphite nodule size and shape of bainitic ferrite along with higher carbon and higher amount of retained austenite (46.7%).

The fracture surfaces of broken charpy impact test specimens of both the weld metals (with and without Ce) after austempering at 300°C and 350°C for different holding time were examined in order to relate impact properties to operative fracture mechanism and are given in **Fig.7.10** and **Fig.7.11**. In both types of welds austempered at 300°C, the fracture surfaces exhibited dimple and cleavage type fracture. Austempering at 350°C, the fracture surface shows predominantly dimpled ductile fracture for both the weld metals. However, dimples are finer in Ce treated weld metal **(Fig. 7.11)** with changing the holding time the shape and size of the dimple also changed. It appears that extensive plastic flow around the graphite nodules results in stress concentration at graphite matrix interface which leads to a decohesion between graphite nodules and the matrix. **Fig.7.10** and **Fig.7.11** illustrate the small graphite nodules within cavities or dimples that initiated the microvoids. Subsequent growth and coalescence of these microvoids produced dimple rupture network. All these fracture surfaces mentioned above are also associated with some cleavage. The crack, which

is likely to initiate near the graphite nodule, propagates through the matrix to reach the adjoining nodules. It is anticipated that plastic deformation in the matrix ahead of the regions of decohesion will thus be confined essentially to the soft regions **[5, 8]** and the crack propagation becomes difficult across the tough austenite to join up with similar microcracks in the neighbouring ferrite needles. Therefore, one can expect improved toughness with increasing the volume fraction of retained austenite.

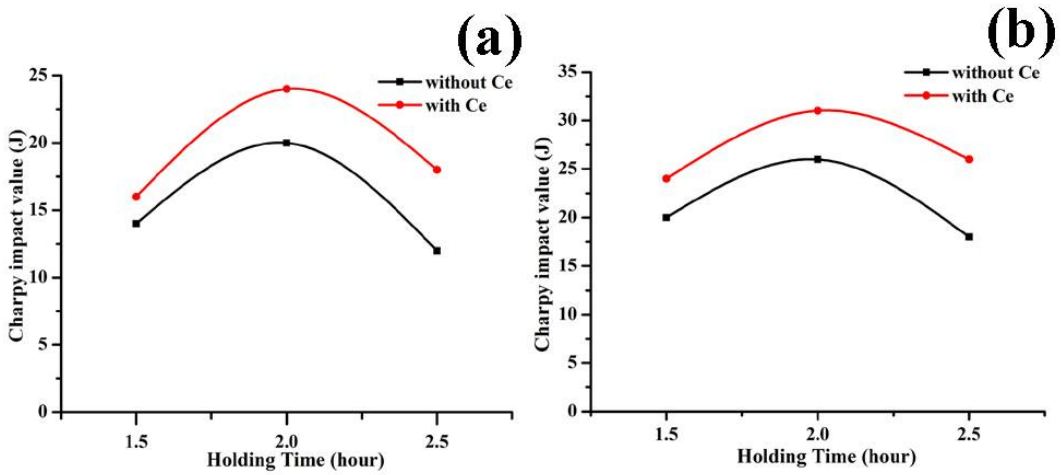

Fig. 7.9: Variation of charpy impact values of heat treated weld metals austempering at (a) 300°C and (b) 350°C for different holding time used with out and with Ce content coated electrodes

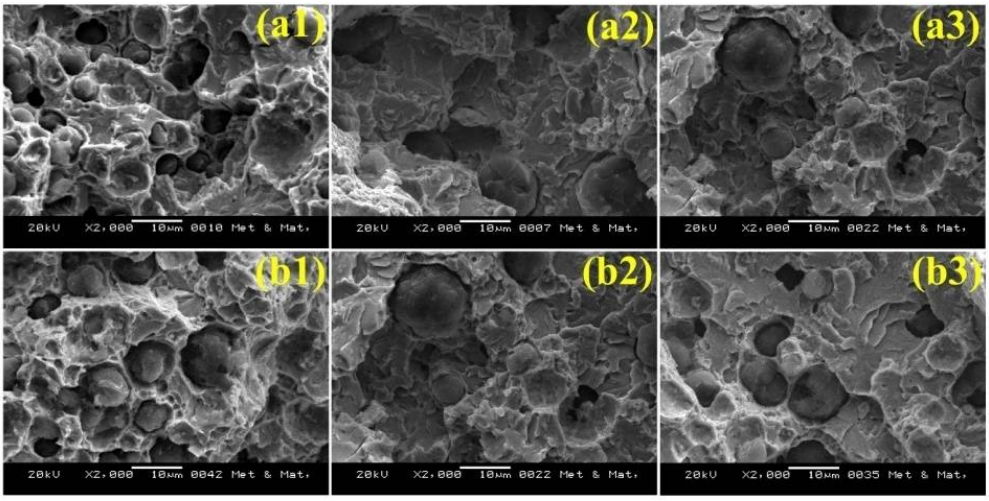

Fig. 7.10: Fracture surface of charpy impact tested without Ce containing welded samples austempering at 300°C for (a1) 1.5 h, (a2) 2h, (a3) 2.5 h and 350°C for (b1) 1.5 h, (b2) 2 h, (b3) 2.5 h holding time

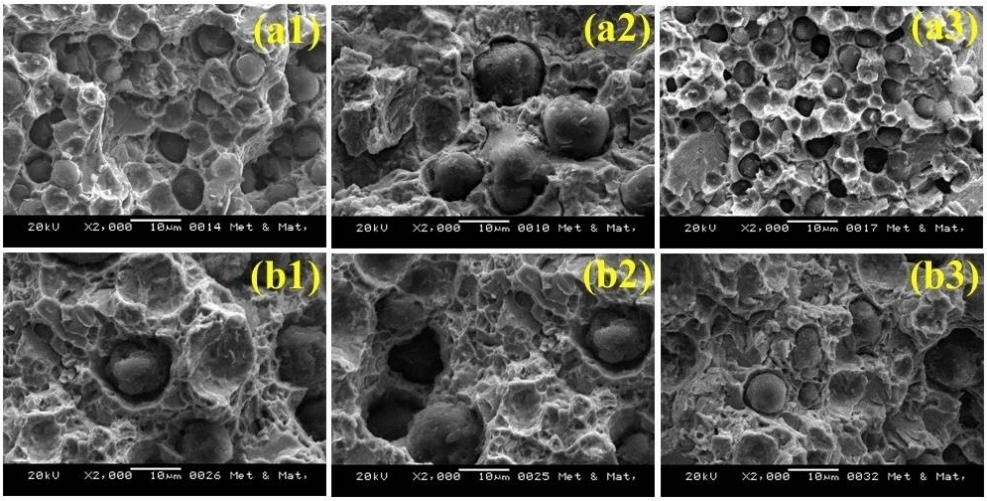

Fig. 7.11: Fracture surface of charpy impact tested without Ce containing welded samples austempering at 300°C for (a1) 1.5 h, (a2) 2 h, (a3) 2.5 h and 350°C for (b1) 1.5 h, (b2) 2 h, (b3) 2.5 h holding time

7.1.6 High cycle fatigue properties

Fatigue failure is the most frequent and serious incident for a mechanical structure. It corresponds to a sequence of complex phenomena: strain hardening, local damage and creation of micro cracks (initiation), then propagation which leads to final fracture. During the last few years, a great deal of research has been carried out on low cycle fatigue. However, high cycle fatigue remains a fundamental field of investigation for mechanical industrial applications. Also there is no published literature available on high cycle behaviour of ADI joints.

High cycle fatigue test was performed under different stress amplitudes i.e. 30% to 70% YS to predict fatigue life and the fatigue test was continued to failure or to 10^7 cycles at which specimen was considered to be stopped. Typical stress amplitude vs. number of cycles to failure plots of different ADI joints are shown in **Fig.7.12**. The S-N curve is drawn through the data point as best fit line and the arrows indicates that the samples didn't fail even after 10^7cycle (endurance limit) **[9-10]**. The highest stress at which specimens endured 10^7 cycles is taken as the fatigue strength. The estimated fatigue strengths and fatigue ratios are shown in **Table 7.2**. During fatigue testing of ADI joints, in case of stress amplitude above 50% YS the fatigue crack initiated at weld metal irrespective of with and without Ce content after after certain no. of cycles loading the crack propagation is stopped **(Fig. 7.13a)**. Whereas, in case of stress amplitudeat and below 50% YS failure of ADI joints took place from the base metals **(Fig. 7.13b)**.

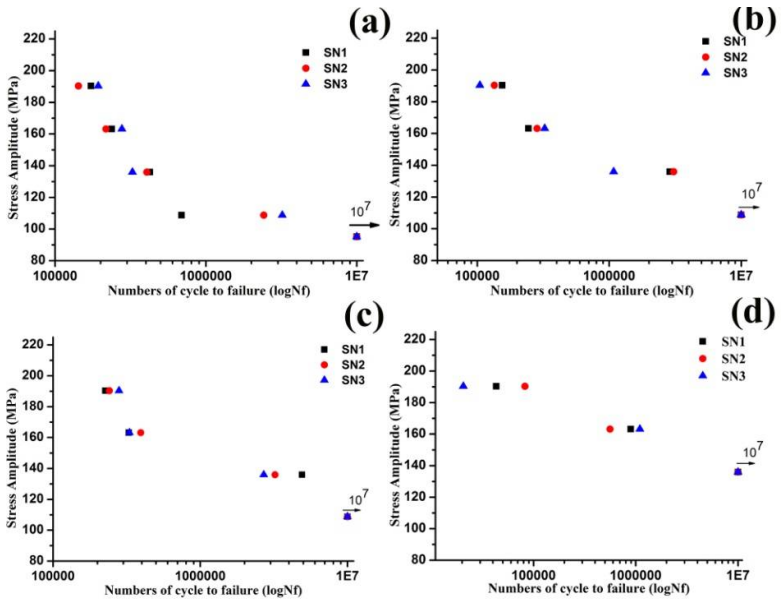

Fig.7.12: S-N curve of high cycle fatigue test for without Ce containing weld joints austempering at (a) 300°C, (b) 350°C at and with Ce containing weld joints at (a) 300°C, (b) 350°C for 2 h holding time (arrow indicating the endurance limit of the each condition)

Table 7.2 Fatigue strength and fatigue ratio of ADI joints with and without Ce content

Electrode Type	Austempering Temp (°C)	Holding Time (h)	Fatigue strength (MPa)	Fatigue ratio (r)
Trial 4	300	2	211.48	0.24
(without Ce)	350		241.69	0.27
Trial 7	300		241.69	0.27
(With Ce)	350		302.11	0.34

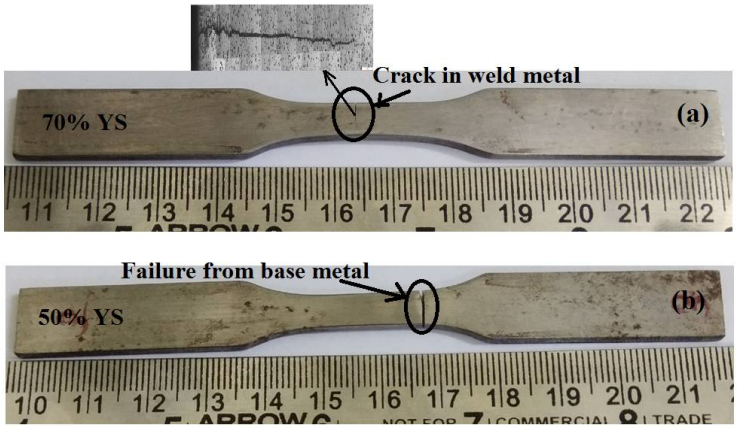

Fig.7.13: ADI fatigue tested sample (a) crack in weld metal (arrow show the macro structure of the crack zone), (b) failure from base metal

In order to find out the cause of failure at weld metal and base metal, microhardness was taken near the crack tip and far away from crack tip of the weld metal **(Fig.7.14b)** as well as in base metal of the same test specimen. Also in case of fractured base metal microhardness was taken at the failure region of the base metal **(Fig. 7.14c)** as well as in weld metal of the same test specimen. The hardness values at different locations of both weld metal and base metal are given in **Table 7.3.**

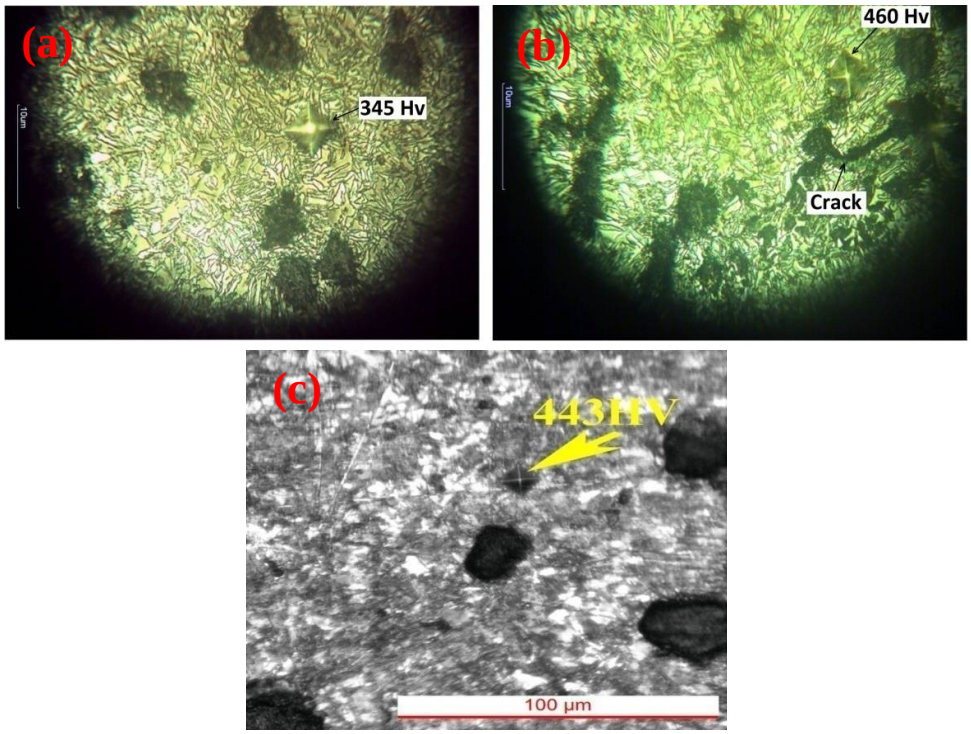

Fig.7.14: Microhardness values at different positions: weld metal (a) far away from crack tip (b) crack tip and (c) base metal of same fatigue specimen

Table 7.3 Microhardness of different positions of weld metal and base metal after fatigue testing of different stress amplitudes

Hardness (HV)	Stress Amplitude				
	Below 50% YS		Above 50% YS		
	BM	WM	BM	WM	
				Matrix	Crack tip
	428	336	387	345	460

It is clearly evident that in weld metal cracked sample the hardness near the crack tip is much higher (460 Hv) than far away from crack tip (345 Hv) of the weld metal indicating hardening near the crack tip. Also the base metal hardness (387 Hv) of the same tested

sample though lower than weld metal; but compare to original base metal (360 Hv), it is significantly higher. The difference in hardness results of base metals clearly reveals hardening of base metal as well. To find out the cause of hardening of both weld metal and base metal, microstructures were taken at respective locations as given in **Fig.s 7.15**. The microstructure near the crack tip of weld metal shows martensite; whereas away from crack tip reveals austempered structure i.e. bainitic ferrite and retained austenite. The base metal of the same fatigue tested sample also shows formation of martensite whichmay form form relatively less stableaustenite.

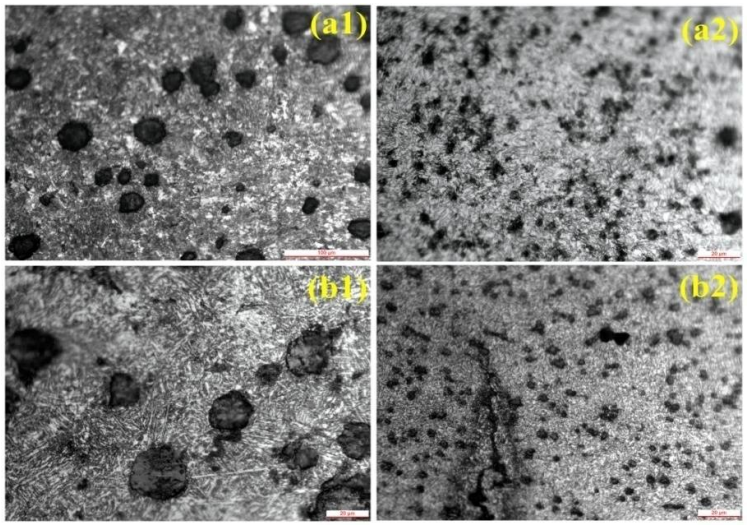

Fig.7.15: Optical microstructure of fatigue tested samples (a1) base metal (a2) weld metal under stress amplitude below 50% YS and (b1) base metal (b2) weld metalunder stress amplitude above 50% YS

The hardness results followed by microstructural studies of cracked weld metal clearly indicate that high stress concentration near the crack tip has caused transformation of martensite even from relatively stable high carbon austenite in weld metal. In fact the stress induced martensite transformation of austenite occurs in the plastic zone ahead of crack so as to relax the stress concentration at the crack tip. The accompanying volume change due to the formation of martensite leading to local compressive stresses also encourages plastically induced crack closure to occur **[9-11]**. However, initiation of crack at weld metal rather than base metal in stress amplitude of above 50% YS is probably due to strain hardening effect which has not reached to saturation point leading to non- transmission of load to the adjacent base metal. Whereas in case of stress amplitude of 50% YS and below no crack was initiated at weld metal and practically no hardening of weld metal took place as revealed from

hardness of weld metal under similar loading condition. This result indicates that retained austenite in weld metal maintained its stability even under stress aplitude of 50% YS and below and also transmited load to the adjacent base metal. But elatively less stable austenite of base metal has undergone stress induced martensite. XRD analysis of the fractured base metal shows 16.5% retained austenite as compared to 31.6% retained austenite content in original (austempered) base metal indicating partial transformation of austenite to martensite. Thus base metal became relatively brittle with the formation of martensite leading to failure under stress amplitude of 50% YS and below.

Fatigue results demonstrate that ADI joint austempered at 350°C provides higher fatigue strength (302.11 MPa) than austempered at 300°C (241.69 MPa). Also for a given austempering temperature, Ce containing weld metal attributed higher fatigue strength than weld metal without Ce content. For example, in case of stress amplitude of about 190.33 MPa that is about 70% YS, fatigue life of Ce containing weld metal is almost three time more (433240 cycles) than that of weld metal without Ce content (154727 cycles).

The fatigue strength of ADI depends on the amount of retained austenite and its carbon contentand fatigue strength increases with increasing the retained austenite content due to the higher strain hardening behaviour of austenite **[12-13]**. In fact higher strain hardening behaviour of austenite delays the formation of persistent slip bands and reduces the nucleating of fatigue crack growth. Thus Ce containing weld metal having higher amount of retained austenite along with higher amount of carbon content improved fatigue strength compare to without Ce containing weld metal at both the austempering temperatutres. Fatigue strength also depends on shape and size of the bainitic ferrite and graphite nodules. However, different effect of bainitic ferrite on the fatigue strength of ADI has been reported. For example, improved fatigue strength is obtained in needle shaped bainitic ferrite than feathery shaped bainitic ferrite **[14-15]**, in upper and lower bainite compared withcoarse upper bainite **[16]**, in coarse ausferrite microstructure and higher volume fraction of retained austenite **[17]**. Regarding graphite, higher nodule count with smaller nodule size exhibits a better fatigue life **[18]**. The improved fatigue strength at 350°C in both the weld metals is considered to be due to higher volume fraction of retained austenite along with high carbon and higher nodule count. Hwang et al **[19]** also found that the 350°C austemper gave the best fatigue crack growth resistance among austempers of 275, 300, 350, 400 and 475°C tested ADI samples.

Whereas, hardness shows opposite to fatigue strength i.e. fatigue strength improves with decreasing hardness. It has been reported **[12-13]** that fatigue strength of ADI is not proportional to tensile strength and hardness, but is related to toughness and the amount of

retained austenite. The present results of high cycle fatigue properties of ADI joints are agreement with the fatigue strength of ADI reported by previous investigators **[20-21]**.

7.1.6.1 Fatigue fracture surface

The fracture surfaces of the fatigue testedspecimens of ADI joints have been examined by SEM in order to understand operative fracture mechanism(s). The fracture surfaces exhibits predominantly quasicleavage **(Fig.7.16a)**. Zones of brittle fracture by transgranular cleavage and intergranular decohesion are also visible **(Fig.7.16b)**. The combination of ductile striation and cleavage plane whose river patterns **(Fig.7.16c)** go into tear-rivers is named as quasi cleavage **[22]**. Other typical and frequent morphologies are steps between different cleavage levels **(Fig.7.16d)**.

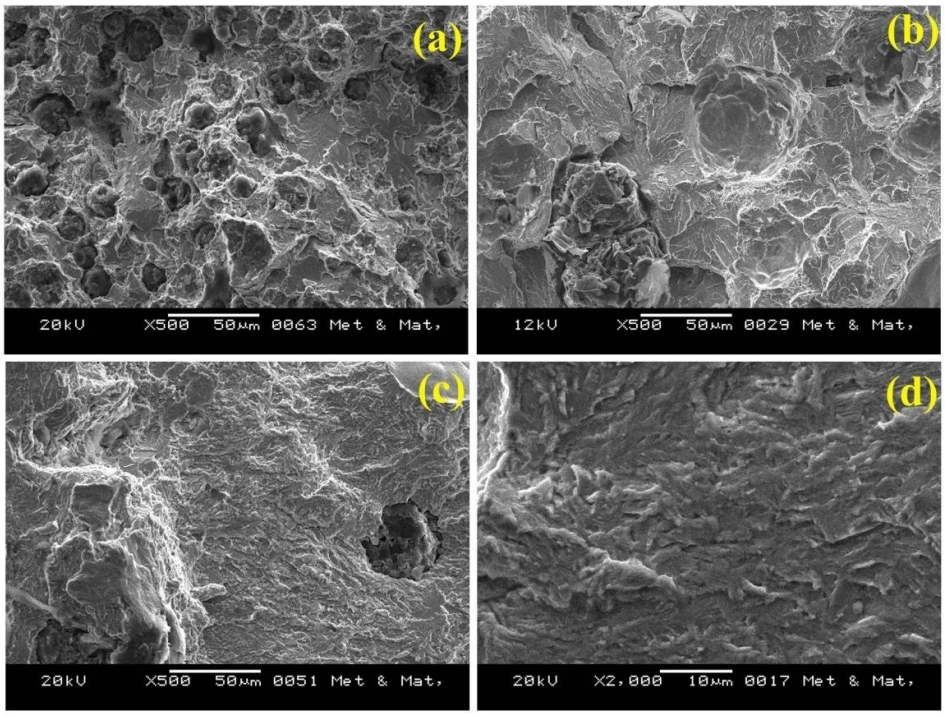

Fig.7.16: Fatigue fracture surface (a) predominantly quasicleavage, (b) transgranular cleavage and intergranular decohesion, (c) river patterns, (d) steps between different clivage level

Several interfacial microcracks formed at the graphite-matrix interface as shown in **Fig.7.17** due to the weak interface bond between graphite and matrix as well as the lower elastic modulus of graphite. Also the stress around the graphite nodules is about three times the average stress in the matrix during elastic deformation **[23]**. Previous investigators **[15-16, 24]** have shown that fatigue cracks initiate at the interface between graphite nodules, and the

matrix or from inclusions and irregularly shaped graphite **[15]**. When the interfacial crack propagated all around a graphite nodule, a micro crack was formed inside the matrix **(Fig.7.17a)**. The crack usually follows the path of least resistance through the matrix between nodules **(Fig.7.17 b, c) [15]**. Thus, microcrack usually propagates along ferrite–austenite interface due to atomic mismatch at the interface **(Fig.7.17b) [23]**. Also during propagation the crack may deflect along another ferrite-austenite interface, which caused the crack to branch **(Fig.7.17d)**. The fact that interconnected nodule graphite causes local reorientation of the propagating crack resulting in a crack branching can reduce the possibilities of the continuous extension of the crack which effectively improves fatigue life.

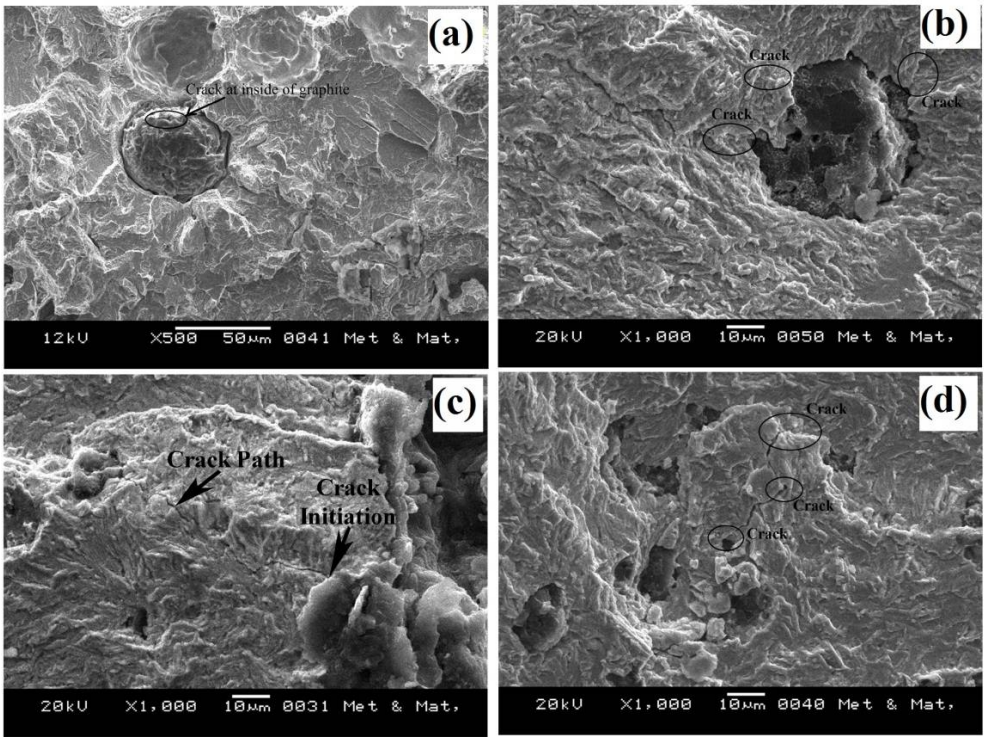

Fig.7.17: (a) microcracks formed at the graphite-matrix interface, (b) interfacial crack around a graphite nodule, (c) crack initiation and propagation path, (d) branch crack

7.2 Conclusions

Based on the above studies, the following conclusions can be drawn.

- Like weld metal microstructure of PMZ shows ledeburitic carbide and alloyed pearlite with graphite nodules except ledeburitic carbides are coarser as well as lesser in amount and graphite nodules are larger in size. However, addition of Ce has minimized ledeburitic carbide and made carbides finer.

- The microhardness of weldments in as-weld condition show higher hardness of weld metal than HAZ and base metal. However, Ce treated weld metal shows comparatively lower hardness than without Ce content due to presence of lower ledebutic carbide and higher alloyed pearlite content. After austempering microhardness shows opposite trend i.e. weld metal shows lowest hardness followed by HAZ and base metal in both without and with Ce treated conditions. However, lowest hardness is obtained at 350ºC for 2 h holding time for both without and with Ce treated weld metals; but like as-welded condition Ce treated austempered weld metal shows comparatively lower hardness than without Ce.
- Transverse tensile testing of all the welded ADI specimens after different austempering conditions shows failure from the base metals indicating that weld metal and even HAZ are stronger than base metal as well as achievement of 100% joint efficiency.
- The charpy impact toughness of Ce treated weld metal improved significantly compared to without Ce at both the austempering conditions. However, highest impact toughness was obtained at 350ºC for 2 h holding time.
- Fatigue strength of both ADI weld joint improved with improving the austempering temperature. At 350ºC feathery shaped bainitic ferrite with higher amount of retained austenite shows higher fatigue strength than needle shaped bainitic ferrite with small amount of retained austenite at 300ºC. Ce containing weld metal shows higher fatigue strength than without Ce content at both the austempering temperatures.
- In case of stress amplitude of above 50% YS the fatigue crack initiated at weld metal irrespective of with and without Ce content for all the ADI joints and after certain no. of cycles the crack propagation is stopped. Whereas, in case of stress amplitude at 50% YS and below failure of ADI joints took place from the base metals. Fractographs of failed ADI joint samples showfatigue crack initiated at graphite nodule/ matrix interface and propagated through least resistance path of matrix to the nearest graphite nodule with crack branching.

References

1. R. C. Voigt, C. R. Loper Jr, "Study of heat-affected zone structures in ductile cast iron", Welding Journal, 62 (1983) 82-88
2. M. Pouranvari, "On the weldability of grey cast iron using nickel based filler metal", Materials & Design, 317 (2010) 3253-3258
3. S. K. Putatunda, C. Martis, "Influence of Two-Step Austempering Process on the Fracture Toughness of a Low Carbon Low Alloy (LCLA) Steel", In Materials Science Forum, Trans Tech Publications, 706 (2012) 2259-2264.
4. S. K. Putatunda, P. K. Gadicherla, "Influence of austenitizing temperature on fracture toughness of a low manganese austempered ductile iron (ADI) with ferritic as cast structure", Materials Science and Engineering A, 268 (1999) 15-31
5. U. Batra, S. Ray, S. R. Prabhakar, "Impact properties of copper-alloyed and nickel-copper alloyed ADI", Journal of materials engineering and performance, 16 (2007) 485-489.
6. P. P. Rao, S. K. Putatunda, "Influence of microstructure on fracture toughness of austempered ductile iron", Metallurgical and Materials Transactions A, 28 (1997) 1457-1470
7. E. Dorazl, M. Holzmann, "Proc. World Conf. on Austempered Ductile Iron, Bloomingdale, IL, Mar. 1991", American Foundryman Society, Des Plaines, IL, (1991) 567–75
8. P. P. Rao, S. K. Putatunda, "Dependence of fracture toughness of austempered ductile iron on austempering temperature", Metallurgical and Materials Transactions A, 29 (1998) 3005-3016
9. D. Krishnaraj, K. V. Rao, S. Seshan, "Influence of matrix structure on the fatigue behavior of ductile iron", AFS Trans, 97 (1989) 345–50
10. D. A. Porter, K. E. Easterling, "Phase Transformations in Metals and alloys", 2nd ed., Chapman & Hall, 1992
11. W. F. Smith, "Structure and Properties of Engineering Alloys", McGraw-Hill,1981
12. J. Yang, S. K. Putatunda, "Influence of a novel two-step austempering process on the strain-hardening behavior of austempered ductile cast iron (ADI)", Materials Science and Engineering A, 382(1-2) (2004) 265-279

13. P. Shanmugam, P. P. Rao, K. R. Udupa, N. Venkataraman, “Effect of microstructure on the fatigue strength of an austempered ductile iron”, Journal of Materials Science, 29(18) (1994) 4933-4940
14. H. L. J. Pang, K. H. Tan, X. Q. Shi, Z. P. Wang, “Microstructure and intermetallic growth effects on shear and fatigue strength of solder joints subjected to thermal cycling aging”, Materials Science and Engineering A, 307(1-2) (2001) 42-50
15. M. Bahmani, R. Elliott, N. Varahram, “The relationship between fatigue strength and micro-structure in an austempered Cu-Ni-Mn-Mo alloyed ductile iron”, Journal of materials science, 32(20) (1997) 5383-5388
16. C. K. Lin, P. K. Lai, T. S. Shih, “Influence of microstructure on the fatigue properties of austempered ductile irons-I. High-cycle fatigue”, International Journal of Fatigue,18 (5) (1996) 297-307
17. C. K. Lin, Chih-Kuang, C. W. Chang, “Influence of heat treatment on fatigue crack growth of austempered ductile iron”, Journal of materials science, 37(4) (2002) 709-716
18. M. Hatate, T. Shiota, N. Takahashi, K. Shimizu, “Influences of graphite shapes on wear characteristics of austempered cast iron”, Wear, 251(1-12) (2001) 885-889
19. B. Stokes, N. Gao, P. A. S. Reed, “Effects of graphite nodules on crack growth behaviour of austempered ductile iron”, Materials Science and Engineering A, 445 (2007) 374-385
20. C. K. Lin, W. J. Lee, “Effects of highly stressed volume on fatigue strength of austem-pered ductile irons”, International journal of fatigue, 20(4) (1998) 301-307
21. A. D. Basso, R. A. Martinez, J. A. Sikora, “Influence of austenitising and austempering temperatures on microstructure and properties of dual phase ADI”, Materials Science and Technology, 23(11) (2007) 1321-1326
22. J. H. Bulloch, “Near threshold fatigue behaviour of flake graphite cast irons micro-structures”, Theoretical and applied fracture mechanics, 24(1) (1995) 65-78
23. G. Toktas, A. Toktas, M. Tayanc, “Influence of matrix structure on the fatigue properties of an alloyed ductile iron”, Materials & Design 29 (2008) 1600–1608
24. C. K. Lin, C. S. Fu, “Low-cycle fatigue of austempered ductile irons in various-sized Y-block casting”, Mater Trans, JIM 38 (1997) 692–700

Chapter 8

Summarized Conclusions

Summarized Conclusions

In the present work, coated electrodes were developed using with and without Ce content for welding DI and converted to ADI after isothermal heat treatment to study and understand the microstructures and mechanical properties of as-welded DI and ADI joints.

The following overall conclusions may be drawn from the results:

- It has been possible to develop coated electrodes without and with Ce content successfully for welding cast DI plate as per AWS(D11) standard. Weld procedure for grove welding of 20 mm thick cast DI plate was established as per AWS(D11) standard using the developed coated electrodes(with and without Ce content) only at preheat of 300°C for 1 h and PWHT immediately after welding at 300°C for 1 h with modified U-groove design.
- All the as-welded DIweld metals show ledeburitic carbide, alloyed pearlite and graphite nodules.With increasing Ce content in DI weld metal from 0.05% to 0.2% amount of ledeburitic carbide increased and became finer compare to without Ce except Ce content of 0.1% which attributed lesser amount of fine ledeburitic carbide. Cerium containing weld metal in general shows smaller size nodule and increased nodule count compare to without Ce.
- All the zones of DI weldments e.g., weld metal, PMZ, HAZ and base metal responded isothermal heat treatment which consists of austenitization at 900°C for 2 h and 300°C and 350°C for 1.5, 2 and 2.5 h holding time.Interestingly, as-welded microstructures including matrix and graphite largely governed the response of isothermal heat treatment cycle. At 300°C microstructure shows needle-shaped bainitic ferrite with film shape austenite and graphite nodules. Whereas, at 350°C shows feathery shape bainitic ferrite with blocky shaped retained austenite. Addition of Ce in general refined bainitic ferrite and retained austenite but reduced vol % of retained austenite except 0.1% Ce which shows maximum vol % of retained austenite. The graphite morphology however remains unaltered after austempering.
- In as-welded condition Ce containing DI weldment show higher hardness than without Ce containing DI weldment. Maximum hardness exhibited in weld metal followed by PMZ, HAZ and base metal. After isothermal heat treatment hardness shows opposite trend i.e. weld metal shows lowest hardness followed by HAZ (PMZ could not be distinguished with HAZ) and base metal in both without and with Ce treated ADI weldment. However,

weld metals containing 0.1% Ce shows the lowest hardness at both the austempering temperatures due to presence of higher vol % of retained austenite.

- The transverse tensile tests results of the ADI welded joints (without and with Ce content) showed that all the test samples failed from base metal indicating weld metal and even HAZ are stronger than base metal as well as achievement of 100% joint efficiency.
- Ce containing weld metals show higher charpy impact toughness than without Ce content and maximum toughness is obtained in weld metal containing 0.1% Ce at 350°C for 2 h holding time.
- Higher fatigue strength is achieved in ADI weld metal containing 0.1% Ce having maximum toughness due to presence of higher amount of high carbon retained austenite. Interestingly, during fatigue testing at stress amplitude of 50% and below YS all ADI joint samples failed from base metal, where as at stress amplitude above 50% YS crack initiated in weld metal, but could not propagate due to formation of martenite at the crack tip.
- With respect to the microstructural constituents (maximum amount of retained austenite) and results of mechanical properties of ADI joints, 0.1% Ce is the optimum Ce content in weld metaland 350°C for 2 h holding time is optimum isothermal heatreated condition in the present study.